8TH INTERNATIONAL CONFERENCE

ON

SIMULATION AND MODELLING

IN THE

FOOD AND BIO-INDUSTRY

2014

FOODSIM'2014

EDITED BY

Alain-Claude Roudot

JUNE 23-25, 2014

BREST, FRANCE

A Publication of EUROSIS-ETI

Printed in Ghent, Belgium

8th International Conference on Simulation and Modelling in the Food and Bio-Industry

BREST, FRANCE

JUNE 23-25, 2014

Organised by

ETI
The European Technology Institute

In Cooperation with

LERCCO

Université de Bretagne Occidentale

Sponsored by

EUROSIS
The European Simulation Society

Technopôle Brest-Iroise

Océanopolis Brest

Ghent University

University of Skövde

Hosted by

Océanopolis Brest
France

EXECUTIVE EDITOR

PHILIPPE GERIL
(BELGIUM)

EDITORS

General Conference Chair

Alain-Claude Roudot, LERCCO, UBO, Brest, France

Local Programme Committee

Gireg Desmeulles, CERV, UBO, Brest, France
Anne-Sophie Ficheux, LERCCO, UBO, Brest, France
Dominique Parent-Massin, LERCCO, UBO, Brest, France
Alain-Claude Roudot, LERCCO, UBO, Brest, France
Nathalie Wesolek, LERCCO, UBO, Brest, France

International Programme Committee

Simulation in Food Engineering and Processing
Lionel Boillereaux (ONIRIS, Nantes, France)
Cedric Brandam (INPT-ENSIACET, Toulouse, France)
Jean-Yves Monteau (ONIRIS, Nantes, France)
Cristina Silva (ESBUCP, Porto, Portugal)
Olivier Vitrac (INRA-UMR FARE, Reims, France)

Simulation in Food Sciences and Biotechnology
Francis Butler (UCD, Dublin, Ireland)
Enda Cummins (UCD, Dublin, Ireland)

Methods and Tools Applied to Food and Bio-Industries
Paolo Masi (University of Naples Federico II, Portici, Italy)
Pierre-Sylvain Mirade (INRA-Theix, St Genes Champanelle, France)
Leon Rothkrantz (Delft University of Technology, Delft, The Netherlands)

Methods and tools applied to Food Quality and Safety Evaluation
Joana Amaral (ESTiG-IPB, Bragança, Portugal)
Ursula Gonzales Barron (University College Dublin, Food Science and Veterinary Medicine, Ireland)
Vasco Cadavez (ESA-IPB, Bragança, Portugal)
Isabel Ferreira (ESA-IPB, Bragança, Portugal)
Isabel Mafra (REQUIMTE, Porto, Portugal)
Isabel M. Vicariao (University of Sevilla, Spain)

Simulation in Functional Foods
Lourdes Amigo Garrido (CSIC, Madrid, Spain)
Gianpaolo Ruocco (University of Basilicata, Potenza, Italy)

Simulation in Food Production Management, Economics and Traceability
Martin Cloutier (UQAM, Montreal, Canada)
Magda Aguiar Fontes (Faculdade de Medicina Veterinária, UTL, Lisboa, Portugal)
Martin Grunow (Technical University of Munich, Munich, Germany)
Vincent Hovelaque (INRA, Rennes, France)

International Programme Committee

Sustainable Food Production
Björn Johansson (Chalmers University of Technology, Sweden)

Innovation in Traditional Food Products
Elsa Ramalhosa (ESA-IPB, Bragança, Portugal)

All articles published in these Proceedings have been peer reviewed

EUROSIS-ETI Publications are ISI-Thomson, IET, SCOPUS and Elsevier Engineering Village referenced
Legal Repository: Koninklijke Bibliotheek van België, Keizerslaan 4, 1000 Brussels, Belgium
CIP 12.620 D/2011/12.620/1

Selected papers of this conference are published in scientific journals.

For permission to publish a complete paper write EUROSIS, c/o Philippe Geril, ETI Executive Director, Greenbridge Science Park, Ghent University Ostend Campus, Wetenschapspark 1, Plassendale 1, B-8400 Ostend, Belgium.

EUROSIS is a Division of ETI Bvba, The European Technology Institute, Torhoutsesteenweg 162, Box 4, B-8400 Ostend, Belgium

Printed and bound in Belgium by Reproduct NV, Ghent, Belgium
Cover Design by Grafisch Bedrijf Lammaing, Ostend, Belgium
Cover picture copyright Océanopolis Brest

EUROSIS-ETI Publication
ISBN: 978-90-77381-84-7
EAN: 978-90-77381-84-7

PREFACE

Dear Colleagues,

It is with a great pleasure, that I welcome you in Brest for this 8th FOODSIM conference.

Brittany is the main area for agriculture and agro-industry in France, and Brest, the main town concerned by this scientific and economic field of activity. As you will see, in our conference center; Océanopolis, sea research is very important in Brest, but agrifood research is also an important element in Brest University with microbiology labs, toxicology lab, plant physiology lab... One of the most interesting and original centers is probably the European Virtual Reality Center located in the vicinity of Brest, where new simulation techniques are developed and applied to biology and food research.

This FOODSIM conference is the unique location, where scientists from such different geographical and research areas can meet: research groups from Europe (Belgium, France, Italy, Spain, Poland) but also from the USA, Mexico, Vietnam, Brazil, Argentina or Senegal with specialties in microbiology, food processing, computer science, risk analysis, electronics, etc. I hope that this diversity will mix and provide new ideas to everybody in order to develop each other's research area with new concepts, theories and practices in order to solve industrial problems. I also hope that new collaborations could come to fruition during this meeting.

To conclude, Brest is an old town as you can see, with its own Castle, the Tanguy Tower, and the picturesque Rue St Malo. Unfortunately, being a major military port, Brest was almost completely destroyed around the end of the 2nd World War. Today the new Brest is largely focused towards the future which, from a research and industrial point of view, is called sea, computing and food research. And last but not least, Brest is situated on a magnificent bay that I encourage you to discover if you decide to stay a few days in our town

Have an excellent 8th FOODSIM conference.

Pr AC Roudot
FOODSIM'2014
General Conference Chair

CONTENTS

CONTENTS

ENVIRONMENTAL FACTORS AND FOOD EXPOSURE

SCIENTIFIC PROGRAMME

METHODOLOGY AND MODELLING

THE USE OF DIMENSIONAL ANALYSIS FOR PROCESS SCALE-UP AND MODELING

Chris Koh, Ph.D. and Sean Eichenlaub, Ph.D.
PepsiCo Global R&D
7701 Legacy Drive
Plano, TX 75244
U.S.A.
Email: chris.j.koh@pepsico.com, sean.eichenlaub@pepsico.com

KEYWORDS
Modeling, Simulation, Dimensional Analysis, seasoning tumbler, Buckingham Pi Theorem

ABSTRACT

Scale up of food process operations is an important task faced by many scientists and engineers. Traditionally, this problem has been approached by experiments (e.g. via design of experiments, followed by modeling of data), relying on our vast experience and intuition, using simple theoretical analysis, and in recent years through the use of computer simulation. In this paper, we discuss the use of dimensional analysis as a complementary technique to simulation that can further enhance its impact and effectiveness. In particular, we evaluate a certain aspect of a seasoning tumbler operation in industrial food production as an example of the application of this concept by combining the so-called Buckingham-Pi Theorem with the use of computer simulation.

INTRODUCTION

Scientists and engineers are often confronted with the question of how to scale up a new unit operation or process, or predict its performance with limited ability to test. In many instances, we can be successful in answering these questions by judiciously designing and executing experiments (e.g. via design of experiments (DOE), followed by modeling of data), relying on our vast experience and intuition, using simple theoretical analysis (for system that such analysis is tractable), and in recent years through the use of computer simulation. However, there are circumstances where the use of dimensional analysis (DA) can further augment the aforementioned tools – to simplify the experimentation (whether real or by computer simulation), ensure that the appropriate range of parameters relevant to the problem is explored, provide physical insights, and bring confidence in model predictions. This is especially true in cases where the fundamental science of the problem is highly convoluted, with many potential parameters that can impact the process. DA – in the form of Buckingham-Pi Theorem – can help simplify the analysis of such problems.

This paper does not introduce any particularly new concepts on dimensional analysis, nor does it report any specific application with real data. Rather, it attempts to illustrate its application and benefits in food process engineering by briefly describing the basic methodology of Buckingham-Pi Theorem, and by exploring a few examples of how DA can complement computer simulation. While the mathematical execution of the theorem is important (and sometimes tedious), it is often the thought process of extracting the relevant physical parameters of the problem prior to the analysis most enlightening, and the evaluation of the output after the mathematical analysis most useful. This work endeavors to highlight these two most stimulating parts of the whole process of using dimensional analysis – and in doing so, it is the authors' hope that the readers will consider dimensional analysis as part of their simulation toolbox in the future .

Many articles have been written on the mathematical basis of dimensional analysis (Eddey, 1945; Evans, 1972;Vignaux, 1992; Sonin, 2004), including the seminal paper by Buckingham (Buckingham, 1914) that led some to synonymously equate dimensional analysis with the "Buckingham-Pi Theorem." Additionally, the literature has many excellent articles detailing the application of this methodology in a wide variety of areas, such as molecular physics (Camblong, 2001), automobile dynamics (O'Brien, 2004), explosive detonation (Schmidt, 1995), ocean engineering (Hughes, 1993), and food engineering (Cheng, 2008; Thurairajasingam, 2002; Rainieri, 2008). As such, only the basic concept of dimensional analysis – as described in Buckingham's paper – is discussed here; for those readers that are interested in more detailed discussion, the above list would serve as a good starting point. More recently, statisticians have begun combining the use of DA with DOE (Albrecht, et al., 2013; Islam & Lye, 2007) and those concepts can be applied not only to real experiments, but also "experiments" performed via simulation.

BASIC THEORY

If a given problem can be described by n physically relevant and dimensional variables ($x_1, x_2, x_3, \ldots x_n$), then these variables can be expressed functionally as

$$F(x_1, x_2, x_3, \ldots x_n) = 0 \quad (1)$$

Drs. Chris Koh & Sean Eichenlaub are employees of PepsiCo Inc. The views expressed in this abstract are those of the authors and do not necessarily reflect the position or policy of PepsiCo Inc.

Furthermore, if there are k dimensionally independent physical quantities that are necessary to describe these n variables, then Buckingham's theorem states that Eqn.1 can be equivalently recasted as

$$\psi(\Pi_1,\Pi_2,..\Pi_{n-k})=0 \tag{2}$$

Where Π_1, Π_2...Π_{n-k} are dimensionless and independent variables, constructed from the original dimensional variables (x_1, x_2, x_3, ...x_n):

$$\Pi_i = x_1^{m_{1i}} x_2^{m_{2i}} \dots x_n^{m_{ni}} \tag{3}$$

It is well to point out that the theorem does not uniquely define the set of these dimensionless variables, nor does it necessarily prescribe the functional relationship, ψ. However, the fact that the two equations above are equivalent provides the first hint of the usefulness of Buckingham's work – that the number of variables describing the problem has been reduced by k through simple rearrangement of the variables, and as such, can significantly reduce the number of simulations necessary to model the problem.

A familiar example: flow in a pipe

To illustrate how the theorem is applied to a physical problem, we turn to the familiar problem of pipe flow. The friction factor, λ, is frequently used to assist in the calculation of pressure drop or head loss for a given flowrate. It is a function of the Reynolds number (N_{RE}) and the pipe roughness factor (ε/R), as commonly shown in the Moody chart (Moody, 1944). The chart is based on the compilation of many experiments in which various relevant parameters, such as velocity (u), density (ρ), viscosity (μ), pipe radius (R), pipe surface roughness (ε) are altered. The complexity of trying to express how the friction factor depends on these parameters can be daunting:

$$\lambda = \lambda(u,\mu,\rho,\mathrm{R},\varepsilon,\dots) \tag{4}$$

So, why does the Moody chart so effectively capture this dependence? Afterall, it is not immediately apparent that the friction factor should functionally be dependent on, and only on, N_{RE} and (ε/R):

$$\lambda = \lambda(\frac{\varepsilon}{\mathrm{R}};N_{\mathrm{RE}}) \tag{5}$$

In the case of the pipe flow problem, a cursory examination of the appropriate form of the steady-state and dimensionless Navier-Stokes equation and boundary conditions would confirm this, as only these two parameters appear in the problem:

$$0=-\frac{\partial P}{\partial z}+\frac{1}{\mathrm{Re}}\left(\frac{\partial^2 u}{\partial z^2}+\frac{1}{r}\frac{\partial u}{\partial z}\right) \tag{6}$$

B.C.1 $u=0$ $\qquad r=1+\frac{\varepsilon}{R}$

B.C.2 $\frac{\partial u}{\partial r}=0$ $\qquad r=0$

Unfortunately, not all problems are readily described by well-established equations where straightforward manipulation of the terms will point to the correct parameter dependency. Buckingham-Pi Theorem is useful in such situations. The following illustrates how it leads to the same conclusions regarding the pipe flow friction factor by examining the relevant physical parameters of the problem.

The procedure is straightforward. First, consider the problem and list all variables and the units associated with each:

1. Pipe radius, R [L]
2. Pipe wall roughness, ε [L]
3. Fluid density, ρ [m/L^3]
4. Fluid viscosity, μ [m/L/t]
5. Average flow velocity, u [L/t]
6. Pressure gradient, ∇P [m/L^2/t^2]

Here, the use of the square brackets [ ] denotes the units of the variable. Here, [L] represents a unit of length, [m] for mass, and [t] for time. From this, one can form the dimension matrix. k, the number of dimensionally independent physical parameters, is given by the rank of the matrix:

	R	ε	ρ	μ	u	∇P
[L]	1	1	−3	−1	1	−1
[m]	0	0	1	1	0	1
[t]	0	0	0	−1	−1	−2

Hence, k = 3 and the problem is described by three dimensionless and independent variables $(n-k=6-3=3)$.

We now select any 3 independent physical parameters (known as "repeating parameters") from the list as the basis to derive the dimensionless variables (Π's). The choice of these parameters is completely up to the reader, so long as they are dimensionally independent of each other. The final outcome may depend on the chosen repeating parameters, but is mathematically the same regardless. Here, we will choose R, u and ρ. Then, the Π's are constructed with the repeating parameters and each of the remaining parameters:

$$\Pi_1 = \mathrm{R}^a u^b \rho^c \varepsilon \quad (7)$$

$$\Pi_2 = \mathrm{R}^d u^e \rho^f \mu \quad (8)$$

$$\Pi_3 = \mathrm{R}^g u^h \rho^i \nabla P \quad (9)$$

To satisfy that each Π is dimensionless, each set of the exponents *(a, b, c)... (g, h, i)* are selected accordingly, for example:

$$[\Pi_1] = [\mathrm{L}]^{a+b-3c+1}[\mathrm{t}]^{-b}[\mathrm{m}]^c \quad (10)$$

So,

$$b = 0$$

$$c = 0$$

$$a + b - 3c + 1 = 0 \Rightarrow a = -1$$

and consequently,

$$\Pi_1 = \varepsilon / R \quad (11)$$

Similarly, it can be shown that:

$$\Pi_2 = \frac{\mu}{\rho u \mathrm{R}} = \frac{1}{N_{\mathrm{RE}}} \quad (12)$$

and,

$$\Pi_3 = \frac{\nabla P}{\rho u^2 / R} \quad (13)$$

Therefore, according to Eqn. 2,

$$\Pi_3 = f(\Pi_1; \Pi_2) \quad (14)$$

or:

$$\frac{\nabla P}{\rho u^2 / R} = f(\frac{\varepsilon}{R}; N_{\mathrm{RE}}) \quad (15)$$

Since the pressure gradient is proportional to the friction factor (Whitaker, 1981) for pipe flow, Eqn. 15 is therefore equivalent to Eqn. 5.

Implication of the analysis

It is well to reiterate that Eqn. 15 is derived from simply identifying the relevant physical parameters of the problem and straightforward application of the Buckingham-Pi Theorem, with no *a priori* knowledge of the detailed physics, mathematical model (Navier-Stokes Equation) or any experimental data. But what are the practical advantages of having done the analysis?

The first advantage facilitates understanding the physics of the problem. In most instances, dimensionless numbers are useful when interpreted as a ratio of two quantities. Here, the dimensionless parameters are N_{Re} and ε/R. The former, Reynolds number, is probably one of the more well-known dimensionless numbers and most readers know that it can be viewed as a ratio of the momentum force to the viscous force. In pipe flow, the magnitude of the N_{RE} governs the flow regime – transitioning from laminar to turbulent as N_{RE} approaches around 2000 for smooth pipe (ε/R~0). Of course, the Buckingham-Pi Theorem does not predict the numerical value of this transition; nonetheless, it is very useful as it does allow one to predict the nature of the flow as long as N_{Re} is known. The second dimensionless parameter, ε/R, is the ratio of the surface roughness to the pipe dimension. Physically speaking, it implies that as far as flow behavior in a pipe is concerned, the roughness of the pipe is relevant only as it relates to the pipe dimension: a surface roughness of 30 microns (peak-to-valley) can have totally different implications to the flow between a tubing of 1 mm and a sewer pipe of 3 meters in diameter.

The second advantage concerns simulation efficiency. In the analysis, we have identified 6 parameters. For discussion purpose, assume for a moment that we know nothing of pipe flow, but are interested in determining the pressure gradient, ∇P, as a function of the rest of the parameters:

$$\nabla \mathrm{P} = F(u, \mathrm{R}, \varepsilon, \rho, \mu) \quad (16)$$

The number of simulations, even with suitable application of design of experiment (DOE), can be daunting. On the other hand, if recasted via the Buckingham-Pi Theorem, the problem can be more compactly described by Eqn. 5.

The number of simulations required is now significantly reduced. For example, a straightforward factorial design in dimensional space would require 2^5= 32 experiments vs. 2^2 = 4 experiments in the dimensionless space. Even with more sophisticated use of DOE, the number of simulations needed to explore the functional dependence of the pressure gradient on the relevant parameters is necessarily more without the benefit of dimensional analysis.

FOOD PROCESSING EXAMPLE

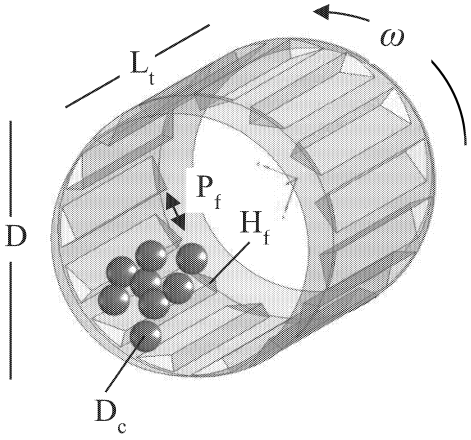

Figure 1: Tumbler Configuration

We now turn to a food processing related problem – understanding the application of seasoning to a food product in a tumbler (Figure 1).

For illustration purpose, we look at the tumbling action only, and the product is spherical. In this example, we will determine the dependency of the average product dwell time, t_D, in the tumbler.

Similar to the previous example, the first step of the analysis is to list all the relevant physical parameters and the associated units.
The dependent variable t_D [t] (product dwell time in the tumbler) is governed by the following independent physical parameters:

1. Angle of inclination of the tumbler, θ [1]
2. Diameter of tumbler, D_t [L]
3. Length of tumbler, L_t [L]
4. Height of flights of tumbler, H_f [L]
5. Pitch of flights of tumbler, P_f [L]
6. Rotational speed of tumbler , ω_t [t^{-1}]
7. Throughput of product, Q_c [mt^{-1}]
8. Characteristic size of product, D_c [L]
9. Density of product, ρ_c [mL^{-3}]
10. Gravitational acceleration, g [Lt^{-2}]
11. Coefficient of friction between product and tumbler wall, μ_{wc} [1]
12. Coefficient of friction between product, μ_{cc} [1]
13. Normal spring stiffness of product, K_n [mt^{-2}]
14. Normal damping of product, N_n [mt^{-2}]
15. Tangential spring stiffness of product, K_t [mt^{-2}]
16. Tangential damping of product, N_t [mt^{-2}]

The last six parameters are required to describe the particle-particle and particle-wall interactions, based on the Hertz-Mindlin contact force model (Di Renzo & Di Maio, 2004). For this problem, we will assume tumbler incline angle, product density, gravitational acceleration, the coefficients of friction, and the spring stiffness and damping (both normal and tangential) remain constant.
The generalized Buckingham-Pi theorem (Sonin, 2004) states that N_D, the number of dimensionless groups that govern the process, is equal to: $N_D = (n-k) - (n_F - k_F)$

where
n = number of independent parameters=16
k = number of dimensionally independent parameters
n_F = number of fixed parameters = 9
k_F = number of dimensionally independent parameters among the fixed parameters

k is equal to the rank of the parameter-units matrix, and k_F is equal to the rank of the fixed-parameter-units matrix. For the tumbler example, both the parameter-units and the fixed-parameter-units matrices have a rank of 3, therefore, $N_D = 7$.
The procedure to identify the dimensionless parameters is similar to the previous example, and it can be readily shown that:

$$\overline{t_D} \equiv t_D \omega_t = f\left(\frac{Q_c}{\omega_t D_t^3 \rho_c}, \frac{\omega_t^2 D_t}{g}, \frac{L_t}{D_t}, \frac{H_f}{D_t}, \frac{P_f}{D_t}, \frac{D_c}{D_t}\right) \quad (17)$$

We shall define $N_L = \frac{Q_c}{\omega_t D_t^3 \rho_c}$ and $N_{FR} = \frac{\omega_t^2 D_t}{g}$

Implication of analysis

It is instructive to briefly review the physical interpretation of each of the dimensionless parameters. The first term, which involves the throughput of product, can be shown to be related to the loading of the tumbler.

The second parameter, $\omega_t^2 D_t/g$, can be viewed as the ratio of the centrifugal force to that of the gravitational force acting on the chips, which is sometimes referred as the Froude number (N_{Fr}) and impacts the path of the product through the tumbler. The rest of the terms are based on the geometric dimensions of the system.

Application Example

To illustrate one benefit of DA, let's assume a simulation model has been constructed based on an existing pilot scale tumbling process, as shown in Figure 1. The following parameters are fixed as below:

1. $\theta = 5^\circ$
2. D_t = 76.2 cm
3. L_t = 127 cm
4. H_f = 4.4 cm
5. P_f = 16.0 cm
6. ω_t = 0.083 – 0.183 s^{-1}
7. Q_c = 0.016 – 0.029 kg/s
8. D_c = 3.81 cm
9. ρ_c = 18 kg/m^3
10. g = 9.8 m/s^2
11. μ_{wc} = 0.4
12. μ_{cc} = 0.7
13. K_n = 0.5 kg/s^2
14. N_n = 0.5 kg/s^2
15. K_t = 0.5 kg/s^2
16. N_t = 0.5 kg/s^2

Using Discrete Element Modeling (Zhu, Zhou, Yang, & Yu, 2007), the trajectory of the spherical particles going through the tumbler is obtained numerically using CD-Adapco DEM software package. Typical output is as shown in Figure 2, from which average residence time data can be calculated.

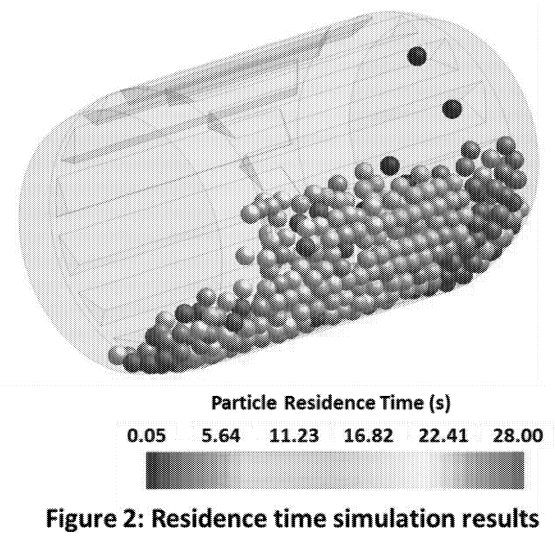

Figure 2: Residence time simulation results

The average dwell-time is calculated for a range of N_{FR} and N_{L}. Figure 3 is a dimensionless dwell-time contour map as a function of N_L and N_{FR}. All the other dimensionless variables are constant.

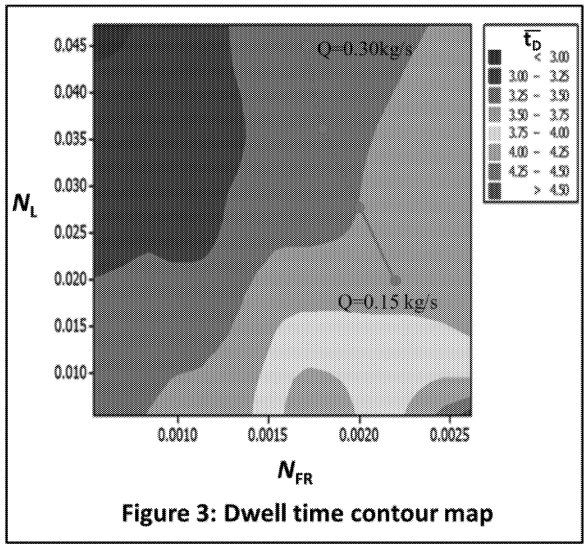

Figure 3: Dwell time contour map

Furthermore, a power law type equation can be fitted to the simulation results to predict the dwell time:

$$t_D\,(\mathrm{s}) = \frac{3.4}{\omega_t} N_{\mathrm{L}}^{-0.135} \cdot N_{\mathrm{FR}}^{0.0787} \qquad (18)$$

As experimental validation is time-consuming and expensive, let's assume that the model has been validated at the pilot scale for a limited number of conditions. In many practical situations, scaling up to commercial scale can be done by pilot-scale testing and simulation techniques. In this example, the goal is to target a commercial product in which the dwell time in the tumbler is 30 seconds; however, the product is twice as big, and that the throughput is at least five times as high as the pilot scale system: t_D= 30s, D_c=7.62cm and $0.15 \le Q_c \le 0.30$ kg/s.

It is reasonable to scale the equipment to be geometrically twice as big as the pilot equipment. One can proceed by building a full scale unit to test (very expensive and time-consuming), or update the computer simulation model with the new geometry (much less expensive, but still time-consuming), or use DA to assess feasibility.

Since the geometric dimensions are scaled twice as big, all the dimensionless geometric factors remain the same and therefore, Eqn. 18 is valid. Substituting the commercial-scale parameters, one can solve for the required N_L and N_{FR} to achieve the required 30 second dwell in the tumbler. The red line in Figure 2 shows the conditions needed at the required range of throughput. The corresponding tumbler rotational speed is shown in Table 1.

Table 1: Throughput vs. tumbler rotational speed

Throughput (kg/s)	Tumbler RPM
0.15	7.2
0.20	6.8
0.25	6.5
0.30	6.3

To confirm the theoretical prediction, one additional simulation has been performed in which the geometry of the system is doubled. The average dwell time was calculated for N_L=0.02 and N_{FR}=0.002 for comparison to the original simulation; results are shown in Table 2.

Table 2: Comparison of throughput for N_L=0.02 and N_{FR}=0.002

Scale	Simulation Average Dwell Time (s)	Simulation Standard Deviation (s)
Pilot	29.5	30.5
Commercial	7.8	6.7

As shown, the dwell time and standard deviation of the simulation at the two different scale are similar, but not identical. This is because the model is written to introduce the spheres into the tumbler at a predefined injection plane (constrained to a certain area) near the inlet. The model then injects spheres at random locations in the plane, and there is some randomness in the number of spheres added per time step - but the model delivers on average the desired throughput. The slight difference between the average dwell time and standard deviation is attributed to the randomness in how the spheres enter the tumbler. Figure 4 shows the histogram of the dwell time in the two simulation runs.

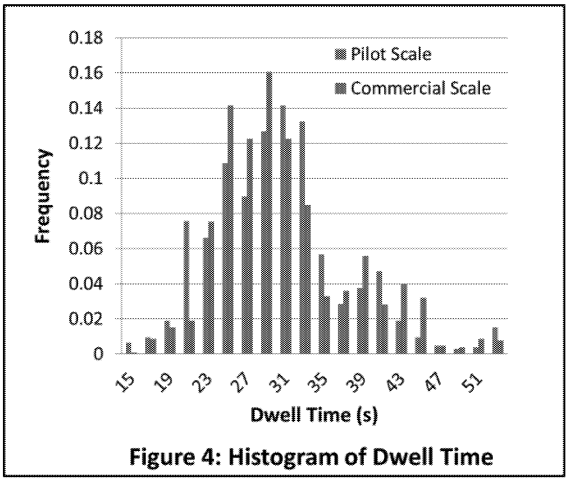

Figure 4: Histogram of Dwell Time

The additional simulation required approximately two engineering hours to modify the simulation model, and eight hours of simulation run time. To recreate the dwell time contour map as shown in Figure 3 for the larger spheres would have added a total of two days of an engineer's time and about two weeks of simulation run time. The use of dimensional analysis can significantly reduce the resource needed in this type of scale-up problems.

CONCLUSIONS

This work discusses the use of the Buckingham-Pi Theorem to augment the traditional approach of computer simulation for the exploration and analysis of new engineering process. Based on the concept of dimensional analysis, the method can provide important insights which can help guide the engineer or scientist in understanding the relevant physics and chemistry of the problem. Furthermore, in many instances, it can not only reduce the number of simulations to ensure optimal usage of experimental resources, but also enhances and provide confidence in scale-up calculations. One food industry scale-up example is shown to highlight the methodology.

REFERENCES

Albrecht, M. C., Nachtsheim, C. J., Albrecht, T. A., & Cook, R. D. (2013). Experimental Design for Engineering Dimensional Analysis. *Technometrics*, 257-270.

Buckingham, E. (1914). On physically similar systems; illustrations of the use of dimensional equations. *Phys. Rev*, 4:345-76.

Camblong, H. e. (2001, November). Quantum anomaly in molecular physics. *Physical Review Letters, 87*, 1-4.

Cheng, H. a. (2008). Expansion of the whole wheat flour extrusion. *Foodsim*, 65-68.

Di Renzo, A., & Di Maio, F. P. (2004). Comparison of contact-force models for the simulation of collisions in DEM-based granular flow codes. *Chemical Engineering Science, 59*, 525-541.

Eddey, E. (1945). Some Engineering Applications of the Buckingham Pi Theorem. *The Ohio State Engineer*.

Evans, J. (1972, December). Dimensionaly Analysis and the Buckingham Pi Theorem. *American Journal of Physics, 40*(12), 1815-1822.

Hughes, S. (1993). *Physical models and laboratory techniques in coastal engineering.* World Scientific.

Islam, M., & Lye, L. M. (2007). Combined use of dimensional analysis and statistical design of experiment methodologies in hydrodynamics experiments. *8th Canadian Marine Hydromechancis and Structures Conference*, (pp. 1-8). St. John's, Newfoundland.

O'Brien, R. (2004). Proceeding of the 2004 American Control Conference., (pp. 3387-3392). Boston.

Rainieri, S. a. (2008). Heat transfer in fluid food processing. In J. (. Cantor, *Progress in Food Engineering Research and Development* (pp. 131-173). Nova Science Publishers, Inc.

Schmidt, R. a. (1995). Problem solving with dimensional analysis. *The Industrial Physicist*, 21-24.

Sonin, A. (2004). A Generalization of the (Pi)-theorem and dimensional analysis. *Proc Natl Acad Sci*, 8525-8526.

Thurairajasingam, E. S. (2002). Modelling of a continuous food pressing process by dimensional analysis. *COmputers & Industrial Engineering*, 343-351.

Vignaux, G. (1992). Dimensional Analysis in Data Modelling. In C. E. Smith, *Maximum Entropy and Bayesian Methods.* Seattle: Kluwer Academic Publishers.

Whitaker, S. (1981). *Introduction to Fluid Mechanics.* Malabar, FL: R.E. Krieger Publishing Company.

Zhu, H., Zhou, Z., Yang, R., & Yu, A. (2007). Discrete particle simulation of particulate systems: theoretical developments. *Chemical Engineering Science*, 3378-3392.

AUTHOR BIOGRAPHIES

CHRIS KOH is Director and PepsiCo Global R&D Fellow, PepsiCo Advanced Research, based in Plano, Texas, U.S.A. Chris received a B.S. from the University of California, Davis, and a Ph.D. from the California Institute of Technology, both in Chemical Engineering. Prior to joining PepsiCo in 2000, Chris was Senior R&D Engineer at Mobil Corporation. Chris' research interests are in the areas of heat, mass and momentum transfer – specifically as applied to food processing. He and his research team leverage fundamental understanding in food chemistry, physics and engineering to develop novel food process technologies. They partner with PepsiCo's development teams worldwide to leverage these technologies to improve the manufacturing of current products and to create new offerings to expand PepsiCo's food portfolio. Email: chris.j.koh@pepsico.com

SEAN EICHENLAUB is a Principal Engineer in PepsiCo Advanced Research, based in Plano, Texas, U.S.A. Sean received a B.S. from the University of Notre Dame and a Ph.D. from Arizona State University, both in Chemical Engineering. Prior to joining PepsiCo in 2010, Sean was a R&D Project Engineer for International SEMATECH. Email: sean.eichenlaub@pepsico.com

EXTENDING A NOVEL CLASS OF PREDICTIVE MODELS TO DESCRIBE THE EFFECT OF pH ON MICROBIAL GROWTH

Simen Akkermans, Estefanía Noriega, Filip Logist, Jan F.M. Van Impe*
CPMF² - Flemish Cluster Predictive Microbiology in Foods – www.cpmf2.be
OPTEC – Centre of Excellence Optimization in Engineering – www.kuleuven.be/optec
BioTeC – Chemical and Biochemical Process Technology and Control – www.cit.kuleuven.be/biotec
Department of Chemical Engineering, KU Leuven
W. de Croylaan 46
B-3001 Leuven, Belgium
*E-mail address: Jan.VanImpe@cit.kuleuven.be

KEYWORDS

Predictive microbiology, secondary modelling, gamma concept, product inhibition.

ABSTRACT

Despite all EU efforts to tackle food poisoning and spoilage, about 5,400 outbreaks and 1.3 billion tons of food waste are reported annually, with a significant impact on EU economy and public health. Modelling and simulation of microbial dynamics as a function of processing, transportation and storage conditions is a useful tool to guarantee food safety and quality. The goal of this research is to improve an existing methodology in order to build accurate predictive models based on multiple environmental conditions. The effect of multiple environmental conditions on microbial dynamics is often described by combining the separate effects in a multiplicative way (gamma concept). This idea was extended further in this work by including the effects of the lag and stationary growth phases on microbial growth rate as independent gamma factors. A mechanistic description of the stationary phase as a function of pH was included, based on a novel class of models that consider product inhibition. Experimental results on *Escherichia coli* growth dynamics indicated that also the parameters of the product inhibition equations can be modelled with the gamma approach. This work has extended a modelling methodology, resulting in predictive models that are (i) mechanistically inspired, (ii) easily identifiable with a limited work load and (iii) easily extendable to additional environmental conditions.

INTRODUCTION

In 2012, 5,363 foodborne outbreaks, causing 5,118 hospitalizations and 41 deaths were reported in the EU. (EFSA and ECDC, 2014). Next to health issues, foodborne outbreaks have a significant economic impact due to productivity losses, marketing campaigns and financial compensations. For instance, the cost of foodborne illness is estimated at £ 1.5 billion and $ 77.7 billion for the UK and USA (UK FSA, 2011; Scharff, 2012). These data show that food safety has a major impact on global economy and public health. Food safety can be improved by studying the effect of food processing, transportation and storage conditions on microbial growth. In predictive microbiology, mathematical models are developed to describe the effect of environmental conditions on microbial dynamics, allowing accurate predictions of microbial behaviour during the complete life-cycle of food products.

In the field of predictive microbiology, a distinction is made between different types of models: (i) primary models describe a microbial response with time for a single set of environmental conditions and (ii) secondary models quantify the effect of environmental conditions on primary model parameters (Whiting and Buchanan, 1993). A typical microbial growth curve described by a primary model includes a lag, exponential and stationary phase of growth. During the stationary phase, the growth rate decreases due to e.g. depletion of a limiting substrate or production of growth-inhibiting metabolites, until the concentration of cells remains constant. Little attention is paid to the description of the stationary phase of growth in predictive microbiology. Many authors argue that only the lag and exponential phase of growth are of importance since many spoilage and pathogenic microorganisms have already caused spoilage or compromised food safety when reaching the stationary phase. However, the growth inhibiting effects during the stationary phase affect the growth rate in a large part of the full growth curve. Additionally, the stationary phase provides e.g. an indication of interactions among species (McMeekin, 2013). Therefore, a better description of the stationary phase will also lead to a better understanding of the microbial growth. Knowledge of these inhibiting effects is even more important in experiments with optical density measurement, since the corresponding cell densities are often much higher than cell concentrations gathered by viable plate counting, and thus, the effect of the stationary phase on microbial growth is much more pronounced. Secondary models including the effects of multiple environmental conditions on the maximum specific growth rate are often built by assuming that these different environmental factors have separate effects. This assumption was first introduced by McMeekin et al. (1987) and later formalized as the gamma hypothesis by Zwietering et al. (1993). This hypothesis allows to build models describing the separate effects of environmental conditions on the maximum specific growth rate. The multiplicative combination of these independent gamma factors results in an expression describing the global effect. The advantage of this approach is that the effect of additional environmental conditions can easily be integrated by adding new factors to an existing model. In several studies, the gamma approach has been acknowledged to successfully describe the combined effect of different environmental conditions on maximum specific growth rate (Wijtzes et al., 1995; Wijtzes et al., 2001; Leroi et al., 2012; Lambert and Bidlas, 2007a; Lambert and Bidlas 2007b). However, other studies suggest that interactions between environmental factors

should be considered at the growth limits (Presser et al., 1998; Augustin and Carlier, 2000; Le Marc et al., 2002; Coroller et al., 2005 and Baka et al., 2013).

The availability of high quality experimental data is decisive for building accurate predictive models, so that an efficient experimental design is essential. During these experiments, it is possible to apply either static or dynamic environmental conditions. With static experiments, a single value for the maximum growth rate can be obtained from every growth curve through independent parameter estimations. These values are subsequently used for the parameter estimation of a secondary model. This approach was for instance implemented by Le Marc et al. (2002) to compose a model based on the gamma concept, which describes the combined effect of temperature, pH and organic acid concentration on the growth rate of *Listeria* spp. Alternatively to static experiments, dynamic experiments offer the possibility to collect more information from a single growth experiment by applying a range of environmental conditions. These dynamic experiments can be combined with optimal experiment design (OED) techniques. The aim of this technique is to collect an optimal amount of information for either parameter estimation or model discrimination. Dynamic experiments were first combined with OED in the field of predictive microbiology by Versyck et al. (1999). The great potential of the combination of dynamic experiments and OED was later confirmed by e.g. Van Derlinden et al. (2010), who designed a single dynamic growth experiment capable of providing sufficient information for an accurate estimation of the cardinal temperatures and optimal growth rate of *E. coli* K12. However, this technique also has limitations. With dynamic experiments, it is often required to combine data from multiple experiments in a single parameter estimation. This may lead to a large number of parameters to be estimated when examining the effect of multiple environmental conditions on the microbial growth rate. The total number of parameters is also high due to many experimental parameters, such as the initial cell density, which are often unknown and should thus be included in the parameter estimation. In the same way, the maximum cell density from the growth model of Baranyi and Roberts (1994) can be included as a separate parameter for every growth curve since it depends on substrate consumption and metabolite production, which are in turn affected by environmental conditions. However, including this empirical value of the maximum cell density in parameter estimations also has drawbacks. At high cell densities during dynamic experiments, growth is inhibited by both the environmental conditions directly and the inhibiting effects of the stationary phase. During a parameter estimation, these effects are hard to distinguish, potentially leading to wrong or inaccurate estimations of the parameters of secondary models.

To identify a full growth model, a modelling strategy with both static and dynamic experiments can be used. (i) In a first step, all environmental conditions should be kept at optimal or reference values during one or more static experiments. This allows the estimation of the optimal growth rate. (ii) Static experiments can be used to investigate the effect of environmental conditions on the lag phase, stationary phase and maximum specific growth. (iii) Using newly gathered, or already existing information on the description of the lag and stationary phase, OED can be used to gather information on the secondary models in an efficient way.

In this paper, the gamma concept will be extended towards primary models, by including the effects of the lag and stationary phase as gamma factors. A more mechanistic description of the stationary phase, based on product inhibition, will also be included in this model. To this end, static experiments are performed at different pH levels with *Escherichia coli* K12. This microorganism is often used as a surrogate for the corresponding pathogenic species, involved, for instance, in a large outbreak in 2011, with 3,816 human cases and 54 deaths (EFSA and ECDC, 2013). The goal of this work is to develop a general modelling approach to build more mechanistic models, which requires a limited amount of experimental effort. This modelling approach will also contribute to the quality of parameter estimations from dynamic experiments.

MATERIAL AND METHODS

Bacterial strain

Escherichia coli K12 MG1655 (CGSC#6300) was acquired from the *E. coli* Genetic Stock Center at Yale University. A stock culture was stored at -80°C in Brain Hearth Infusion broth (BHI, Oxoid), supplemented with 20% (w/v) glycerol (Acros Organics).

Inoculum preparation

The inoculum was prepared in a three step procedure: (i) A 10 µL loopful of the stock culture was spread onto a BHI agar plate, (BHIA, BHI supplemented with 14 g/L technical agar nr. 3, Oxoid) and incubated overnight at 37°C. (ii) Then, a single colony was transferred into a 50 mL Erlenmeyer containing 20 mL BHI and stored at 37°C for 9 h. (iii) Finally, 20 µL of the stationary phase culture was inoculated into 20 mL fresh BHI and incubated at 37°C for 17 h. A 1:800 dilution of this preculture was used to inoculate the bioreactors at about $1.1x10^3$ CFU/mL (or 7 ln(CFU/mL)). The exact volume of preculture to be added to the bioreactor was calculated for each experiment based on the optical density of a 1:10 dilution of the preculture (reference absorbance 0.130 at 600 nm).

Experimental method

Experiments were performed in computer controlled bioreactors (BioFlo 3000, New Brunswick Scientific Inc.). The reactor vessel was filled with 3.5 L BHI. Temperature was controlled at 37°C for all experiments. pH was controlled at different constant values (5.0, 6.0, 7.0, 8.0, 8.5 and 9.0) by addition of acid (1 N H_2SO_4, Sigma-Aldrich) or base (1 N KOH, Thermo Fisher Scientific). The reactor was aerated with filtered air at 2 L/min and stirred at 400 rpm. To avoid foaming, 500 µL of an anti-foaming agent (Y-30 emulsion, Sigma-Aldrich) was added to the bioreactor prior to the experiment. Approximately every hour after inoculation, a sample was taken from the bioreactor and the appropriate dilutions were made in BHI

and plated onto BHIA plates using a spiral plater (Eddy Jet, IUL Instruments s.a.). These plates were incubated at 37°C for about 15 h and then colonies were counted to obtain viable cell numbers (CFU/mL). Experiments lasted between 12 and 36 h.

Models

The primary growth model of Baranyi and Roberts (1994) is often used in predictive microbiology. This model was used here to set a benchmark for the comparison with other models. The equations are written using the natural logarithm of the cell density n [ln(CFU/mL)] and the natural logarithm of the physiological state of the cell q [-]:

$$\frac{dn(t)}{dt} = \mu_{max}(\mathrm{pH}) \cdot \left(\frac{1}{\exp(-q(t)) + 1}\right) \cdot (1 - \exp(n(t) - n_{max}))$$

$$with\ n(t=0) = n_0$$

$$\frac{dq(t)}{dt} = \mu_{max}(\mathrm{pH})$$

$$with\ q(t=0) = q_0$$

where μ_{max} [1/h] is the maximum specific growth rate at a given pH value and n_{max} [ln(CFU/mL)] is the maximum cell density. In this work, a novel class of secondary models is built by combining the effect of pH, lag and stationary phase on the growth rate (gamma factors) with a basic primary model. The gamma factor representing the inhibiting effects of the stationary phase is based on the product inhibition factor of the P-model developed by Van Impe et al. (2005):

$$\frac{dN(t)}{dt} = \mu_{max}(\mathrm{pH}) \cdot \left(\frac{Q(t)}{Q(t)+1}\right) \cdot \left(1 - \frac{P(t)}{K_P}\right) \cdot N(t)$$

$$with\ N(t=0) = N_0$$

$$\frac{dQ(t)}{dt} = \mu_{max}(\mathrm{pH}) \cdot Q(t)$$

$$with\ Q(t=0) = Q_0$$

$$\frac{dP(t)}{dt} = Y_{P/N} \cdot \mu_{max} \cdot \left(\frac{Q(t)}{Q(t)+1}\right) \cdot \left(1 - \frac{P(t)}{K_P}\right) \cdot N(t)$$

$$with\ P(t=0) = 0$$

with N [CFU/mL] the cell density, Q [-] the dimensionless physiological state of the cell, P [M] the concentration of growth inhibiting metabolic products, K_P [M] the maximum concentration of growth inhibiting metabolic products, $Y_{P/N}$ [M/(CFU/mL)] the yield of growth inhibiting metabolic products. This model was chosen since it has an equal quality of fit as the widely used Baranyi and Roberts model, but includes a more mechanistic description of the stationary phase through product inhibition. The assumption was made that no inhibiting product is present in the bioreactor at the beginning of the experiment.

To describe the effect of pH on the maximum specific growth rate $\gamma_{\mu,\mathrm{pH}}(\mathrm{pH})$, the Cardinal pH Model (CPM, Rosso et al., 1995) was used:

$$\mu_{max}(\mathrm{pH}) = \begin{cases} \mathrm{pH} < \mathrm{pH}_{min}, 0 \\ \mathrm{pH}_{min} < \mathrm{pH} < \mathrm{pH}_{max}, \mu_{opt} \cdot \gamma_{\mu,\mathrm{pH}}(\mathrm{pH}) \\ \mathrm{pH} > \mathrm{pH}_{max}, 0 \end{cases} \quad (1)$$

$$\gamma_{\mu,\mathrm{pH}}(\mathrm{pH}) = \frac{(\mathrm{pH} - \mathrm{pH}_{min}) \cdot (\mathrm{pH} - \mathrm{pH}_{max})}{(\mathrm{pH} - \mathrm{pH}_{min}) \cdot (\mathrm{pH} - \mathrm{pH}_{max}) - (\mathrm{pH} - \mathrm{pH}_{opt})^2}$$

with $\gamma_{\mu,\mathrm{pH}}$ [-] the reduction of the maximum specific growth rate due to a deviation from the optimal pH (pH_{opt}) at which the maximum specific growth rate is equal to the optimal growth rate (μ_{opt} [1/h]). pH_{min} and pH_{max} are the limits of the pH range where growth is possible. The CPM model is presumed to be symmetrical, meaning that only two cardinal pH values have to be estimated (here pH_{min} and pH_{opt}).

Parameter estimation and confidence intervals

Model parameters were estimated using the *lsqnonlin* routine of the Optimization Toolbox of Matlab version 7.14 (The Mathworks, inc.). A multistart routine was built to help finding the global minimum of the optimization function. This routine was executed at least 25 times for every parameter estimation. The 95% confidence interval of every parameter p_i was calculated based on the Student's t-distribution:

$$\left[p_i \pm t_{0.975, n_s - n_p} \cdot \sqrt{s^2_{p,i}}\right]$$

where n_s and n_p are respectively the number of samples and the number of parameters and thus $n_s - n_p$ is the number of degrees of freedom. $s^2_{p,i}$ is the variance on the parameters and is found as the main diagonal elements of the variance covariance matrix which is approximated as the inverse of the Fisher Information Matrix (F):

$$F = \frac{1}{MSE} \cdot J^T \cdot J \quad with \quad MSE = \frac{SSE}{n_t - n_p}$$

$$V = F^{-1}$$

$$s^2_{p,i} = V(i,i)$$

with J the Jacobian matrix, MSE the mean sum of squared errors and SSE the sum of squared errors (Walter and Pronzato, 1997). The MSE value is used as an indicator for the goodness of fit.

RESULTS AND DISCUSSION

Effect of pH on the growth of *E. coli* K12

To build the model, a set of six static experiments was performed at different pH values. The results from these experiments are shown in Figure 1 and Figure 2. A typical sigmoidal shape is found for all six growth curves. Figure 1 shows the growth curves in an acidic and neutral environment. These growth curves show that both the maximum specific growth rate and maximum cell density

decrease when the environment becomes more acidic with respect to a neutral environment. Figure 2 shows the growth curves in an alkaline environment. Here, both the maximum specific growth rate and maximum cell density decrease as the environment becomes more alkaline. The growth curves at pH 7.0 in Figure 1 and at pH 8.0 in Figure 2 are very similar regarding maximum specific growth rate and maximum cell density.

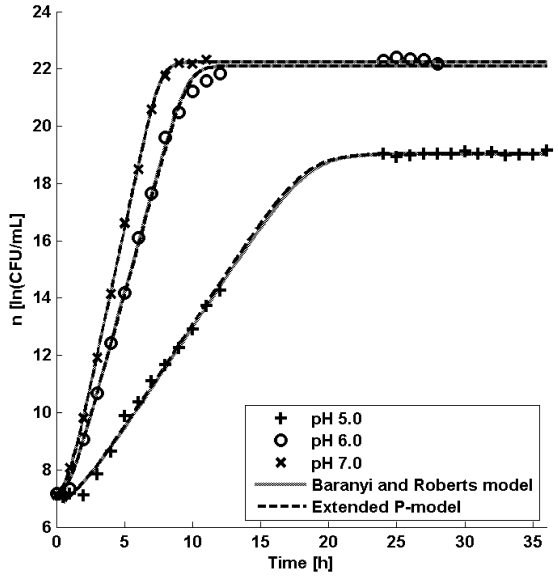

Figure 1: Growth curves from static experiments with E. coli K12 at pH *values of 5.0, 6.0 and 7.0.*

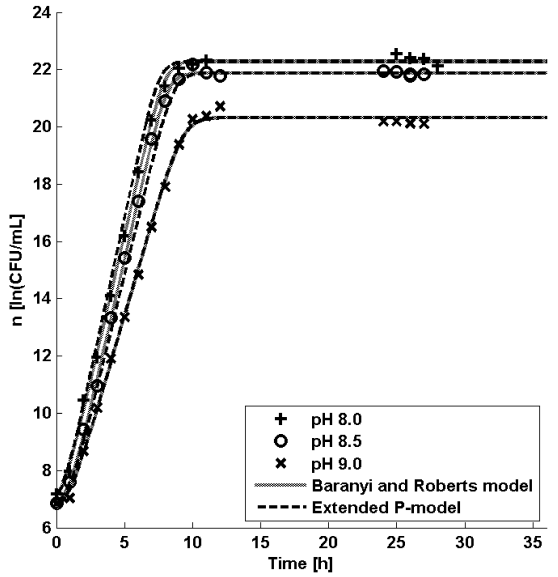

Figure 2: Growth curves from static experiments with E. coli K12 at pH *values of 8.0, 8.5 and 9.0.*

Parameter estimation with Baranyi and Roberts model

As pointed out by Van Impe et al. (2005), the model of Baranyi and Roberts is widely used due to its (i) easy implementation, (ii) applicability under dynamic conditions, (iii) good quality of fit, and (iv) biological interpretability of most of the model parameters. Accordingly, this model is ideal to set a benchmark for a good model fit of the experimental data shown in Figure 1 and Figure 2. In this parameter estimation, different values are estimated for n_i, Q_i, μ_{max} and n_{max} for every experiment, since these parameters are dependent on the environmental conditions. The fit of the Baranyi and Roberts model is shown in Figure 1 and Figure 2. Parameter estimates are listed in Table 1. In Figure 3 and Figure 4, the effect of pH on parameter estimates is illustrated. Since this research focuses on the exponential and stationary phase of the growth curve, the results of μ_{max} and n_{max} are presented here. Both μ_{max} and n_{max} show lower values in more acidic and alkaline environments compared to neutral conditions. This was also described in the previous section, directly from the growth curves. The MSE of this parameter estimation is 0.037.

pH	μ_{max} [1/h]	n_{max} ln(CFU/mL)
5.0	0.71±0.05	19.03±0.09
6.0	1.73±0.06	22.10±0.14
7.0	2.20±0.09	22.24±0.21
8.0	2.05±0.08	22.26±0.15
8.5	2.07±0.08	21.89±0.12
9.0	1.62±0.07	20.33±0.15

Table 1: Parameter estimation values and 95% confidence bound for μ_{max} and n_{max} using the model of Baranyi and Roberts.

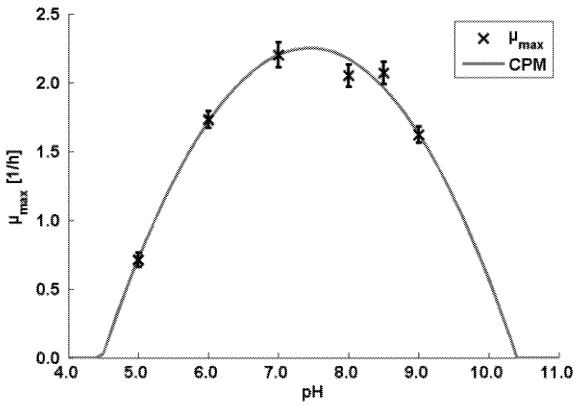

Figure 3: The effect of pH *on the maximum specific growth rate: individual parameter estimates with 95% confidence bounds (symbols) and the fit of the CPM model (continuous line).*

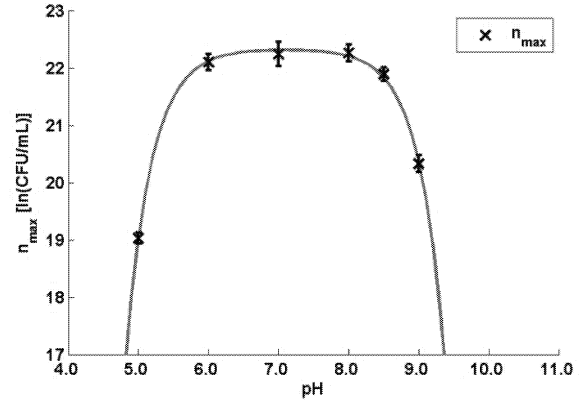

Figure 4: The effect of pH *on the maximum cell density: individual parameter estimates with 95% confidence bounds (symbols) and the expected trend (continuous line).*

Description of the modelling approach

The first step in composing a primary growth model is to start with the following first order differential equation (or the ln-transformed equivalent):

$$\frac{dN(t)}{dt} = \mu(\cdot) \cdot N(t) \quad with\ N(t=0) = N_0$$

or

$$\frac{dn(t)}{dt} = \mu(\cdot) \quad with\ n(t=0) = n_0 \qquad (2)$$

in which $\mu(\cdot)$ [1/h] is the specific growth rate. In this paper, the primary model for the evolution of the cell density with time will not be extended itself to describe the effects of the lag and stationary phase. Instead, the growth inhibiting effects during the lag and stationary phase are described as gamma factors $\gamma_l(\cdot)$ and $\gamma_s(\cdot)$, respectively. These gamma factors are combined with the gamma factor of the CPM model:

$$\mu(\cdot) = \mu_{opt} \cdot \gamma_l(\cdot) \cdot \gamma_{\mu,pH}(\mathrm{pH}) \cdot \gamma_s(\cdot) \qquad (3)$$

The gamma factor, representing the effect of the lag phase on the maximum specific growth rate, is provided with the same structure as the factor describing the lag phase in the model of Baranyi and Roberts. This mechanistically inspired factor is based on Michaelis-Menten kinetics (Baranyi et al., 1993). Consequently, the following definition for the gamma factor $\gamma_l(*)$ and additional differential equation are included in the model:

$$\gamma_l(\cdot) = \frac{1}{1 + \exp(-q(t))} \qquad (4)$$

$$\frac{dq(t)}{dt} = \mu_{max}(\mathrm{pH}) \quad with\ q(t=0) = q_0 \qquad (5)$$

For the dimensionless physiological state of the cell $Q(t)$, the gamma factor is expressed as: $Q(t)/(1+Q(t))$, where $Q(t)$ is an exponentially increasing value. This leads to calculations where two very large values are divided by one another and thus, large numerical errors may occur or even undefined values, if infinity is divided by infinity. These problems are avoided in the above equations by using the natural logarithm of the dimensionless physiological state of the cell $q(t)$.

Next, an equation is required to express the growth inhibiting effects during the stationary phase as a gamma factor. The description of the stationary phase in the Baranyi and Roberts model is based on the logistic model of Verhulst (1838) and is expressed with a maximum carrying capacity, called n_{max} in this instance. However, this maximum carrying capacity is not related to the underlying mechanisms that inhibit growth and is thus an empirical parameter. Van Impe et al. (2005) proposed to use additional equations to describe the consumption of growth-limiting substrates (S-model) and/or the production of growth inhibiting toxic components (P-model). These equations were combined with factors that describe the inhibiting effect of substrate depletion and toxic products on the growth rate, resulting in a more mechanistic model. This modelling technique was successfully applied in Poschet et al. (2005) to make a more complex model describing coculture growth based on lactic acid formation. The structure of the P-model is given in Materials and methods. As a case study, this model will be further extended to incorporate the effect of pH, using the gamma approach. The factor describing the effect of the stationary phase can also be defined as a gamma factor:

$$\gamma_s(\cdot) = \left(1 - \frac{\mathrm{P(t)}}{K_P}\right)$$

$$\frac{dP(t)}{dt} = Y_{\frac{P}{N}} \cdot \mu(\cdot) \cdot \exp(n(t))$$

Since product concentrations were not experimentally determined, these equations are rewritten using the inhibiting product concentration relative to the maximum inhibiting product concentration $p(t)$:

$$\gamma_s(\cdot) = (1 - p(t)) \qquad (6)$$

$$\frac{dp(t)}{dt} = \frac{Y_{\frac{P}{N}}}{\mathrm{K_P}} \cdot \mu(\cdot) \cdot \exp(n(t)) \qquad (7)$$

$$with\ p(t=0) = 0$$

In the equations above, $Y_{\frac{P}{N}}/\mathrm{K_P}$ can be reduced to a single parameter ψ [mL/CFU], which expresses the ratio between the yield of growth inhibiting metabolites $Y_{\frac{P}{N}}$ and the maximum concentration of a growth inhibiting metabolites $\mathrm{K_P}$.

The gamma factor describing the effect of pH on the growth rate is expressed using the CPM model.

Parameter estimation with the extended P-model

A parameter estimation was performed on the full dataset using the model described by Equations (1)-(7). The CPM model was used to express the dependence of the maximum specific growth rate on pH and the parameters pH_{min}, pH_{opt} and μ_{opt} are shown in Table 2. The obtained CPM model is shown in Figure 3. Individual parameters for the yield coefficient ψ were estimated since these are still dependent on the environmental pH. These yield coefficients are inverted and ln-transformed (Table 3) to allow comparison with the description of the stationary phase in the Baranyi and Roberts model through the values of n_{max} (Table 1). Due to the small deviation between the maximum specific growth rates and the CPM model (Figure 3), the MSE value of the extended P-model (0.042) is slightly higher than the MSE value of the Baranyi and Roberts model (0.037). Figure 1 and Figure 2 also clearly show that the extended P-model provides an accurate fit to the experimental data.

Parameter	*Value*
$\mathbf{pH}_{min}$	4.48±0.06
$\mathbf{pH}_{opt}$	7.44±0.05
μ_{opt} **[1/h]**	2.25±0.05

Table 2: Parameter estimation of CPM parameters with 95% confidence bounds.

pH	ln(1/ψ) [ln(mL/CFU)]
5.0	19.03±0.10
6.0	22.11±0.15
7.0	22.24±0.22
8.0	22.25±0.15
8.5	21.89±0.13
9.0	20.32±0.16

Table 3: Parameter estimation of yield coefficients for individual growth curves with 95% confidence bounds.

The obtained parameter ψ, or it's components $Y_{\frac{P}{N}}$ and K_P, have biological meaning and can also be modelled as a function of environmental conditions. This approach has already been performed for e.g.: the effect of pH, substrate and oxygen on lactic acid production (Fu and Mathews, 1999); the effect of temperature and pH on citric acid production (Ambati and Ayyanna, 2001); the effect of temperature and pH on bacteriocin production (Messens et al., 2002 and 2003) and the effect of temperature on ethanol fermentation (Phisalaphong et al., 2006). Most of these models are, however, of an empirical nature. In the general gamma approach, the yield parameter ψ could be expressed as:

$$\psi = \psi_{opt} \cdot \gamma_{\psi,\mathrm{pH}}(\mathrm{pH})$$

where $\gamma_{\psi,\mathrm{pH}}(\mathrm{pH})$ represents the change in production rate of inhibiting product relative to optimal conditions. Similarly to the gamma approach for the maximum specific growth rate, this expression allows several effects to be investigated separately and to be combined afterwards, with or without interactions. Following the assumption of product inhibition with *E. coli* K12, this gamma factor can be built based on experimental data of the metabolite production. The effect could be explained for instance through the presence of different concentrations of undissociated weak acids and bases at different pH values, since these components are responsible for changes in the intracellular pH (Repaske and Adler 1981).

The modelling methodology proposed here has the following benefits: (i) different experiments are performed for the identification of different model parameters to allow for accurate and unambiguous parameter estimations, (ii) the model structures contain general information about microbial behaviour, making them suitable for general use (e.g. properties of the Cardinal Temperature Model from Rosso et al., (1993)) and (iii) models containing the effect of many environmental effects can be built with a limited experimental load.

CONCLUSIONS

In this paper, a modelling methodology is presented to build more mechanistic predictive models with a limited experimental load. As a case study, the P-model was extended to describe the effect of pH on the growth of *E. coli* K12. In this model, the inhibiting effects during the lag and stationary phase are also included as gamma factors along with the CPM model. The effect of the stationary phase on the growth rate was described by a gamma factor that considers product inhibition. A comparison between the extended P-model and the Baranyi and Roberts model revealed that the first one has a good fitting capacity. Based on the new model structure and results from the parameter estimation, it was concluded that the yield of growth inhibiting metabolites and/or the maximum growth inhibiting metabolite concentration are also a function of pH. Consequently, these parameters can also be described with a gamma approach. The results presented in this research contribute to a global modelling methodology that allows to build accurate predictive models with multiple environmental conditions and requires only a limited experimental effort.

ACKNOWLEDGEMENTS

The research was supported by the KU Leuven Research Fund: OT/10/035, PFV/10/002 (Center of Excellence OPTEC-Optimization in Engineering); the Research Foundation Flanders (FWO): FWO KAN2013 1.5.189.13, FWO-G.0930.13 and the Belgian Federal Science Policy Office: IAP VII/19 (DYSCO). Author Jan Van Impe holds the chair Safety Engineering sponsored by the Belgian chemistry and life sciences federation essenscia.

REFERENCES

Ambati, P. and C. Ayyanna. 2001. "Optimizing medium constituents and fermentation conditions for citric acid production from palmyra jaggery using response surface method." *World Journal of Microbiology & Biotechnology*, 17: 331-335.

Augustin, J.C. and V. Carlier. 2000. "Modelling the growth rate of *Listeria monocytogenes* with a multiplicative model including interactions between environmental factors." *International Journal of Food Microbiology*, 56: 53-70.

Baka, M.; E. Van Derlinden; K. Boons; L. Mertens; J.F. Van Impe. 2013. "Impact of pH on the cardinal temperatures of *E. coli* K12: Evaluation of the gamma hypothesis." *Food Control*, 29: 328-335.

Baranyi, J.; T.A. Roberts and P. McClure. 1993. "A non-autonomous differential equation to model bacterial growth." *Food Microbiology*, 10: 43-59.

Baranyi, J. and T.A. Roberts. 1994. "A dynamic approach to predicting bacterial growth in food." *International Journal of Food Microbiology*, 23: 277-294.

Coroller, L.; V. Guerrot; V. Huchet; Y. Le Marc; P. Mafart; D. Sohier; D. Thuault. 2004. "Modelling the influence of single acid and mixture on bacterial growth." *International Journal of Food Microbiology*, 100: 167-178.

EFSA (European Food Safety Authority) and ECDC (European Centre for Disease Prevention and Control). 2013. "The European Union summary report on trends and sources of zoonoses, zoonotic agents and food-borne outbreaks in 2011." *EFSA Journal*, 11: 3129-3378.

EFSA (European Food Safety Authority) and ECDC (European Centre for Disease Prevention and Control). 2014. "The European Union summary report on trends and sources of zoonoses, zoonotic agents and food-borne outbreaks in 2012." *EFSA Journal*, 12: 3547-3758.

Fu, W. and A.P. Mathews. 1999. "Lactic acid production from lactose by *Lactobacillus plantarum*: kinetic model and effects of pH, substrate, and oxygen." *Biochemical Engineering. Journal*, 3: 163-170.

Lambert, R.J.W. and E. Bidlas. 2007a. "An investigation of the Gamma hypothesis: A predictive modelling study of the effect of combined inhibitors (salt, pH and weak acids) on the

growth of *Aeromonas hydophila*." *International Journal of Food Microbiology*, 115: 12-28.

Lambert, R.J.W. and E. Bidlas. 2007b. "A study of the Gamma hypothesis: Predictive modelling of the growth and inhibition of *Enterobacter sakazakii*." *International Journal of Food Microbiology*, 115: 204-213.

Le Marc, Y.; V. Huchet; C.M. Bourgeois; J.P. Guyonnet; P. Mafart and D. Thuault. 2002. "Modelling the growth kinetics of *Listeria* as function of temperature, pH and organic acid concentration." *International Journal of Food Microbiology*, 73: 219-237.

Leroi, F.; P.A. Fall; M.F. Pilet; F. Chevalier; R. Baron. 2012. "Influence of temperature, pH and NaCl concentration on the maximal growth rate of *Brochothrix thermosphacta* and biotective bacteria *Lactococcus piscium* CNCM I-4031." *Food Microbiology*, 31: 222-228.

McMeekin, T.A.; R.E. Chandler; P.E. Doe; C.D. Garland; J. Olley; S. Putro and D.A. Ratkowsky. 1987. "Model for combined effect of temperature and salt concentration/water activity on the growth rate of *Staphylococcus xylosus*." *Journal of Applied Bacteriology*, 62: 543-550.

McMeekin, T.; J. Olley; D. Ratkowsky; R. Corkrey and T. Ross. 2013. "Predictive microbiology theory and application: Is it all about rates?" *Food Control*, 29: 290-299.

Messens, W.; P. Neysens; W. Vansieleghem; J. Vanderhoeven and L. De Vuyst. 2002. "Modeling growth and bacteriocin production by *Lactobacillus amylovorus* DCE 471 in response to temperature and pH values used for sourdough fermentations." *Applied and Environmental Microbiology*, 68: 1413-1435.

Messens, W.; J. Verluyten; F. Leroy and L. De Vuyst. 2003. "Modelling growth and bacteriocin production by *Lactobacillus curvatus* LTH 1174 in response to temperature and pH values used for European sausage fermentation processes." *International Journal of Food Microbiology*, 81: 41-52.

Poschet, F.; K.M. Vereecken; A.H. Geeraerd; B.M. Nicolaï and J.F. Van Impe. 2005. Analysis of a novel class of predictive microbial growth models and application to coculture growth." *International Journal Food of Microbiology*, 100: 107-124.

Presser K.A.; T. Ross and D.A. Ratkowsky. 1998. "Modelling the growth limits 'growth/no growth interface) of *Escherichia coli* as a function of temperature, pH, lactic acid concentration, and water activity." *Applied and Environmental Microbiology*, 64(5): 1773-1779.

Phisalaphong, M.; N. Srirattana and W. Tanthapanichakoon. 2006. "Mathematical modelling to investigate temperature effect on kinetic parameters of ethanol fermentation." *Biochemical Engineering Journal*, 28: 36-43.

Repaske, D.R. and J. Adler. 1981. "Change in intracellular pH of *Escherichia coli* mediates the chemotactic response of certain attractants and repellents." *Journal of Bacteriology*, 145(3): 1196-1208.

Rosso L.; J.R. Lobry and J.P. Flandrois. 1993. "An unexpected correlation between cardinal temperatures of microbial growth highlighted by a new model." *Journal of Theoretical. Biology*, 162: 447-463.

Rosso L.; J.R. Lobry; S. Bajard and J.P. Flandrois. 1995. "Convenient model to describe the combined effect of temperature and pH on microbial growth." *Applied and Environmental Microbiology*, 61(2): 610-616.

Scharff L. 2012. "Economic burden from health losses due to foodborne illness in the United States." *Journal of Food Protection*, 75(1), 123-131.

UK FSA (Food Standards Agency). 2011. "Foodborne disease strategy 2010-15." *UK Food Standards Agency Report*.

Van Derlinden; E., K. Bernaerts and J.F. Van Impe. 2010. "Simultaneous versus sequential optimal experiment design for the identification of multi-parameter microbial growth kinetics as a function of temperature." *Journal of Theoretical Biology*, 264: 347-355.

Van Impe, J.F.; F. Poschet; A.H. Geeraerd and K.M. Vereecken. 2005. "Towards a novel class of predictive microbial growth models." *International Journal of Food Microbiology*, 100: 97-105.

Verhulst, P.F. 1838. "Notice sur la loi que la population suit dans son accroissement." *Correspondance Mathématique et Physique*, 10: 113-121.

Versyck K.J.; K. Bernaerts; A.H. Geeraerd and J.F. Van Impe. 1999. "Introducing optimal experimental design in predictive modelling: A motivating example." *International Journal of Food Microbiology*, 51: 39-51.

Walter, E. and L. Pronzato. 1997. *Identification of parametric models from experimental data.* Springer, Germany, Berlin.

Wijtzes, T.; J.C. De Wit; J.H. Huis in 't Veld; K. van 't Riet; M.H. Zwietering. 1995. "Modelling bacterial growth of *Lactobacillus curvatus* as a function of acidity and temperature." *Applied and Environmental Microbiology*, 61(7): 2533-2539.

Wijtzes, T.; F.M. Rombouts; M.L.T. Kant-Muermans, K. van 't Riet; M.H. Zwietering. 2001. "Development and validation of a combined temperature, water activity, pH model for bacterial growth of *Lactobacillus curvatus*." *International Journal of Food Microbiology*, 63: 57-64.

Whiting, R.C. and R.L. Buchanan. 1993. "A classification of models for predictive microbiology – a reply to K.R. Davey." *Food Microbiology*, 10: 175-177.

Zwietering, M.H.; T. Wijtzes; F.M. Rombouts and K. van 't Riet. 1993. "A decision support system for prediction of microbial spoilage in foods." *Journal of Industrial Microbiology*, 12: 324-329.

An individual-based model for anaerobic dynamics of *Escherichia coli* colonies

Ignace Tack, Filip Logist, Estefanía Noriega Fernández, Jan Van Impe

CPMF^2 - Flemish Cluster Predictive Microbiology in Foods - www.cpmf2.be
OPTEC - Center of Excellence Optimization in Engineering - www.kuleuven.be/optec
BioTeC - Chemical and Biochemical Process Technology and Control - cit.kuleuven.be/biotec,
Department of Chemical Engineering, KU Leuven,
Willem de Croylaan 46 box 2423, B-3001 Leuven, Belgium
E-mail: {ignace.tack|filip.logist|estefania.noriegafernandez|jan.vanimpe}@cit.kuleuven.be

KEYWORDS

predictive microbiology, individual-based modeling, microbial colony dynamics, mixed acid fermentation

ABSTRACT

Traditional models in predictive microbiology describe microbial dynamics in homogeneous liquid food systems. However, most food systems have a semi-solid structure, in which microbial cells grow locally as colonies. Due to the high cell density in these colonies, the environment becomes inhomogeneous as a result of nutrient overconsumption and cell product accumulation.
Hence, the individual cells exhibit strongly different behavior according to their position in the colony. Consequently, an individual-based modeling approach, considering the cell as the basic modeling unit, is most appropriate to describe colony dynamics in full detail. In this paper, an individual-based model is developed for anaerobic colony behavior of *Escherichia coli* K-12. From the simulation, characteristic colony dynamics emerge, such as a linear radius increase. These dynamics result from the pH drop and concomitant cellular stress in the colony center due to accumulation of lactic acid.

INTRODUCTION

In the whole food production and supply chain, accurate assessment and control of microbiological quality and safety are required. In the EU, 5363 foodborne outbreaks were reported in 2012 (EFSA and ECDC, 2014), implying the need for more effective control measures. For this purpose, mathematical models are developed in predictive microbiology to describe and predict microbial behavior as a function of environmental conditions resembling food processing and storage (Buchanan, 1993). Most of these predictive models consider microbial population dynamics in liquid food systems. However, most food products have a semi-solid structure where microorganisms grow locally as colonies.
The relatively high cell density in these colonies induces a local increase in the cellular uptake of organic nutrients (e.g., glucose) and oxygen. Ultimately, the overconsumption of these substrates leads to nutrient depletion due to nutrient diffusion limitations in the food system. Under anaerobic conditions, e.g., in vacuum-packed food products, *E. coli* converts glucose through the mixed acid fermentation process leading to the excretion of weak lipohilic acids into the environment, such as acetic, formic, lactic and succinic acid (Clark, 1989). This local production of weak acids causes a gradual acidification of the colony environment, inhibiting microbial growth (Malakar et al., 2000).

As nutrient and oxygen limitations start in the colony center, individual cells in the colony exhibit different behaviors along the colony radius. Hence, microbial colony dynamics are most appropriately described by a *spatially-explicit individual-based model* (*IbM*) with the cell as the basic modeling unit, in contrast to traditional predictive models considering the global behavior of the microbial population in the whole food medium.

Several IbMs are already available for the description of microbial colony dynamics, e.g., Bacsim (Kreft et al., 1998) and INDISIM (Ginovart et al., 2002). Based on these models, the MICRODIMS IbM for colony behavior has been developed at the KU Leuven/BioTeC research group in user-friendly IbM software toolkits (Verhulst et al., 2011). However, IbMs including the excretion of weak acid metabolites under anaerobic conditions have not been implemented yet.

Therefore, a metabolic model has been developed for anaerobic *E. coli* K-12 MG1655 growth on glucose, since this bacterial strain is frequently applied as a model organism for pathogenic *E. coli* strains in predictive microbiology, an increasing trend of *E. coli* infections is observed in the EU from 2008 to 2012 (EFSA and ECDC, 2014), and due to the abundant information that is available about this organism from systems biology. This metabolic model is subsequently incorporated in MICRODIMS to simulate anaerobic colony behavior of *E. coli*. The relative importance of the glucose depletion and environmental acidification pattern is investigated.

MATERIALS AND METHODS

The extended version of MICRODIMS is described by means of the *ODD* protocol of Grimm et al. (2010).

Overview

Purpose
The aim of this model is to describe a two-dimensional monolayer colony of *Escherichia coli* K-12 MG1655 in a homogeneous gel medium under anaerobic conditions. More specifically, the growth-limiting effects of glucose depletion and weak acid accumulation are compared.

Entities, state variables and scales
The simulation contains two types of entities: microbial cells and their environment.
In the graphical display, cells are represented as a disk. Each individual cell is defined by its radius, mass, spatial coordinates, and maximum specific glucose uptake rate. A list variable stores the progress of ongoing DNA replication cycles, according to the cell reproduction model of Cooper and Helmstetter (1968). Finally, the cell color indicates the cell activity level; growing microorganisms are green, starving cells are shrinking and turn red.
The two-dimensional environment represents a 200 μm x 200 μm section of a 200 μm thick gel system, discretized in equally-sized square units. These square patches are characterized by their glucose, acetate, formate and lactate concentration. The pH value in the environmental unit is defined by the weak acid concentrations. As the simulation of local acidification and cellular glucose competition is the primary goal of the IbM, the patch dimension is selected to be in the same order of magnitude as the cell size, viz., 2 μm (Kreft et al., 1998).

Process overview and scheduling
The IbM contains four process categories: intracellular processes, intercellular interactions, interactions between the cell and its surrounding medium, and diffusion processes in the medium.
Cell growth and maintenance, DNA replication and cell division, and cell starvation are intracellular processes. Due to the high cell density in a colony, biomass growth causes pressure between the colony organisms or, equivalently, spatial overlap of neighboring cell disks in the simulation, which is relieved by cell shoving. In order to sustain growth and other active intracellular processes, cells take up glucose from the surrounding medium. Under anaerobic conditions, this glucose consumption leads to the release of acid metabolites into the environment. Local glucose uptake and metabolite excretion result in concentration gradients and diffusion of these substances in the medium.
In the process schedule, i.e., the order in which the aforementioned processes are executed, two time resolutions are applied: a smaller time step Δt_1 of 0.0005 min for processes with fast dynamics (i.e., diffusion, glucose uptake, cell growth and maintenance, and metabolite excretion) and a larger time step Δt_2 of 0.1 min for cellular functions with slower dynamics (cell reproduction and shoving). The slow processes are executed as follows: firstly DNA replication and cell division, and secondly cell shoving. During a large time step, the fast cellular processes are completed 200 times in a logical order: glucose uptake, cell growth, maintenance and starvation, and lastly the release of weak acids to the environment. Each small time step, the order in which the microorganisms execute their actions, is shuffled to avoid favoritism with respect to nutrient uptake. Finally, the diffusion process levels glucose and weak acid concentration gradients caused by nutrient uptake and metabolite excretion.

Design concepts

Interaction
Glucose depletion results in intercellular nutrient competition. Metabolic production of weak acids involves an environmental stress condition for microbial cell growth.
Apart from these two cellular interactions mediated by the surrounding medium, the simulated microorganisms interact in a more direct way by repelling each other in case of spatial overlap.

Emergence
It is observed when and to which extent cell starvation emerges from the simulation due to glucose overconsumption and the presence of weak acids in the colony center. Due to cell starvation in the colony center, the increase of the colony radius slows down.

Sensing
When the cell is starving, the progress of all ongoing DNA replication and cell division cycles is inhibited to prevent detrimental cell reproduction leading to inviably small cells. Hence, it is important that the microbial cell senses the glucose and weak acid concentrations in the environment to stop its reproduction processes in time. In addition, the cell is able to detect overlap with its neighbors in support of the cell shoving mechanism.

Stochasticity
The IbM includes two stochasticity sources: the direction in which daughter cells are positioned after cell division, and a stochastic element on the maximum specific glucose uptake rate of the cells to take into account cell variability and growth asynchrony.

Observation
To validate the model against observations and experimental data in literature, the evolution of the colony radius is set out in a time chart. The colony radius is defined as the distance between the center of the square environment, where the inoculum cell is situated, and the microorganism furthest away from this position.

Secondly, the total cell number and the share of starving cells is monitored in a time graph. A third type of time graps illustrates the evolution of glucose concentration, pH and weak acid concentrations in the center of the environment. From these time plots, the dynamics and causes of the cell starvation zone in the colony center are inferred.
Finally, the local glucose depletion and acidification patterns, and concomitant cell starvation are presented in graphical displays presenting the environmental pH, and glucose or weak acid concentrations.

Details

Initialization
At the start of the simulation, one cell is positioned in the center of the environment. This inoculum cell has an initial mass equal to the cell mass required to initiate DNA replication. The environment has a homogeneous initial glucose concentration $C_{S,init}$ of 1.0 g/L or $5.56{\cdot}10^{-3}$ mol/L. Initially, the food system does not contain any acid substances or oxygen.

Boundary conditions
The environment is characterized by Dirichlet boundary conditions, i.e., at the environmental boundaries, the glucose and weak acid concentrations are held constant at their initial value. This implies that the environment is surrounded by an infinitely large glucose reservoir or metabolite sink without diffusion limitations.

Submodels

Glucose consumption. Cellular glucose uptake from the environment is assumed to follow Monod kinetics:

$$-\frac{\Delta S^k_{(i,j)}}{\Delta t_1} = v^k_S = q^k_{S,max} \cdot \frac{C_{S,(i,j)}}{K_S + C_{S,(i,j)}} \cdot X^k \qquad (1)$$

In this formula, $C_{S,(i,j)}$ [mol/L] is the glucose concentration of the environmental unit with coordinates (i,j) in which the cell is situated, $\Delta S^k_{(i,j)}$ [mol] the glucose uptake by cell k from its environment, K_S [mol/L] the Monod half-saturation constant, v^k_S [mol/min] the glucose uptake rate of cell k, $q^k_{S,max}$ $\left[\frac{\text{mol}}{\text{gDW}\cdot\text{min}}\right]$ the maximum specific glucose uptake rate, and X^k [gDW] the cell mass. If the glucose amount in environmental unit (i,j) is smaller than $\Delta S^k_{(i,j)}$, the nutrient uptake reduces to the available amount of glucose.
To take asynchrony in cell growth and division into account, the maximum specific glucose consumption rate of a cell is composed of a deterministic and a normally-distributed stochastic part:

$$q^k_{S,max} = q^m_{S,max} \cdot (1 + CV) \qquad (2)$$

with $q^m_{S,max}$ the mean maximum specific glucose uptake rate over all the cells, and CV [-] the coefficient of variation of the maximum specific glucose consumption rate. Numerical values for the parameters in the nutrient uptake process are included in Table 1.

Cell growth and maintenance. Consumed glucose is in the first place employed to meet maintenance requirements, and secondly to support cell growth and reproduction. The specific glucose uptake rate q_S is linked to the cellular maintenance needs and microbial growth according to the model of Schulze and Lipe (1964):

$$q_S = \frac{\mu}{Y_{X/S}} + m_S, \qquad (3)$$

with μ [min^{-1}] the specific cellular growth rate, $Y_{X/S}$ [gDW/mol] the theoretical cell yield coefficient on glucose, and m_S $\left[\frac{\text{mol}}{\text{gDW}\cdot\text{min}}\right]$ the maintenance coefficient. This leads to the following expression for the biomass growth rate of cell k:

$$\frac{\Delta X^k}{\Delta t_1} = \mu^k \cdot X^k = (q^k_S - m_S) \cdot Y_{X/S} \cdot X^k. \qquad (4)$$

The maintenance and biomass yield coefficient depend on the intracellular metabolic flux distribution. Under anaerobic conditions, energy is generated as ATP by conducting glucose through the glycolytic pathway to pyruvate (see Figure 1). Subsequently, depending on the environmental pH, pyruvate is converted to lactic acid, or acetyl-CoA and formic acid. At low pH, cells exhibit a homolactic metabolism mediated by the lactate dehydrogenase (LDH) enzyme, while acetyl-CoA and formic acid are mainly produced through pyruvate formate lyase (PFL) at neutral or higher pH values, as illustrated in Figure 2. Hence, the maintenance and cell yield coefficient are expressed as a linear combination of these coefficients under both metabolic regimes:

$$Y_{X/S} = \alpha \cdot Y^{LDH}_{X/S} + (1-\alpha) \cdot Y^{PFL}_{X/S}, \qquad (5)$$

$$m_S = \alpha \cdot m^{LDH}_S + (1-\alpha) \cdot m^{PFL}_S, \qquad (6)$$

$$\alpha = \frac{1}{1 + \exp(1.9547 \cdot (pH - 5.7809))}, \qquad (7)$$

with α the normalized version of the sigmoid function in Figure 2. The biomass yield coefficient of the PFL metabolism $Y^{PFL}_{X/S}$ is derived by means of a flux balance analysis (FBA) with the `iAF1260` metabolic model of Feist et al. (2007) in the COBRA toolbox for MATLAB® (Becker et al., 2007). For the LDH metabolism, the biomass coefficient $Y^{LDH}_{X/S}$ is obtained by eliminating the PFL reaction in the `iAF1260` model. The production of succinic acid from phosphoenolpyruvate (PEP), depicted in Figure 1, and its concomitant influence on the biomass yield coefficient is not taken into account, as it is negligible with respect to the excretion of the other acid metabolites for wild type *E. coli* strains (Stokes, 1949; Clark, 1989).

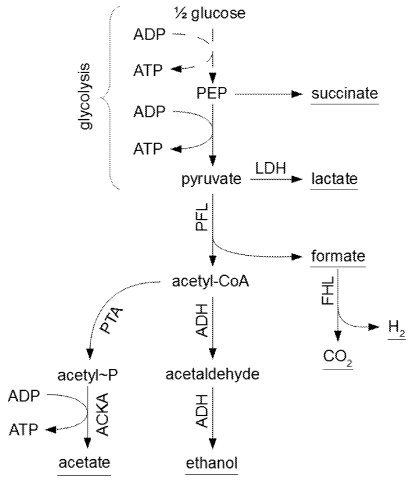

Figure 1: Anaerobic metabolism of *E. coli*. Glucose is converted to phosphoenolpyruvate (PEP) and pyruvate through glycolysis. From PEP and pyruvate, metabolic products are formed in reactions catalyzed by lactate dehydrogenase (LDH), pyruvate formate lyase (PFL), phosphotransacetylase (PTA), acetate kinase (ACKA), alcohol dehydrogenase (ADH), and formate hydrogen lyase (FHL). The underlined metabolic products are excreted to the environment.

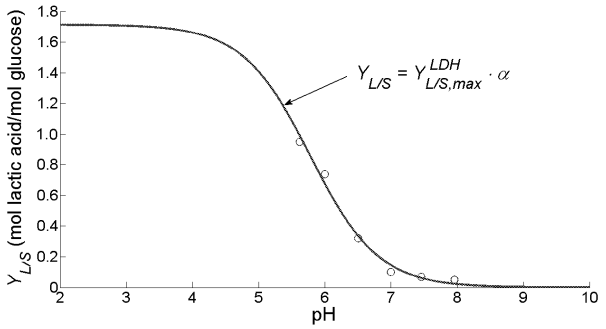

Figure 2: Lactic acid yield coefficient $Y_{L/S}$ fitted as a sigmoid function of pH (MSSE = 0.0022). Experimental data (○) are taken from Stokes (1949). The maximum lactic acid yield $Y^{LDH}_{L/S,max}$in the homolactic LDH metabolic regime at low pH values is determined by means of an FBA analysis with the `iAF1260` metabolic model (Feist et al., 2007) in the COBRA toolbox for MATLAB (Becker et al., 2007).

The cellular maintenance requirements are influenced by the environmental pH and the presence of weak lipophilic acids. Decreasing pH values have an inhibitory influence on cell growth, proportional to the extracellular hydrogen ion concentration (Cole et al., 1990). Weak organic acids exhibit an additional growth-restrictive effect, principally in their undissociated form (Eklund, 1989). The lipophilic undissociated acid enters through the cell membrane, and disturbs the intracellular pH by dissociation. It is hypothesized that growth inhibition by weak acids is linearly dependent on the undissociated acid concentration, similar to the aforementioned proton effect. Therefore, the maintenance coefficient in both the LDH- or PFL-mediated metabolism is expressed as

$$m^*_S = m^*_{S,ref} + A^* \cdot \frac{[H^+] - 10^{-7}}{[H^+_{min}] - 10^{-7}} + B^* \cdot \sum_i \frac{[U_i]}{[U_{i,min}]}. \tag{8}$$

In this formula, the maintenance coefficient consists of three terms: (*i*) the reference maintenance coefficient $m^*_{S,ref}$ in a medium at neutral pH and without weak acids, (*ii*) supplementary maintenance requirements due to increasing extracellular proton concentrations $[H^+]$, and (*iii*) an additional maintenance term taking the effect of undissociated weak acids $[U_i]$ into account. The coefficients A^* are calculated by filling in this general maintenance coefficient definition in Equation 4, and considering the specific case of a glucose-rich food system free of weak acids in which the proton concentration is equal to the minimimal hydrogen ion concentration inhibiting cell growth, $[H^+_{min}]$:

$$\begin{aligned} 0 &= (q^m_{S,max} - m^*_{S,ref} - A^*) \cdot Y^*_{X/S} \\ &\Rightarrow A^* = q^m_{S,max} - m^*_{S,ref}. \end{aligned} \tag{9}$$

In a similar way, the coefficients B^* are calculable from the minimum inhibition concentration of undissociated acetic, formic and lactic acid, $[U_{i,min}]$, experimentally measured by Östling and Lindgren (1993).

Metabolite excretion. Figure 1 illustrates how glycolytic pyruvate is converted to excreted metabolites. At low pH values, formic acid is decomposed to water and carbon dioxide before excretion by means of the formate hydrogen lyase (FHL) complex. However, in the pH range from 6.0 to 7.5, the stability of the formate dehydrogenase FDH_H component of the FHL complex reduces drastically (Axley et al., 1990). In Figure 3, the fraction of decomposed formic acid β is depicted as a sigmoid function of pH:

$$\beta = \frac{1}{1 + \exp(11.3021 \cdot (pH - 6.3133))}. \tag{10}$$

On the basis of the sigmoid functions α and β, mathematical expression for the specific metabolite excretion rates are derived:

$$q_A = (1-\alpha) \cdot \left(Y^{PFL}_{A/S} \cdot q_S + \frac{m^{PFL}_S}{m^{PFL}_{S,ref}} \cdot q_{A,ref}|_{q_S=0} \right), \tag{11}$$

$$q_F = (1-\beta) \cdot (1-\alpha) \cdot \left(Y^{PFL}_{F/S} \cdot q_S + \frac{m^{PFL}_S}{m^{PFL}_{S,ref}} \cdot q_{F,ref}|_{q_S=0} \right), \tag{12}$$

$$q_L = \alpha \cdot \left(Y^{LDH}_{L/S} \cdot q_S + \frac{m^{LDH}_S}{m^{LDH}_{S,ref}} \cdot q_{L,ref}|_{q_S=0} \right), \tag{13}$$

with q_A, q_F, and q_L the specific production rates of acetic, formic, and lactic acid, respectively. These specific excretion rates are linked to the specific glucose uptake rate, q_s, by the maximum production yield coefficients of the excreted metabolites, $Y^*_{i/S}$, in the respective metabolite production regime. Reference specific excretion rates at zero glucose concentration, $q_{i,ref}|_{q_S=0}$, are obtained from flux balance analyses in the COBRA toolbox. Values for these parameters are included in Table 1.

Cell starvation. Microbial cells starve when their maintenance requirements are not met and, consequently, their specific growth rate is negative. Cell division and DNA replication processes, addressed in one of the next paragraphs, stop progressing in starving cells.

Diffusion. Diffusion of glucose and acid metabolites through the isotropic food medium is modeled by means of the second law of Fick in two dimensions:

$$\frac{\partial C_i}{\partial t} = \mathcal{D}_i \cdot \left(\frac{\partial^2 C_i}{\partial x^2} + \frac{\partial^2 C_i}{\partial y^2} \right), \tag{14}$$

with C_i [g/L] the concentration of substance i, $\mathcal{D}_i$ [μm^2/min] the diffusion coefficient of substance i in the food system, x [μm] and y [μm] the spatial dimensions, and t [min] the temporal dimension.
This partial differential equation does not have an analytical solution for the applied initial and boundary conditions. Therefore, Equation (14) is discretized according to the Alternating Direction Implicit (ADI) scheme of Peaceman and Rachford (1955), in order to solve the PDE numerically as a difference equation by means of the computationally efficient Thomas algorithm (Thomas, 1949).
The diffusion coefficients $\mathcal{D}_i$ are influenced by the gel matrix structure. At a temperature of 37°C, the diffusion coefficient of glucose in a 5% (w/w) agarose gel has a value of $6.7925 \cdot 10^{-10}$ m^2/s or 40755 μm^2/min (Andersson and Öste, 1994), approximately 75% of the glucose diffusivity in water at the same temperature. Diffusivities of acetic, formic and lactic acid are included in Table 1.

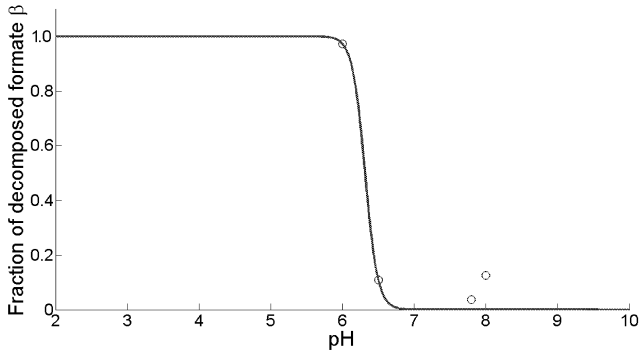

Figure 3: Fraction of decomposed formic acid β fit as a function of pH (MSSE = 0.0085). Experimental data ($\circ$) are taken from Blackwood et al. (1956), Higgins and Johnson (1970), and Karel and Robertson (1989).

Updating the environmental pH. In an environmental unit, the pH is determined by the concentration of weak acids. The hydrogen ion concentration is equal to the sum of the dissociated acid molarities $[D_i]$ and hydroxyl concentration. Using the definitions of the acid and water dissociation constants, $K_{a,i}$ and K_w,

$$K_{a,i} = \frac{[H^+] \cdot [D_i]}{[U_i]} = 10^{-pK_{a,i}}, \tag{15}$$

$$K_w = [H^+] \cdot [OH^-], \tag{16}$$

this leads to the following quintic equation for the proton concentration:

$$[H^+]^5 + a \cdot [H^+]^4 + b \cdot [H^+]^3 + c \cdot [H^+]^2 + d \cdot [H^+] + e = 0, \tag{17}$$

with the coefficients

$$a = K_{a,A} + K_{a,F} + K_{a,L}, \tag{18}$$

$$b = K_{a,A} \cdot (K_{a,F} - [A]) + K_{a,F} \cdot (K_{a,L} - [F]) + K_{a,L} \cdot (K_{a,A} - [L]) - K_w, \tag{19}$$

$$c = K_{a,A} \cdot K_{a,F} \cdot K_{a,L} - K_{a,A} \cdot ((K_{a,F} + K_{a,L}) \cdot [A] + K_w) - K_{a,F} \cdot ((K_{a,A} + K_{a,L}) \cdot [F] + K_w) - K_{a,L} \cdot ((K_{a,A} + K_{a,F}) \cdot [L] + K_w), \tag{20}$$

$$d = -K_{a,F} \cdot K_{a,L} \cdot (K_{a,A} \cdot [A] + K_w) - K_{a,A} \cdot K_{a,L} \cdot (K_{a,F} \cdot [F] + K_w) - K_{a,A} \cdot K_{a,F} \cdot (K_{a,L} \cdot [L] + K_w), \tag{21}$$

$$e = -K_{a,A} \cdot K_{a,F} \cdot K_{a,L} \cdot K_w, \tag{22}$$

where $[A]$, $[F]$, and $[L]$ are the total concentration of acetic, formic and lactic acid in both dissociated and undissociated form. Equation (17) is solved by means of Halley's method. This iterative algorithm is initialized with a value $[H^+]_0$ of 0.01 mol/L in order to ensure that the algorithm converges to the largest root of the quintic equation, which is the real proton concentration.

DNA replication and cell division. The cell generation cycle consists of two or three stages: (*i*) the *C*-phase in which the cellular DNA is replicated, (*ii*) the *D*-phase between the completion of DNA replication and cell division in two equally large daughter cells, and (*iii*) a possible *B*-phase between cell birth and initiation of DNA replication in the daughter cells. In Figure 4, the duration of the $C + D$-period [min] is fitted as a function of the specific cellular growth rate:

$$C+D = \begin{cases} 3.50 \cdot (\mu^k)^{-0.658} \\ \qquad \text{for } 0 \text{ min} < \mu^k \leq 0.011 \text{ min} \\ 67.92 \quad \text{for } \mu^k > 0.011 \text{ min} \end{cases} \tag{23}$$

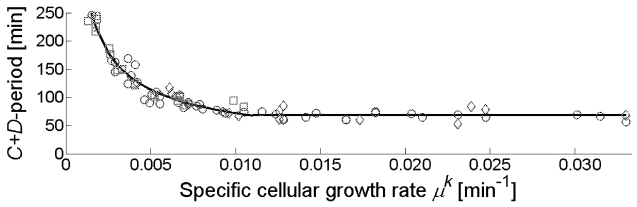

Figure 4: $C+D$-period fitted as a function of the specific cellular growth rate μ^k (MSSE = 13.93 min^2). Symbols represent batch data for *E. coli* K-12 listed in Table 3 of Michelsen et al. (2003) (○), chemostat data from Table 4 in Michelsen et al. (2003) (□), and *E. coli* K-12 data selected from Table 1 in Helmstetter (1996) (◇).

The C-phase is initiated at a critical ratio X^c [gDW] of the cell mass to the number of ongoing DNA replication rounds (Donachie, 1968). Consequently, cell masses at which the DNA replication is initiated, are

$$\begin{aligned} \frac{X_{init}}{n_i} &= X^c \\ \Rightarrow X_{init} &= X^c \cdot n_i \\ &= X^c \cdot 2^j \quad \text{with } j = 0, 1, 2, ... \end{aligned} \tag{24}$$

The critical initiation ratio is derived from the mean cell mass at division X_D^m [gDW] in exponentially growing cultures (Dens et al., 2005):

$$\begin{aligned} & X_D^m(\mu^m) = X^C \cdot \exp(\mu^m \cdot (C+D)) \\ \Rightarrow \quad & X^C = \frac{2 \cdot X_B^m}{\exp(\mu^m \cdot (C+D))} = \frac{2 \cdot \rho_{DW} \cdot V^m}{Z \cdot \exp(\mu^m \cdot (C+D))}, \end{aligned} \tag{25}$$

with, V^m [L] the mean cell volume, X_B^m [gDW] the mean cell mass at birth, ρ_{DW} [gDW/L] the density of dry biomass, and Z [-] the ratio of the mean cell mass to the mean cell mass at birth. This Z ratio has a value of 1.377 for cells with a specific growth rate CV of 0.10 (Koch, 1993).
Wold et al. (1994) observed a linear decrease of X^C as a function of the mean specific growth rate:

$$X^C(\mu^m) = E - F \cdot \mu^m, \text{ or} \tag{26}$$

$$V^m(\mu^m) = \frac{Z \cdot \exp(\mu^m \cdot (C+D))}{2 \cdot \rho_{DW}} \cdot (E - F \cdot \mu^m). \tag{27}$$

The E and F constants are determined by fitting Equation (27) to the mean cell volume data of Volkmer and Heinemann (2011) as a function of specific growth rate: E = 610.7 fgDW and F = 8315.1 fgDW · min.

Cell shoving. Cellular movements are hindered due to the structure of the food system. On the other hand, due to biomass growth, an outward pressure emerges in the colony as cells avoid spatial overlap. This pressure is relaxed by cell shoving. In the cell shoving mechanism, the vector sum of all positive overlap radii with neighboring microorganisms is calculated

Symbol	Value	Reference
ρ_{DW}	301.6 gDW/L	Godin et al. (2007)
CV	0.10	Koch (1993)
$\mathcal{D}_A$	7092.7 μm^2/min	Azevedo and Oliveira (1995)
$\mathcal{D}_F$	1.17 * $\mathcal{D}_A$	Cussler (1984)
$\mathcal{D}_L$	5101.4 μm^2/min	(Øyaas et al., 1995)
$\mathcal{D}_S$	4075.5 μm^2/min	Andersson and Öste (1994)
$[H^+_{min}]$	$10^{-3.95}$ mol/L	Baka et al. (2013)
K_S	$2.994 \cdot 10^{-6}$ mol/L	Ihssen et al. (2007)
$m_{S,ref}^{LDH}$	$6.992 \cdot 10^{-5}$ $\frac{\text{mol}}{\text{gDW} \cdot \text{min}}$	iAF1260 model
$m_{S,ref}^{PFL}$	$5.085 \cdot 10^{-5}$ $\frac{\text{mol}}{\text{gDW} \cdot \text{min}}$	iAF1260 model
$pK_{a,A}$	4.756	Speight (2005)
$pK_{a,F}$	3.751	Speight (2005)
$pK_{a,L}$	3.858	Speight (2005)
pK_w	13.64	Speight (2005)
$q_{A,ref}\|_{q_S=0}$	$1.529 \cdot 10^{-5}$ $\frac{\text{mol}}{\text{gDW} \cdot \text{min}}$	iAF1260 model
$q_{F,ref}\|_{q_S=0}$	$1.012 \cdot 10^{-5}$ $\frac{\text{mol}}{\text{gDW} \cdot \text{min}}$	iAF1260 model
$q_{L,ref}\|_{q_S=0}$	$2.007 \cdot 10^{-5}$ $\frac{\text{mol}}{\text{gDW} \cdot \text{min}}$	iAF1260 model
$q_{S,max}^m$	$17.3 \cdot 10^{-3}$ mol/L	Portnoy et al. (2010)
s	1.3	Kreft et al. (1998)
$U_{A,min}$	$6.25 \cdot 10^{-3}$ mol/L	Östling and Lindgren (1993)
$U_{F,min}$	$1.075 \cdot 10^{-3}$ mol/L	Östling and Lindgren (1993)
$U_{L,min}$	$4.75 \cdot 10^{-3}$ mol/L	Östling and Lindgren (1993)
$Y_{L/S}^{LDH}$	1.713 mol/mol	iAF1260 model
$Y_{X/S}^{LDH}$	19.465 gDW/mol	iAF1260 model
$Y_{A/S}^{PFL}$	0.801 mol/mol	iAF1260 model
$Y_{F/S}^{PFL}$	1.699 mol/mol	iAF1260 model
$Y_{X/S}^{PFL}$	27.075 gDW/mol	iAF1260 model
Z	1.377	Koch (1993)

Table 1: Parameter values for the IbM simulation

for each cell. The overlap radius r_o [μm] of a cell with a neighboring organism is defined as

$$r_o = s \cdot r_k + r_n - d, \tag{28}$$

with r_k [m] and r_n [μm] the radius of cell k and its neighbor n, d [μm] the distance between the centers of these two cells, and s [-] a factor to obtain realistic minimum distances between neighboring cells in the simulation.

Software

MICRODIMS is implemented in Java with the Repast Simphony software toolkit (North et al., 2013). Repast S is selected over other software toolkits for its simulation speed, and because Java provides efficient array structures and for-loops to iterate over array elements. These features are required for an efficient implementation of the ADI diffusion scheme with the Thomas algorithm.

RESULTS AND DISCUSSION

Cell growth inhibition in colony center

In the colony center, cell growth is inhibited by glucose depletion or environmental acidification. From the IbM simulation, it is concluded that the pH drop in the colony center is the determining growth-limiting factor and that glucose depletion is negligible under anaerobic conditions, as illustrated in Figures 5 and 6. Figure 7 shows that this pH decline is induced by the excretion of lactic acid, while the accumulation of acetic and formic acid is insignificant. However, the minimum inhibitory concentration of undissociated lactic acid is not reached. The growth-limiting pH effect starts to get important around t = 25 h, when the first starving (red) cell emerges from the simulation (see Figure 8).

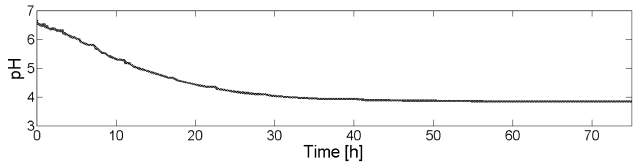

Figure 5: pH drop in the center of the environment.

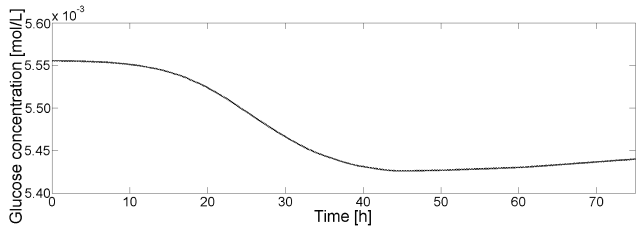

Figure 6: Glucose availability in the environment center is nearly constant over time.

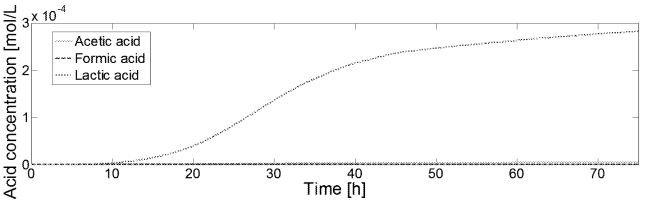

Figure 7: Presence of weak acids in the environment center over time.

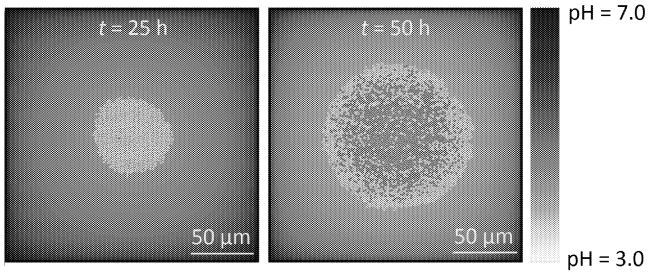

Figure 8: Emergence of a cell starvation zone in the colony center due to environmental acidification.

Colony growth

The acidification of the colony center has implications on the colony dynamics. Firstly, cell starvation emerges and spreads, mainly in the colony center, as presented in Figure 8. In general, cells are growing faster at the colony boundary. Figure 9 depicts that the number of growing cells stays more or less constant after the emergence of cell starvation.

Secondly, Figure 10 demonstrates that the colony radius growth consists of three phases: a superlinear phase at the start of the simulation (I), a linear phase after the growth-limiting effect of decreasing pH and cell starvation become significant (III), and a transition phase between both (II). The transition phase begins

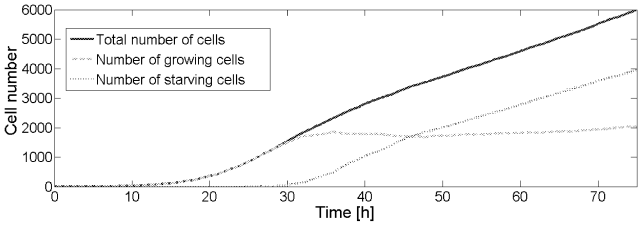

Figure 9: Evolution of the cell number.

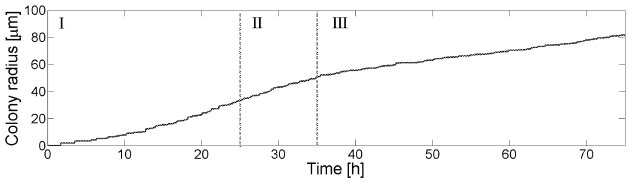

Figure 10: Three-phase colony radius dynamics: superlinear phase (I), transition (II), and linear phase (III).

when the first starving cell emerges around $t = 25$ h (Figures 8 and 10). This simulated colony radius evolution has been experimentally observed by Mitchell and Wimpenny (1997).

CONCLUSION

An individual-based model (IbM) has been developed to describe the dynamics of anaerobic monolayer colonies. Colony dynamics are qualitatively reproduced, such as the linear radius increase and emergence of a starvation zone in the center. The IbM demonstrates that these phenomena are caused by the pH decrease in the colony center due to the cellular excretion of lactic acid. Hence, this IbM is a first step in the simulation of surface colony dynamics on vacuum-packed food products.

The general merit of individual-based modeling in predictive microbiology is the elucidation of experimentally observed colony behavior in terms of cell physiological mechanisms and interactions. Incorporation of this knowledge in classical differential equation models for colony growth will allow rapid and more accurate assessments of microbiological quality and safety in structured food systems.

ACKNOWLEDGEMENTS

The research of I. Tack is funded by Ph.D. grant IWT SB-111565 of the Agency for Innovation by Science and Technology (IWT). In addition, this work is supported by projects FWO-G.0930.13 and FWO KAN2013 1.5.189.13 of the Research Foundation - Flanders (FWO), project PFV/10/002 (Center of Excellence OPTEC-Optimization in Engineering) of the KU Leuven Research Fund, Knowledge Platform KP/09/005 (SCORES4CHEM) of the KU Leuven Industrial Research Fund, and the Belgian Program on Interuniversity Poles of Attraction, initiated by the Belgian Federal Science Policy Office (IAP Phase VII - 19 DYSCO). J. Van Impe holds the chair Safety Engineering sponsored by the Belgian chemistry and life sciences federation essenscia.

REFERENCES

Andersson, A. P. and Öste, R. E. (1994). Diffusivity data of an artificial food system. *Journal of Food Engineering*, 23:631–639.

Axley, M. J., Grahame, D. A., and Stadtman, T. C. (1990). *Escherichia coli* formate-hydrogen lyase. Purification and properties of the selenium-dependent formate dehydrogenase component. *Journal of Biological Chemistry*, 265:18213–18218.

Azevedo, I. C. A. and Oliveira, F. A. R. (1995). A model food system for mass transfer in the acidification of cut root vegetables. *International Journal of Food Science & Technology*, 30(4):473–483.

Baka, M., Van Derlinden, E., Boons, K., Mertens, L., and Van Impe, J. F. (2013). Impact of ph on the cardinal temperatures of *E. coli* K12: Evaluation of the gamma hypothesis. *Food Control*, 29(2):328–335.

Becker, S. A., Feist, A. M., Mo, M. L., Hannum, G., Palsson, B. Ø., and Herrgard, M. J. (2007). Quantitative prediction of cellular metabolism wit constraint-based models: the COBRA Toolbox. *Nature Protocols*, 2:727–738.

Blackwood, A. C., Neish, A. C., and Ledingham, G. A. (1956). Dissimilation of glucose at controlled pH values by pigmented and nonpigmented strains of *Escherichia coli*. *Journal of Bacteriology*, 72:497–499.

Buchanan, R. L. (1993). Predictive food microbiology. *Trends in Food Science & Technology*, 4:6–11.

Clark, D. P. (1989). The fermentation pathways of *Escherichia coli*. *FEMS Microbiology Letters*, 63(3):223–234.

Cole, M. B., Jones, M. V., and Holyoak, C. (1990). The effect of pH, salt concentration and temperature on the survival and growth of *Listeria monocytogenes*. *Journal of Applied Bacteriology*, 69(1):63–72.

Cooper, S. and Helmstetter, C. E. (1968). Chromosome replication and the division cycle of *Escherichia coli* B/r. *Journal of Molecular Biology*, 31:519–540.

Cussler, E. L. (1984). *Diffusion: Mass Transfer in Fluid Systems*. Cambridge University Press.

Dens, E. J., Bernaerts, K., Standaert, A. R., and Van Impe, J. F. (2005). Cell division theory and individual-based modeling of microbial lag: Part I. the theory of cell division. *International Journal of Food Microbiology*, 101(3):303–318.

Donachie, W. D. (1968). Relationship between cell size and time of initiation of DNA replication. *Nature*, 219:1077–1079.

EFSA and ECDC (2014). The European Union summary report on trends and sources of zoonoses, zoonotic agents and food-borne outbreaks in 2012. *EFSA Journal*, 12(2):3547.

Eklund, T. (1989). Organic acids and esters. In Gould, G. W., editor, *Mechanisms of action of food preservation procedures*, pages 160–200. London: Elsevier Science Publishers Ltd.

Feist, A. M., Henry, C. S., Reed, J. L., Krummenacker, M., Joyce, A. R., Karp, P. D., Broadbelt, L. J., Hatzimanikatis, V., and Palsson, B. Ø. (2007). A genome-scale metabolic reconstruction for *Escherichia coli* K-12 MG1655 that accounts for 1260 orfs and thermodynamic information. *Molecular Systems Biology*, 3(121).

Ginovart, M., López, D., Valls, J., and Silbert, M. (2002). Individual based simulations of bacterial growth on agar plates. *Physica A: Statistical Mechanics and its Applications*, 305(3-4):604–618.

Godin, M., Bryan, A. K., and Burg, T. P. (2007). Measuring the mass, density and size of particles and cells using a suspended microchannel resonator. *Applied PHysics Letters*, 91(123121).

Grimm, V., Berger, U., DeAngelis, D. L., Polhill, J. G., J., G., and Railsback, S. F. (2010). The ODD protocol: A review and first update. *Ecological Modelling*, 221(23):2760–2768.

Helmstetter, C. E. (1996). Timing of synthetic activities in the cell cycle. In Neidhardt, F. C., Curtiss III, F., Ingraham, R., Lin, J., Low, E., Magasanik, K., Reznikoff, W., Riley, M., Schaechter, M., and Umbarger, H., editors, *Escherichia coli and Salmonella: Cellular and molecular biology*, volume 2, chapter 102, pages 1627–1637. Washington D.C.: ASM Press, 2nd edition.

Higgins, T. E. and Johnson, M. J. (1970). Pathways of anaerobic acetate utilization in *Escherichia coli* and *Aerobacter cloacae*. *Journal of Bacteriology*, 101(3):885–891.

Ihssen, J., Grasselli, E., Bassin, C., François, P., Piffaretti, J.-C., Köster, W., Schrenzel, J., and Egli, T. (2007). Comparative genomic hybridization and physiological characterization of environmental isolates indicate that significant (eco-)physiological properties are highly conserved in the species *Escherichia coli*. *Microbiology*, 134(7):2052–2066.

Karel, S. F. and Robertson, C. R. (1989). Cell mass synthesis and degradation by immobilized *Escherichia coli*. *Biotechnology and Bioengineering*, 34(3):337–356.

Koch, A. L. (1993). Biomass growth rate during the prokaryote cell cycle. *Critical reviews in microbiology*, 19(1):17–42.

Kreft, J.-U., G., B., and Wimpenny, J. W. T. (1998). BacSim, a simulator for individual-based modelling of bacterial colony growth. *Microbiology*, 144(12):3275–3287.

Malakar, P. K., Brocklehurst, T. F., Mackie, A. R., Wilson, P. D. G., Zwietering, M. H., and van 't Riet, K. (2000). Microgradients in bacterial colonies: use of fluorescence ratio imaging, a non-invasive technique. *International Journal of Food Microbiology*, 560:71–80.

Michelsen, O., Teixeira de Mattos, M. J., Jensen, P. R., and G., H. F. (2003). Precise determination of C and D periods by flow cytometry in *Escherichia coli* k-12 and b/r. *Microbiology*, 149(4):1001–1010.

Mitchell, A. J. and Wimpenny, J. W. T. (1997). The effects of agar concentration on the growth and morphology of submerged colonies of motile and non-motile bacteria. *Journal of Applied Microbiology*, 83(1):76–84.

North, M. J., Collier, N. T., Ozik, J., Tatara, E. R., Altaweel, M., Macal, C. M., Bragen, M., and Sydelko, P. (2013). Complex adaptive systems modeling with Repast Simphony. *Complex Adaptive Systems Modeling*, 1(3).

Östling, C. E. and Lindgren, S. E. (1993). Inhibition of enterobacteria and *Listeria* by lactic, acetic and formic acids. *Journal of Applied Bacteriology*, 75(1):18–24.

Øyaas, J., Storre, I., Svendsen, H., and Levine, D. W. (1995). The effective diffusion coefficient and the distribution constant for small molecules in calcium-alginate gel beads. *Biotechnology & Bioengineering*, 47(4):492–500.

Peaceman, D. W. and Rachford, H. H. (1955). The numerical solution of parabolic and elliptic differential equations. *Journal of the Society of Industrial and Applied Mathematics*, 3:28–41.

Portnoy, V. A., Scott, D. A., Lewis, N. E., Tarasova, Y., Osterman, A. L., and Palsson, B. Ø. (2010). Deletion of genes encoding cytochrome oxidases and quinol monooxygenase blocks the aerobic-anaerobic shift in *Escherichia coli* K-12 MG1655. *Applied Environmental Microbiology*, 76(19):6529–6540.

Schulze, K. L. and Lipe, R. S. (1964). Relationship between substrate concentration, growth rate, and respiration rate of *Escherichia coli* in continuous culture. *Archiv für Mikrobiologie*, 48:1–20.

Speight, J. G. (2005). *Lange's Handbook of Chemistry*. New York: McGraw-Hill Inc.

Stokes, J. L. (1949). Fermentation of glucose by suspensions of *Escherichia coli*. *Journal of Bacteriology*, 57(2):147–158.

Thomas, L. H. (1949). *Elliptic Problems in Linear Differential Equations over a Network*. New York: Columbia University, Watson Scientific Computing Lab.

Verhulst, A., Cappuyns, A. M., Van Derlinden, E., Bernaerts, K., and Van Impe, J. F. (2011). Analysis of the lag phase to exponential growth transition by incorporating inoculum characteristics. *Food Microbiology*, 28(4):656–666.

Volkmer, B. and Heinemann, M. (2011). Condition-dependent cell volume and concentration of *Escherichia coli* to facilitate data conversion for systems biology modeling. *PLoS ONE*, 6(7).

Wold, S., Skarstad, K., Steen, H. B., Stokke, T., and Boye, E. (1994). The initiation mass for DNA replication in *Escherichia coli* K-12 is dependent on growth rate. *EMBO Journal*, 13(9):2097–2102.

FOOD PROCESSING

MODELLING OF WATER TRANSFER IN BREAD DURING STALING

Jean-Yves Monteau[a,b], Emmanuel Purlis[a,b,c], Emna Besbes[a,b], Vanessa Jury[a,b], Alain Le Bail[a,b]
[a] Oniris, département GPA, rue de la Géraudière, B.P. 82 225, 44322 Nantes CEDEX 3, France
[b] UMR 6144 GEPEA CNRS
[c] CIDCA - CONICET La Plata, Facultad de Ciencias Exactas, UNLP, 47 y 116, 1900 La Plata, Argentina
email: jean-yves.monteau@oniris-nantes.fr

KEYWORDS
Sandwich bread, Staling, Modelling, Water transfer

Abstract

Retrogradation of starch and water loss have an effect of the same intensity on the firmness increase in the phenomenon of bread staling. To understand the transfer of water during staling, we developed three models. In the first two models, crust is considered as a membrane characterised by its water vapour permeability. In the third model, crust is considered a material similar to the crumb but with its peculiar characteristics. In the first model, internal pressure is constant and equal to atmospheric pressure. In the second and third models, the dry air content is determined by solving the corresponding mass balance; air pressure and total pressure are deducted afterwards. The aim of this study is to compare the results of the three models and to conclude on their individual interests. The first two models give relatively similar results, but the third one has significant differences.

INTRODUCTION

Staling of bread is defined as its firming over time, and results in a loss of smoothness (Roussel and Chiron 2002). Besides modification of textural properties, modification of aromatic properties are noted. This evolution is perceptible for a product like sandwich bread, packed in an tight packing. Retrogradation of starch is essential for staling (Hug-Iten et al. 1999), but water migration plays an important part through its distribution among the bread components. In fact, bread with crust loses its freshness quickly, while bread without crust stays fresh (Bechtel et al. 1953, Besbes et al. 2014). However the effect of the presence of the crust is exerted on the exchange of water between the crumb, the crust and the atmosphere, not on the starch retrogradation. According to Ronda et al. (2011), the starch retrogradation and the loss of water have an effect of same intensity on the increase of bread firming. Water migration results in a balancing of the water content between the crust and the crumb at the macroscopic scale, and in redistribution of the moisture between the components at the microscopic scale. This equilibrium is unstable and may drift towards softening of the crust and drying of the crumb.

Water transfer in a product is driven according to various mechanisms: molecular diffusion (gas phase), convection and liquid capillarity. Several authors used a simple model based on molecular diffusion in dense, homogeneous and isotropic media with the second Fick's law to describe the mass transfer (Datta 2005). Mass transfer in liquid water form, or in vapour water form, were not differentated. Other authors prefer the using of the Fick's law in separating liquid water tansfer and vapour water transfer. For instance the works of Thorvaldsson and Janestad (1999) may be quoted. Nevertheless, the Fick's law alone does not explain the mass transfer in porous media because the diffusion is not the only responsible mechanism. Therefore, it is necessary to add to the diffusion term a convection term based on the Darcy's law: the transfer is then due also to a pressure gradient. A synthesis of formulations of heat and mass transfer problems was achieved by Datta (2007a).

To understand the mechanisms of water transfer in bread during staling, we developed models of the system. Modelling a process involves a number of assumptions and choices for the equations. This is why a same process can be described by several models, the most complex in its equations being not necessarily the wiser. For bread staling we tested three models. The aim of this work is to compare the results given by these three models and to conclude as to their respective interests.

MODELLING

The Models

The modelling is greatly inspired by the model of Whitaker (1977) developed for the drying process, with some adaptations to our staling problem. The problem is an isotherm one. Thus, there is no heat transfer equation. We are interested in particular in three quantities varying in time and 2D-space. These three variables are local content of liquid water, water vapour and dry air.

The geometry is a slice of sandwich bread, horizontally disposed in order to eliminate the gravitational effect. For the two first models, the crust is supposed to be a membrane characterised by its water vapour permeability. In the first model, the pressure of the bread slice is assumed equal to the atmospheric pressure. Thus we have two governing equations, one for liquid water and one for water vapour, the dry air content being deduced with algebraic equations. In the second model, the dry air content is calculated using a differential equation similar to that used for the water vapour. Then, the pressures of water vapour, dry air and the total pressure are calculated with algebraic equations. In, the third model, the crust is a domain with its own characteristics (density, porosity, etc.) different from the crumb. The content in dry air is calculated, as in the 2nd model, using the corresponding mass balance.

First Model

The variation of the local water content, X_{liq}, is described by Darcy flow (due to liquid pressure: $P_{liq} = P - P_c$) with addition of an evaporation-condensation volumetric rate, I:

$$\frac{\partial X_{liq}}{\partial t} = \nabla \cdot \left[\rho_{liq} \frac{k_{liq}}{\mu_{liq}} \nabla \left(P - P_c \right) \right] - I \tag{1}$$

where P_c is the capillary pressure. Since liquid water is strongly bound to starch, total pressure driven flow is not significant in our case, so the following expression is used:

$$\frac{\partial X_{liq}}{\partial t} = \nabla \cdot \left(D_{liq} \nabla X_{liq} \right) - I \tag{2}$$

where D_{liq} is the capillary diffusivity of liquid water, defined as (Datta 2007b):

$$D_{liq} = -\rho_{liq} \frac{k_{liq}}{\mu_{liq}} \frac{\partial P_c}{\partial X_{liq}} \tag{3}$$

The variation of water vapour, X_{vap}, is represented by a diffusion equation with the corresponding source term:

$$\frac{\partial X_{vap}}{\partial t} = \nabla \cdot \left[\rho_g \Phi \left(1 - S \right) D_{av} \nabla \frac{\rho_{vap}}{\rho_g} \right] + I \tag{4}$$

The air-vapour diffusion coefficient D_{av} is weighted by the ratio of gas volume on total volume, i.e. the porosity Φ multiplied by the gas fraction in the pores, $1 - S$; S is the water saturation in the pores, and ρ_g is the gas density.

The evaporation-condensation rate is supposed proportional to the difference between the equilibrium water vapour, $a_w \, P_{sat}(T)$, and the vapour pressure in the pores P_{vap}. a_w is the crumb water activity, and $P_{sat}(T)$ is the saturation pressure of the water vapour at temperature T:

$$I = C \left(a_w \, P_{sat}(T) - P_{vap} \right) \tag{5}$$

C is the proportionality coefficient. The crumb water activity was experimentally determined to fill a table function of the local water content (table not given here). This table is interpolated using piecewise cubic functions.

The water vapour pressure is derived from the perfect gas law:

$$P_{vap} = \frac{X_{vap} \, R \, T}{M_{vap} \, \Phi \left(1 - S \right)} \tag{6}$$

where R is the perfect gas law constant, and M_{vap} is the molar mass of water vapour.

This first model is characterised by a total pressure supposed as constant and equal to atmospheric pressure. Thus, the dry air pressure is derived by substracting the water vapour pressure to the total pressure:

$$P_{air} = P - P_{vap} \tag{7}$$

Then, the dry air content X_{air} is derived using the perfect gas law:

$$X_{air} = \frac{P_{air} \, M_{air} \, \Phi \left(1 - S \right)}{R \, T} \tag{8}$$

where M_{air} is the molar mass of dry air.

The water vapour and dry air densities can be calculated from mass concentrations in the porous matrix:

$$\rho_{vap} = \frac{X_{vap}}{\Phi \left(1 - S \right)} \tag{9}$$

$$\rho_{air} = \frac{X_{air}}{\Phi \left(1 - S \right)} \tag{10}$$

The saturation pressure is calculated with the Dupré formula, formula usable from -50 to 200 °C:

$$P_{sat}(T) = 133.32 \, e^{46.784 - \frac{6435}{T} - 3.868 \, \ln T} \tag{11}$$

where T is in K and P_{sat} in Pa. The problem is isotherm, thus P_{sat} is constant.

The pores saturation is calculated with the following equation:

$$S = \frac{X_{liq}}{\rho_{liq} \, \Phi} \tag{12}$$

for which ρ_{liq} is the density of liquid water.

Lastly, the gas density is the sum of dry air and water vapour densities:

$$\rho_g = \rho_{vap} + \rho_{air} \tag{13}$$

Boundary conditions:

The mass transfer with the ambient is assumed to be only in gaseous phase. Consequently, the liquid water flow at the surface is equal to zero, as well as at the left and bottom boundaries because of the symmetries (see Fig. (1)). Thus, in all boundaries, the boundary condition for liquid water is

$$n \cdot \left(D_{liq} \nabla X_{liq} \right) = 0 \tag{14}$$

with n being the outward normal to the boundary. Regarding X_{vap}, on left and bottom boundaries, the vapour flow is equal to zero,

$$n \cdot \left[\rho_g \, \Phi \, (1 - S) \, D_{av} \, \nabla \, \frac{\rho_{vap}}{\rho_g} \right] = 0 \tag{15}$$

and at the surface is determined by the water vapour permeability of the crust WVP:

$$n \cdot \left[\rho_g \, \Phi \, (1 - S) \, D_{av} \, \nabla \, \frac{\rho_{vap}}{\rho_g} \right] = \mathrm{WVP} \, \frac{P_{vap,a} - P_{vap}}{e} \tag{16}$$

where e is the crust thickness. The vapour pressure in the ambient is calculated conventionally by

$$P_{vap,a} = \mathrm{RH} \, P_{sat}(T) \tag{17}$$

with RH the relative humidity of ambient.

Second Model

In the second model, X_{air} is calculated using a diffusion equation similar to the one used for X_{vap}, but without the evaporation-condensation term:

$$\frac{\partial \, X_{air}}{\partial \, t} = \nabla \cdot \left[\rho_g \, \Phi \, (1 - S) \, D_{av} \, \nabla \frac{\rho_{air}}{\rho_g} \right] \tag{18}$$

The equation (8) is rewritten to calculate P_{air},

$$P_{air} = \frac{X_{air} \, R \, T}{M_{air} \, \Phi \, (1 - S)} \tag{19}$$

and also the equation (7) to calculate P:

$$P = P_{vap} + P_{air} \tag{20}$$

The boundary conditions are unchanged.

Third Model

The third model involves all mechanisms included in the second model, but it incorporates explicitly the presence of the crust. An external layer (5 mm-thickness) is added to crumb (Fig. 1 b) to represent the crumb-crust composite system. Furthermore, crumb and crust have different properties, mainly due to differences in structure developed during baking. For instance, the following expressions inspired from (Datta 2007b) and fitted to our product were used for the capillary diffusivity of liquid water:

$$D_{liq,crumb} = 1.5 \, 10^{-9} \, e^{(-2.8 + 2 \, X_{ms})} \, \Phi \tag{21}$$

$$D_{liq,crust} = 1 \, 10^{-9} \, e^{(-2.8 + 2 \, X_{ms})} \, \Phi \tag{22}$$

Regarding the water activity of crust, a water sorption isotherm obtained at 15 °C is used (Besbes et al. 2013).

Boundary conditions are the same as before, where the value $\frac{\mathrm{WVP}}{e}$ represents a mass transfer coefficient. In the interface crumb-crust, continuity condition of flows is applied (no consumption/generation at interface).

Parameters

The models constants either are known physical constants (D_{av}, R, M_{vap}, ...), peculiar values to our product (D_{liq}, Φ, WVP, ...), or the environmental parameters T and RH. They are given in Table 1.

Table 1: Models Parameters

Physical constants		
D_{av}	$(\mathrm{m^2\,s^{-1}})$	$2.34\,10^{-5}$
R	$(\mathrm{J\,mol^{-1}\,K^{-1}})$	8.3145
M_{vap}	$(\mathrm{kg\,mol^{-1}})$	$18.02\,10^{-3}$
M_{air}	$(\mathrm{kg\,mol^{-1}})$	$28.96\,10^{-3}$
ρ_{liq}	$(\mathrm{kg\,m^{-3}})$	998.98
Product constants		
D_{liq} [a]	$(\mathrm{m^2\,s^{-1}})$	$1.34\,10^{-10}$
Φ_{crumb}		0.811
Φ_{crust}		0.750
C	$(\mathrm{s\,m^{-2}})$	$5\,10^{-4}$
$\rho_{app,s,crumb}$	$(\mathrm{kg\,m^{-3}})$	192
$\rho_{app,s,crust}$	$(\mathrm{kg\,m^{-3}})$	330
WVP	$(\mathrm{kg\,m^{-1}\,s^{-1}\,Pa^{-1}})$	$4.67\,10^{-11}$
e	(m)	0.005
Environmental parameters		
T	(°C)	15
RH		0.9

[a] 1st and 2nd model.

Initial conditions

For the first model, the initial conditions necessary to solve the two differential equations were:

$$X_{liq} = 160 \, \mathrm{kg\,m^{-3}} \quad (X_{ms} = 0.83) \tag{23}$$

$$X_{vap} = 8 \, 10^{-3} \, \mathrm{kg\,m^{-3}} \tag{24}$$

For the second model, the boundary condition necessary to solve Equation (18) was added:

$$X_{air} = 0.785 \, \mathrm{kg\,m^{-3}} \tag{25}$$

For the third model, initial conditions for crust are also necessary:

$$X_{liq} = 75.9 \, \mathrm{kg\,m^{-3}} \quad (X_{ms} = 0.23) \tag{26}$$

$$X_{vap} = 7.2 \, 10^{-3} \, \mathrm{kg\,m^{-3}} \tag{27}$$

$$X_{air} = 0.815 \, \mathrm{kg\,m^{-3}} \tag{28}$$

Programming, Geometry and Mesh

Programming was achieved using Comsol 4.2 and 4.3. The geometry used the symmetries of the product: a quarter of bread slice was drawn. In order to validate the models by use of comparisons between numerical

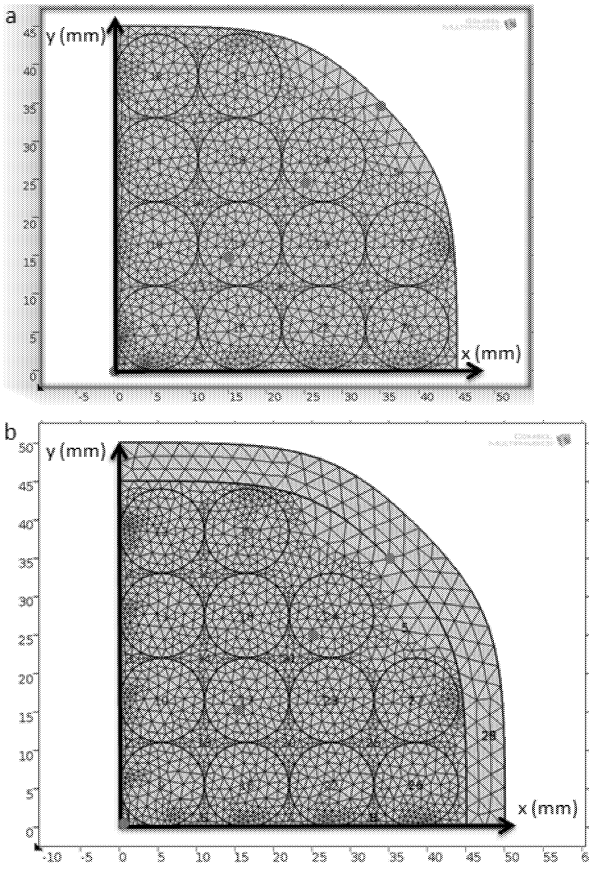

Figure 1: Geometry and Mesh. a: 1st and 2nd Models, b: 3rd Model

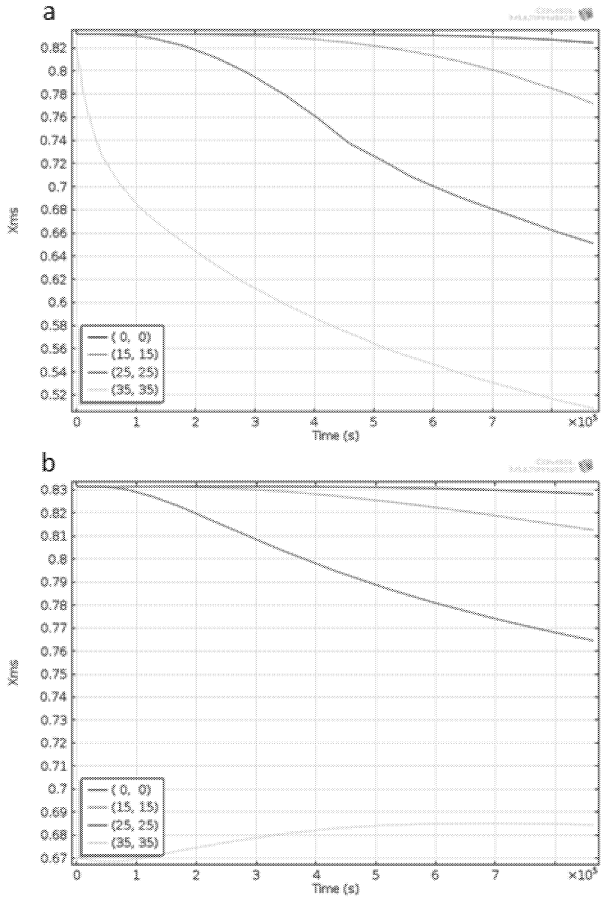

Figure 2: Time Variation of Local Water Content Dry Basis. a: 1st Model, b: 3rd Model

results and measurements of average water content on some areas of the slice, these areas were represented by discs on the entire surface of the slice. This resulted in a modification of the mesh (Fig. 1).

PARAMETER ESTIMATION AND MODEL VALIDATION

The models were validated by comparing the numerical and experimental average water content of circular areas. The evaporation coefficient C can not be experimentally determined. C was used as a fitting parameter to find the experimental results at best.

RESULTS AND DISCUSSION

The following figures present the time variation of the main variables at points shown on Figure 1 (0 mm, 0 mm) (central point), (15 mm, 15 mm), (25 mm, 25 mm) and (35 mm, 35 mm) (surface point).

Time Variation of Main Variables

The analysis presented in this paragraph is performed on the results given by the first model. The local water content is given on a dry basis, X_{ms}, according to the use in food process engineering. The relationship between X_{liq} and X_{ms} is

$$X_{ms} = \frac{X_{liq}}{\rho_{app,s}} \tag{29}$$

where $\rho_{app,s}$ is the bulk density of dry matter.

X_{ms} and I: X_{ms} monotonically decreases, starting by the surface (Fig. 2 a). This results from an evaporation zone which propagates from the surface towards the centre (Fig. 3 a). In fact, the time variation of the I profile on a segment (0,0)-(35,35) reveals that at certain times there is condensation around the evaporation peak.

X_{vap} and P_{vap}: the vapour content first increases near the surface, then at the central area (Fig. 4). The vapour pressure in ambient always is lower than the vapour pressure at the product surface. Thus, there is always a vapour flow from the crust towards the ambient. Nevertheless, X_{vap} increases because is supplied with evaporation inside the product. This evaporation rate is important because the vapour

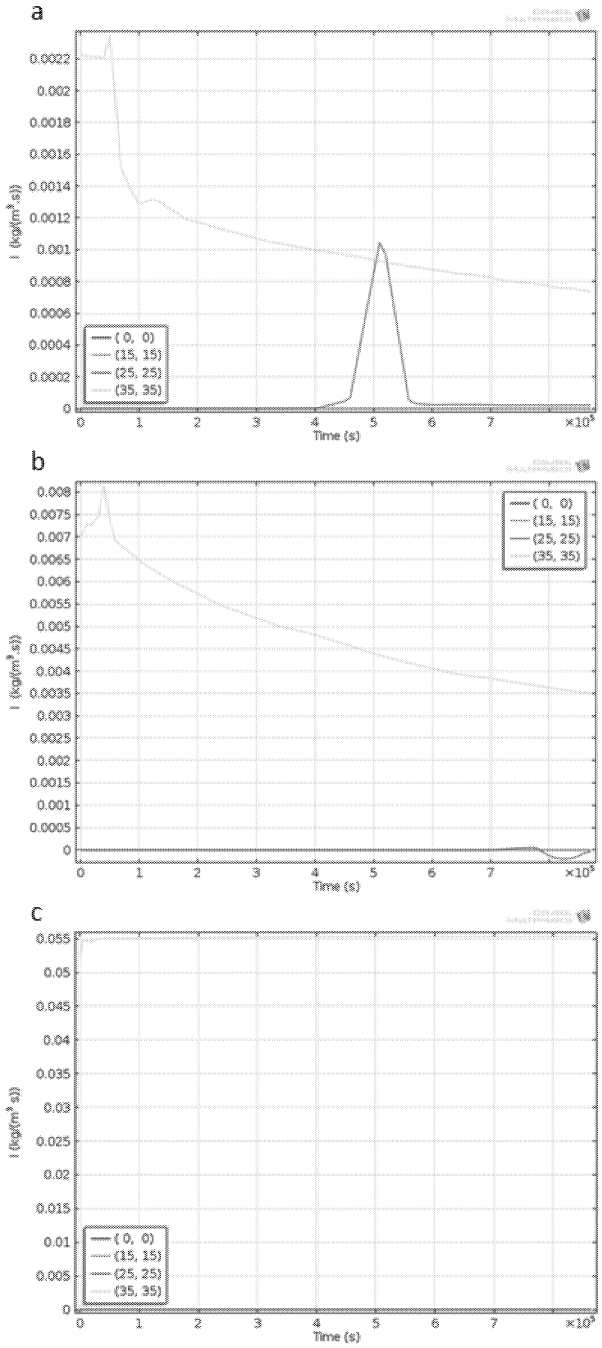

Figure 3: Time Variation of Evaporation Rate. a: 1st Model, b: 2nd Model, c: 3rd Model

pressure is always lower than the equilibrium pressure given by the sorption isotherm. The equation for I (Eq. ((5)) means that the vapour pressure is different from the equilibrium pressure. That is questionable. A noteworthy point is that P_{vap} decreases while X_{vap} increases (Fig. 5). That is explained by the pores saturation, S, which decreases quickly enough so that the vapour pressure increases instead of decreasing, according to the equation $P_{vap} = \frac{RT}{M_{vap}\,\Phi}\,\frac{X_{vap}}{1-S}$ (Fig. 6).

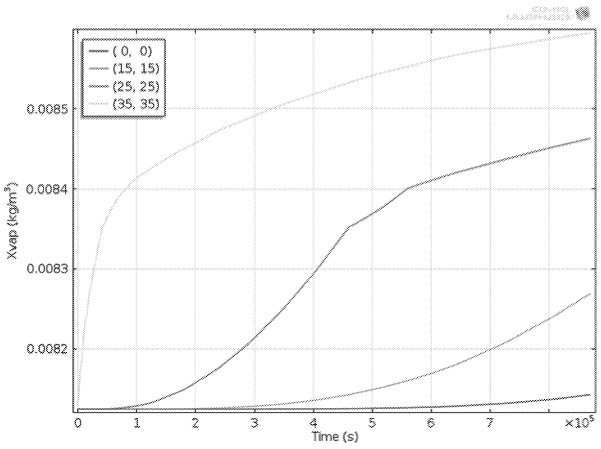

Figure 4: Time Variation of Water Vapour Content, 1st Model

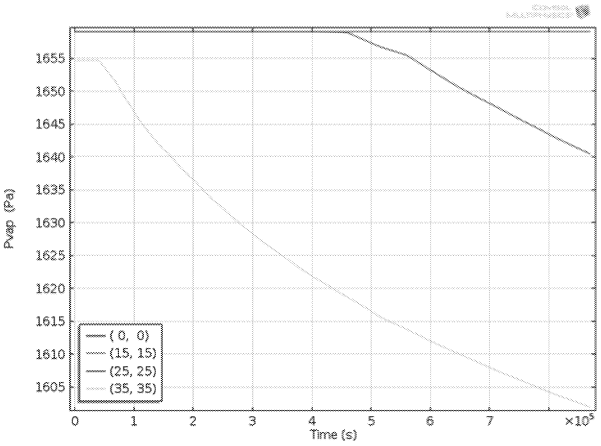

Figure 5: Time Variation of Water Vapour Pressure, 1st Model

X_{air} and P_{air}: the air pressure increases because the total pressure in the product is equal to P_{atm} and the vapour pressure decreases. Consequently X_{air} increases (Figs 7 a, 8 a).

S: the pores saturation decreases over time at the four points. Again, the phenomenon begins at the surface, and then propagates towards the centre. At the end of the simulation, the saturation just started to decrease at the central point (Fig. 6).

Differences between the Three Models

The results obtained with the two first models are quite similar. Nevertheless, there are some differences. For the second model, compared to the first, curves often present the same shape, but amplified. A slower inward propagation of the phenomena can be observed. However, there are noteworthy differences for I, X_{air},

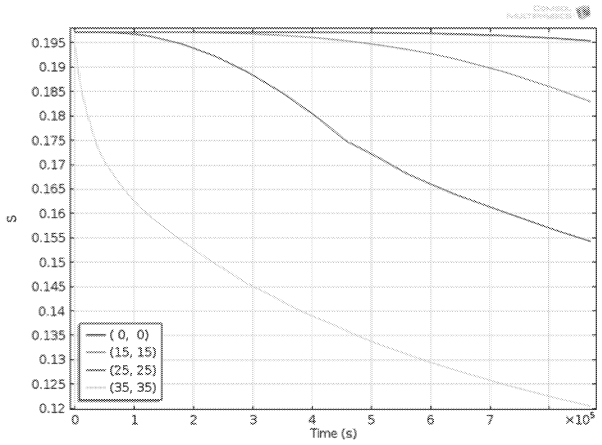

Figure 6: Time Variation of Pores Saturation, 1st Model

P_{air}. Besides, P is calculated in the second model and not in the first one:

I: the evaporation rate presents the same variation at the surface but the peak is much higher, 0.008 instead of $0.0023\,\mathrm{kg\,m^{-3}\,s^{-1}}$ (Fig. 3 a, b). For the point (25,25), I stays at 0 except at the end of the simulation, where there is a trend for evaporation at $7\,10^5$ s, and then a condensation phase before returning to zero evaporation. With the first model, an evaporation peak of $0.001\,\mathrm{kg\,m^{-3}\,s^{-1}}$ was obtained at about $5\,10^5$ s. For the points (15,15) and (0,0), evaporation remains 0 for the two first models.

X_{air} and P_{air}: at the surface, in the first model, P_{air} increases. In the second model, the Dirichlet condition imposes that P_{air} be constant and equal to air pressure in ambiant air (Fig. 7 b). For the other points, at the beginning a rapid increase is noticed, then a plateau before a slower increase, with the three curves almost the same. However, in (25,25), P_{air} begins to decrease at the end of the simulation, at $8\,10^5$ s. $P_{air} = \frac{RT}{M_{air}\,\Phi}\,\frac{X_{air}}{1-S}$. This equation explains the plateau which comes from the change of X_{air} given by the diffusion equation. However, for X_{air}, the three curves are not the same (Fig. 8 b). The decrease in (25,25) comes from the ratio $\frac{X_{air}}{1-S}$, because of a significant decrease of water saturation at the surface.

P: in the first model the total pressure is fixed constant and equal to atmospheric pressure. In the second model, the total pressure is the sum of P_{vap} and P_{air}. The results of this model show a pressure which changes over time, the curves similar to P_{air}, although P_{vap} decreases (Fig. 9 a). In fact, the P_{air} values are about 100 times the values of P_{vap}, which explains this result.

When analysing the results of the third model, some others differences are found, which is expected due to

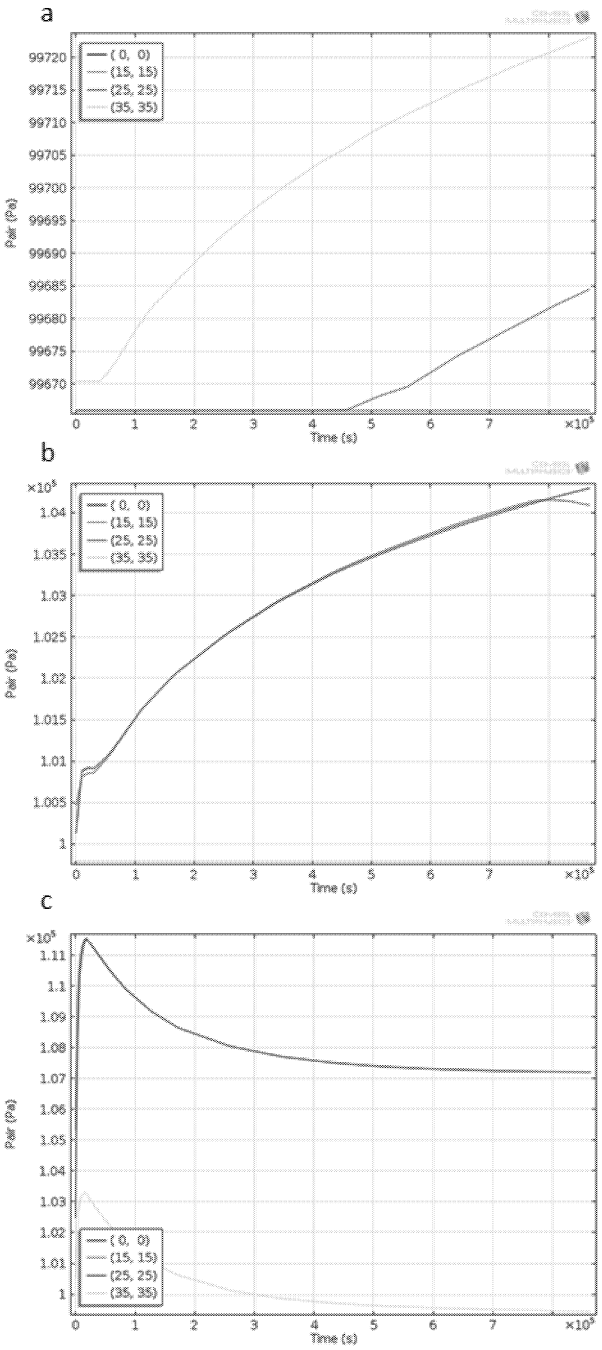

Figure 7: Time Variation of Air Pressure. a: 1st Model, b: 2nd Model, c: 3rd Model

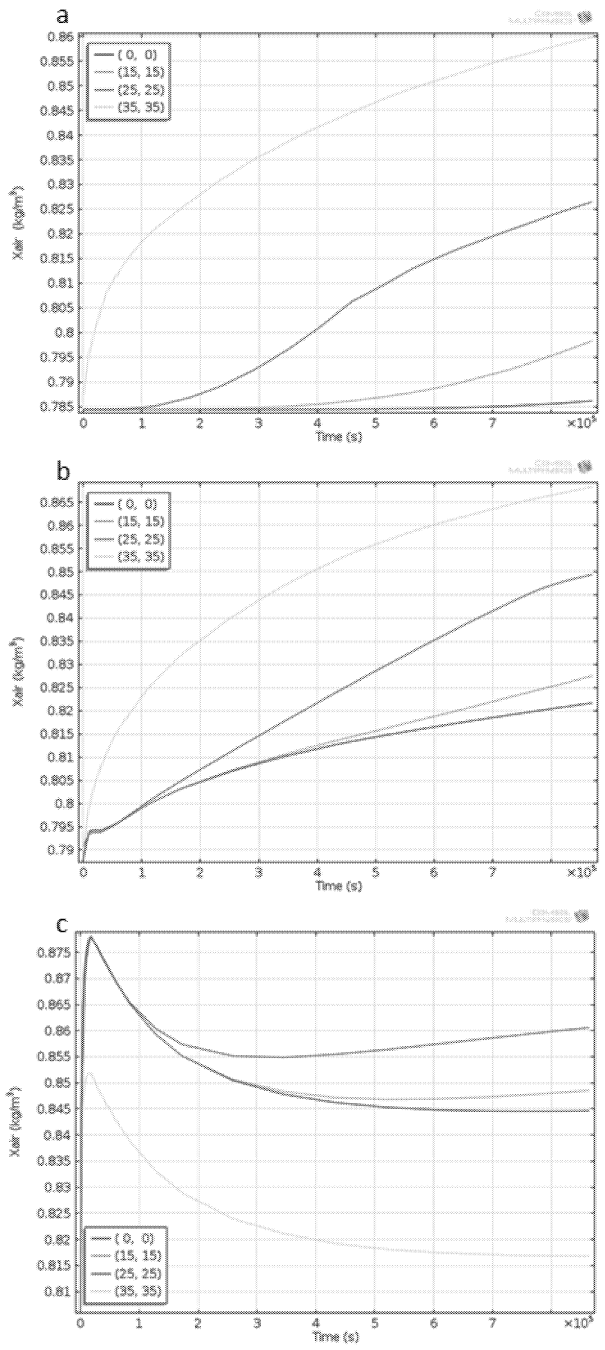

Figure 8: Time Variation of Dry Air Content. a: 1st Model, b: 2nd Model, c: 3rd Model

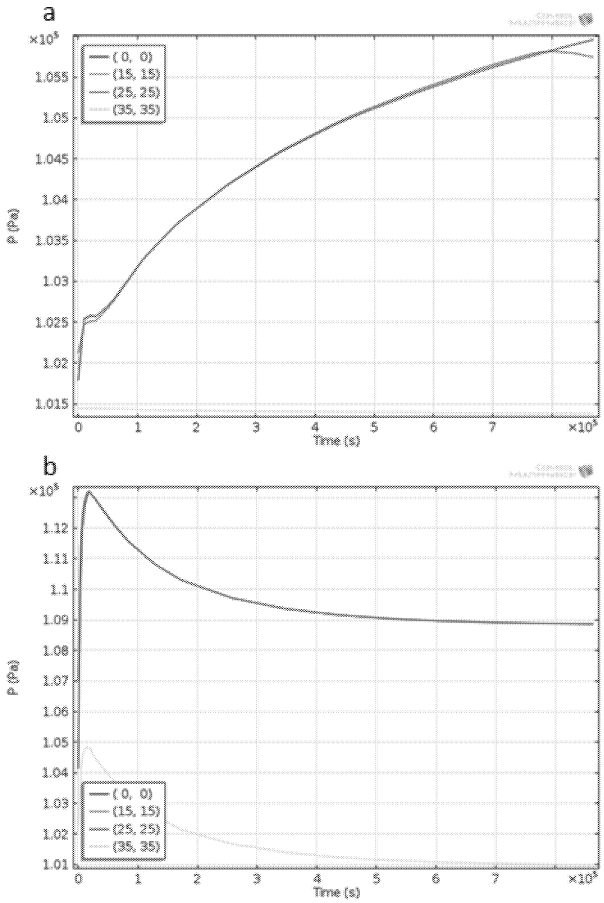

Figure 9: Time Variation of Total Pressure, a: 2nd Model, b: 3rd Model

the incorporation of the crust to the system. Firstly, the evolution of variables at interface point (35,35) is affected by the presence of the crust, which initially has lower water content and associated water activity (0.836) than crumb (and even than ambient; RH = 0.9) (Fig. 2 b). In this sense, the interface point presents a different behaviour being the intermediate between the (slow) dehydration of crumb and the gain of moisture of crust during the process. Regarding the evaporation term, it is one order higher than previous models and it is located at interface (Fig. 3 c); inside crumb, evaporation seems to be not significant. This can be explained by the difference established between vapour pressure given by water activity and vapour pressure given by transport equations (see definition of I, Eq. (5)).

With respect to air pressure, air concentration and total pressure, a first increase in all zones is found (Figs 7 c, 8 c, 9 b), but then values tend to equilibrium according to transport resistance (inner crumb) and ambient conditions (interface crumb-crust). Finally, some points inside crust were analysed to assess the expected mois-

ture increase during staling, which has been verified; values tend to equilibrium given by relative humidity of ambient (results not shown).

CONCLUSION

A priori, the first model is more simple and gives useful results, but the second model is more realistic based on equations, since it supposes the same mechanisms for air and water vapour. Furthemore, the third model, although more complex than the other ones, represents better the real system crumb-crust.

Adjustment of properties and parameters is still under work in order to validate the proposed hypotheses. The presented models can be useful for different objectives: the first and second models could be implemented to assess water loss properties of crumb during staling, in a relatively easy way; the third model could be utilised to obtain additional information about the crust, once properties depending on structure are known.

These models have to be still adjusted by varying environmental parameters (temperature and humidity), and some parameters peculiar to the product as the water vapour permeability, the diffusion coefficient of liquid water, the evaporation coefficient.

References

Bechtel W.G.; Meisner D.F.; and Bradley W.B., 1953. *The effect of the crust on the staling of bread. Cereal Chemistry*, 30, 160–168.

Besbes E.; Jury V.; Monteau J.Y.; and Le Bail A., 2013. *Water vapor transport properties during staling of bread crumb and crust as affected by heating rate. Food Research International*, 50, no. 1, 10–19.

Besbes E.; Jury V.; Monteau J.Y.; and Le Bail A., 2014. *Effect of baking conditions and storage with crust on the moisture profile, local textural properties and staling kinetics of pan bread. LWT - Food Science and Technology.* doi:http://dx.doi.org/10.1016/j.lwt.2014.02.037.

Datta A., 2005. *Modelling heat and mass transfer in food systems: current state and needs.* In G. Pagliarini and S. Rainieri (Eds.), *Heat and Mass Transfer in Food Processing - Eurotherm Seminar 77.* Università degli Studi di Parma, Parma, 3–8.

Datta A.K., 2007a. *Porous media approaches to studying simultaneous heat and mass transfer in food processes. I: Problem formulations. Journal of Food Engineering*, 80, no. 1, 80–95.

Datta A.K., 2007b. *Porous media approaches to studying simultaneous heat and mass transfer in food processes. II: Property data and representative results. Journal of Food Engineering*, 80, no. 1, 96–110.

Hug-Iten S.; Handschin S.; Conde-Petit B.; and Escher F., 1999. *Changes in Starch Microstructure on Baking and Staling of Wheat Bread. LWT - Food Science and Technology*, 32, no. 5, 255–260.

Ronda F.; Caballero P.A.; Quilez J.; and Roos Y.H., 2011. *Staling of frozen partly and fully baked breads. Study of the combined effect of amylopectin recrystallization and water content on bread firmness. Journal of Cereal Science*, 53, 97–103.

Roussel P. and Chiron H., 2002. *Les pains français. Évolution, qualité, production.* MAE Editeurs ERTI, Vesoul. ISBN 2-84601-693-3.

Thorvaldsson K. and Janestad H., 1999. *A model for simultaneous heat, water and vapour diffusion. Journal of Food Engineering*, 40, 167–172.

Whitaker S., 1977. *Simultaneous heat, mass, and momentum transfer in porous media: a theory of drying. Advances in Heat Transfer*, 13, 119–203.

HYBRID MODELLING OF COOLING-DRYING PROCESS IN ANIMAL FEED-PELLETS INDUSTRIES

Charlène Lambert
Francis Courtois
AGROPARISTECH, INRA,CNAM, UMR1145 GénIAL
1 avenue des Olympiades
91744 Massy Cédex, France
charlene.lambert@agroparistech.fr
francis.courtois@agroparistech.fr

Hadyan Fibrianto*
Lionel Boillereaux
ONIRIS*, GEPEA, UMR 6144
Rue de la Géraudière, BP 82225
44322 Nantes Cédex 03, France
hadyan.fibrianto@oniris-nantes.fr
lionel.boillereaux@oniris-nantes.fr

Sandy Rouchouse
Fabrice Putier
TECALIMAN*
Rue de la Géraudière, BP 71627
44316 Nantes Cédex 03, France
s.rouchouse@tecaliman.com
f.putier@tecaliman.com

KEYWORDS
Hybrid model, switched continuous distributed parameter system, mass and heat transfers, cooling and drying processes, animal feed-pellets, vertical cooler.

ABSTRACT

Drying/cooling stages in the animal feed sector aim to bring hot, damp pellets produced by a press into thermal and hygrometric balance with the ambient air, in the quickest and most cost-effective manner possible. The purpose of this manufacturing stage is to perform both at once: drying and cooling. This is a delicate process as the ambient air used acts both as a drying and cooling vector. Industrialists have demonstrated poor management of this operation and have a tendency to over-dry/excessively cool the pellets to ensure the stability over time, which has both a substantial energy and economic cost.
This paper aims at introducing simulated cooler operating conditions in order to enable industrialists to anticipate their actions and to design operation regulation and control. A hybrid approach has been proposed and discussed.

INTRODUCTION

Industrialists must resolve the problem of the contradictory objectives of final pellet moisture, the energy spent by the process and cohesion of pellets in real-time. To do so they require:

- Relevant information in real-time,
- Control algorithms related to ventilation,
- Software tools to be able to manage the great diversity of pellet types and drying/cooling technologies, and to be able to design optimized processes (reverse engineering).

The objective is therefore to develop a new direction for optimizing drying/cooling process performance in livestock feed production factories. One needs to implement intelligent measurement and simulation in order to improve the product quality management and to optimize the energy efficiency of the process. Thus we will contribute to reducing greenhouse gas emissions.

This objective involves improving knowledge of drying/cooling processes and the behavior of pellets during this process. Knowledge is furthered in this field by technical and scientific bibliographic studies (Fairfield 2003; Maier and Bakker-Arkema 1992), industrial instrumental test campaigns and characterization of the behavior of pellets during drying and cooling in pilot tests. This will enable creation of a software simulator.

In this paper, we show that hybrid approach allows a more accurate model of the drying-cooling process.

This work is part of OPSERA research project managed by TECALIMAN and funded by ADEME.

PELLET COOLER

In product conservation, the cooling/drying process is a must step, as it is impossible to stock hot and humid animal feed-pellets without quality damage and microbial problems.

This operation consists in drying and cooling the hot-humid pellets through forced convection phenomenon. Ambient air, basically dry and colder than the product, is blown inside the vessel containing hot and humid pellets provoking water evaporation, drying the pellets. The cooling process can also be adjusted by the air inlet temperature, although it is not done yet currently (see Figure 1).

The drying process implies mass (moisture content) and heat (enthalpy) exchanges between the air and product. The ambient air, which is in countercurrent with the hot product flow, becomes progressively hotter by the contact with this one.

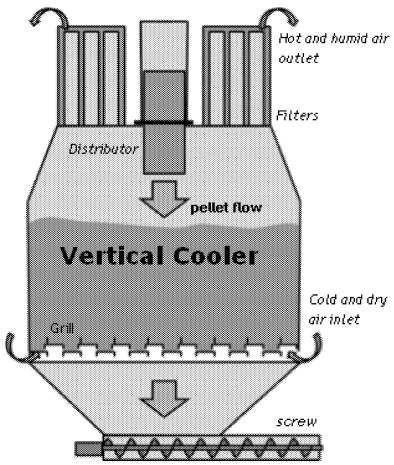

Figure 1: Common Vertical Cooler

These exchanges will depend on the following factors:
- Product temperature after the press stage (where hot-humid pellets are formed),
- Air velocity (i.e. flow rate) inside the cooler,
- Production flow rate,
- Pellets size,
- Ambient air properties …etc.

The initial temperature of pellets may vary between 50°C and 90°C and their relative humidity are generally between 14% and 17%. Industrialists' goal will be to achieve a temperature of 5 to 10°C above the ambient and humidity below 14% (based on the regulation) at the output. A very dry product is however not recommended by industrialists, as it means also loss of economic value.

The final quality of pellets will be related to their: hardness (resistance to compression) and durability (resistance to frictions), which will be measured after the cooling-drying phase.

There are also other types of coolers, such as a horizontal cooler, which has air flow perpendicular to the product direction. Nevertheless, this is not discussed in this article.

MASS BALANCE - HEAT TRANSFER COUPLING

The following assumptions are considered for the pellets:

- Shape is assumed to be an infinite cylinder;
- Isotropic behavior is assumed within them (heat and mass transfers are in the radial direction);
- Conduction heat transfer between them is negligible;
- Shrinkage is negligible;
- Thermal expansion coefficient is negligible;
- Evaporation only occurs at the surface.

It was developed for thin and thick layer drying. Furthermore, the heat and mass Biot number values (Bi_{th} and Bi_m) are respectively between 0.1 and 100 and much higher than 100. Therefore, the following phenomena are considered (Bird et al. 2002):

- Heat conduction and liquid water diffusion within the particles;
- Water evaporation and heat and mass convection at their surface.

One usually assimilates the thick layer as a series of thin layers for which the only transfers are between air and particle, and a thin layer as a single particle (see Figure 2). Moreover, thick layer drying involves energy and mass transfer in air, after each thin layer crossing (Courtois 1991; Courtois et al. 1991, 2001). The heat and mass Peclet number values (Pe_{th} and Pe_m) are much higher than 1, therefore a plug-type airflow and no pressure variation are assumed.

Partial differential equations (P.D.E.) are discretized in space using volume finite approach, O.D.E. are solved using the MATLAB solver, named ode23tb®.

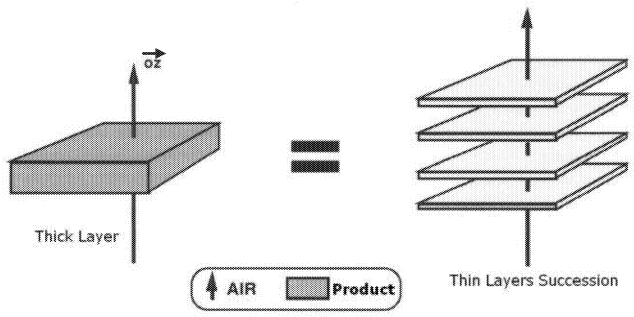

Figure 2: Thick layer decomposition

HYBRID APPROACH

Mathematical model called hybrid system combines both discrete and continuous events in a single formalism. It is very adapted to systems with various phases. The main application of this approach is real-time systems where the processes are controlled on-line.

A hybrid system is composed of continuous and discrete dynamical parts. A way to represent correctly this combination is using *hybrid automatons/ automata* (Alur et al. 1995; Henzinger 1996). They can be seen as finite state automata for which continuous-time model is added to each discrete state, called location. A hybrid automaton is defined by a finite set of vertices, called locations, continuous state space, a set of transitions between locations, a set of invariant and a set of applications associated at each location.

In food process control and modeling field, several references can be found in literature (Boillereaux et al. 2002; Fibrianto et al. 2003a and b). Those papers deal with heat transfer modeling in food thawing and freezing using high pressure technology. Hybrid approach has successfully overcome the modeling problem of discontinuities due to phase changes (liquid-melting-solid) of water as well as pressure steps generating discrete changes of thermo-physical properties. Technically the pressure is regulated around several setting points.

Regarding vertical cooling-drying process, the dynamics can be divided into three stages: *filling* phase (increasing pellets level without extraction), *steady* stage (extraction phase by maintaining the pellets level) and *draining* phase (extraction stage by decreasing pellets level), as shown in Figure 3.

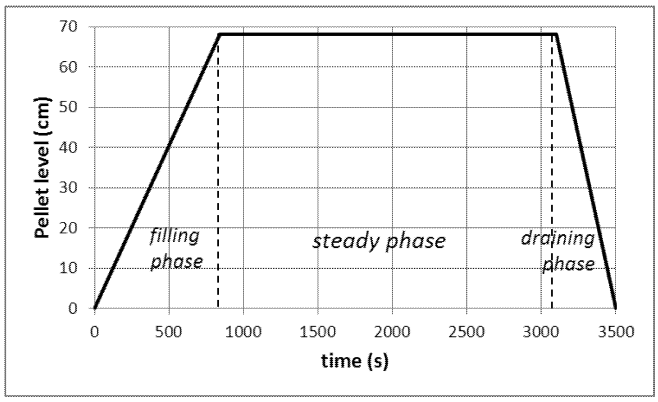

Figure 3: Three stages in cooling-drying process

By considering hybrid approach, one can express a ramp as steps succession, as described by Figure 4. The hybrid model in this case can be implemented on the filling and draining phases.

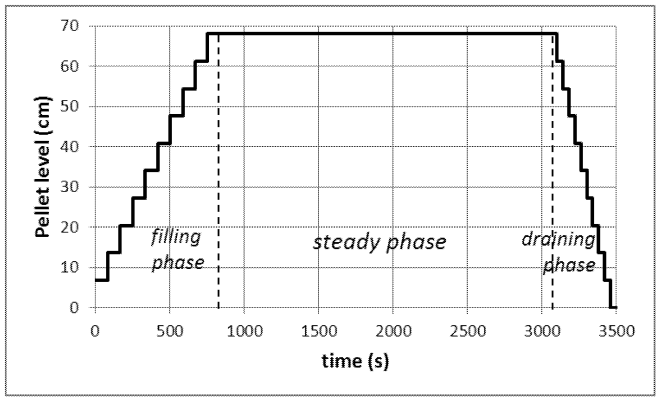

Figure 4: Three cooling-drying stages by hybrid approach

This approach facilitates the use of layer-decomposition methodology previously mentioned. Each step will represent a specific number of layers and can be modeled by a continuous-time system describing the dynamics of product temperatures and moisture content (i.e. humidity), as well as those of air. During filling phase, the number of layers increases according to the steps, while it decreases during the draining phase.

Mathematically, the process can be represented by Equation (1), where x includes the state variables, such as the moisture content (humidity) and temperatures of product (X_p and T_p respectively) and also of air (Y and Ta respectively) at various positions with respect to time.

$$\frac{\partial x(t)}{\partial t} = f(x(t), u) \qquad (1)$$

Here, the thermo-physical properties are basically known or can be easily identified.

The continuous system dynamics of the drying model uses the thick-thin layers drying approach involving energy and mass transfer equations, which can be found in the literature (Courtois 1991; Courtois et al. 1991, 2001).

Therefore, one can design hybrid automata describing the system dynamics during filling phase as follow (Figure 5).

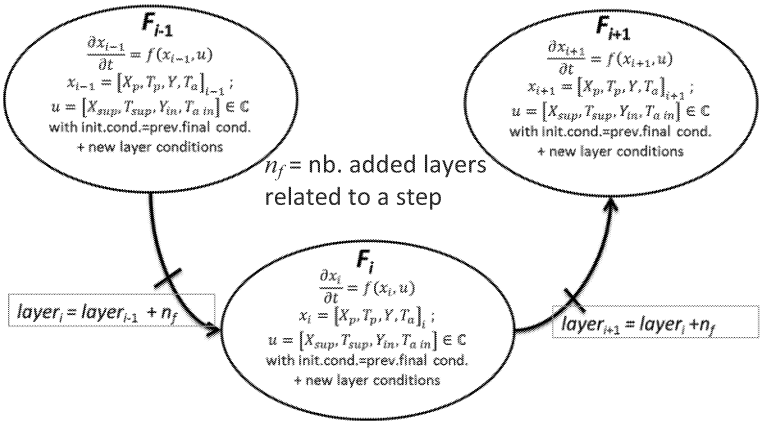

Figure 5: Hybrid automata in filling phase

Now let us focus on the steady phase. This stage contains indeed discontinuities due to extractions, which usually occur in regular interval. This phenomenon can also be seen as discrete events between continuous systems (see Figure 6).

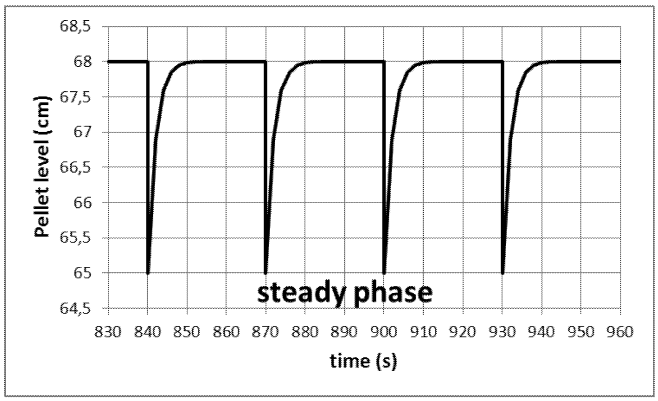

Figure 6: Discontinuities during steady phase

In hybrid representation, this dynamics can be modeled as below.

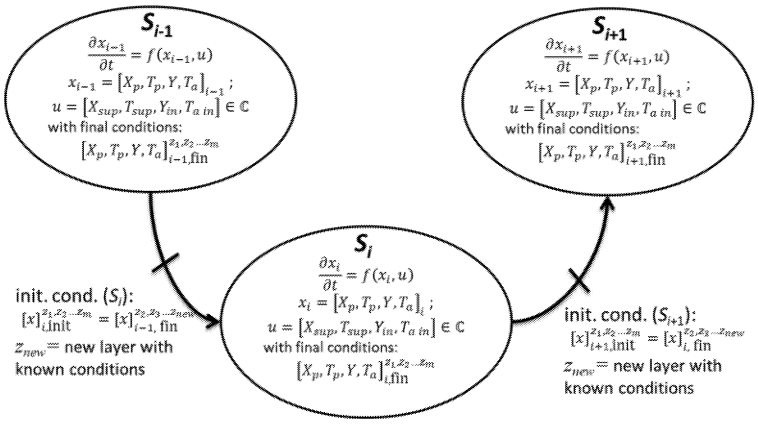

Figure 7: Hybrid automata in steady phase

The product height (i.e. number of layers) is maintained by continuous filling such as it remains constant.

The draining stage is the combination of extractions and diminution of number of layers. From hybrid approach, it is hence the combination between filling-phase automata and steady-phase automata.

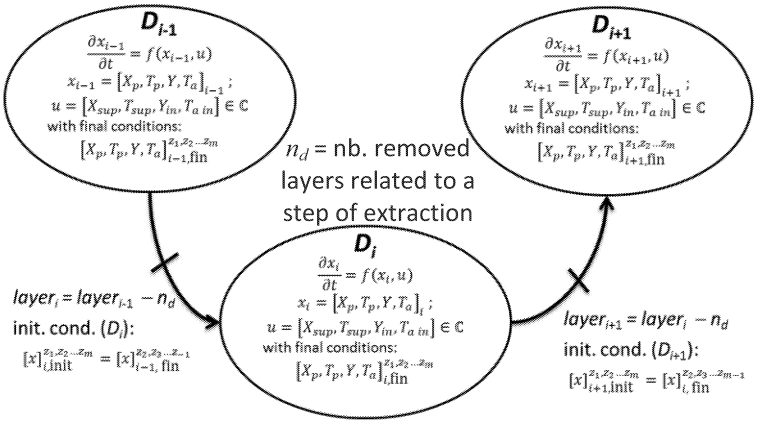

Figure 8: Hybrid automata in draining phase

SIMULATIONS

In this section, we will show simulations in comparison with experimental data.

Our experiments use the configuration in Table 1, which is related to chicken feed pellets, composed of cereals like wheat, corn and others. Also the cooling – drying process is set up under real industrial conditions.

Table 1: Experimental properties

Pellet properties		**Cooler properties**	
$C_{p\ \text{dry pellet}}$	1,660 J/kg/K	Total Height	2 m
$C_{p\ \text{water}}$	4,180 J/kg/K	Length	8 m
λ_{pellet}	0.22 W/m/K	Width	1.9 m
density	1,400 kg/m^3	Air flow rate	7700 m^3/h
Initial T°	80 °C	Inlet air T°	10.4 °C
porosity	0.48 [-]	Air HR inlet	81.4 %
HR $_{\text{pellet}}$ in	15.5 %	ρ air	1.2 kg/m^3
Pellet level	0.68 m	$C_{p\ \text{wet air}}$	1,660 + 2,030.Y J/kg/K

Basically the specific heat of pellets at constant pressure is the sum of that of its components.

Humid pellets are introduced to the cooler where we place thermocouples in 2 places: in the center at different levels and in the side (against the wall) also at different levels (i.e. 20 - 35 - 39 - 44 - 50 - 68 - 76 - 83 - 88 - 93 - 99 cm). The evolution of average temperatures at those levels can be found in Figure 9.

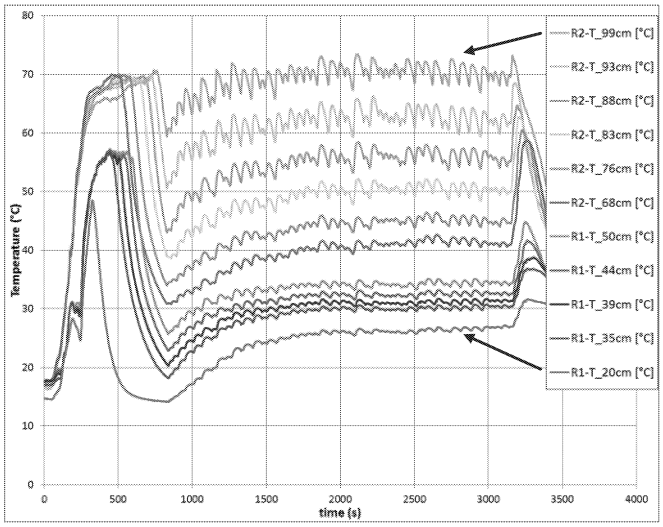

Figure 9: Temperatures data at different levels

Note that first 15 minutes correspond to the filling phase; no extraction is done and the level is increasing according to the filling flow rate. During the same time, ambient air is blown up from the bottom of the cooler. These 15 minutes lead to the pellets level of 68 cm.

Then the extraction starts and is repeated every 30 seconds, by maintaining the 68-cm level by continuous feeding and a level sensor. Each extraction occurs during 4.5 seconds. This is called the steady phase. It lasts for about 35 minutes.

Last phase deals with the draining. The feeding is stopped; only extractions happen until no more pellets inside the cooler. The total process takes about one hour, actually.

The outlet air temperature is 44.24°C in average; with relative humidity of 60% (i.e. absolute humidity of outlet air is 0.0358 dry basis [db.] vs. that of inlet of 0.0064 [db.] corresponding to 81.4% HR at 10.4°C). The whole operation is held under atmospheric conditions.

As result, the output pellets have a relative humidity around 12.2% at a temperature of 19°C in average.

Now, let us see the numerical simulations. We used simple tool developed under MATLAB software for this purpose. Those parameters previously mentioned have been applied on the model (Boillereaux et al. 2002; Courtois 1991; Courtois et al. 1991, 2001; Fibrianto et al. 2003a and b), which lead to the following graphs.

Pellets and air temperatures at specific levels (i.e. 20 - 35 - 39 - 44 - 50 cm) are illustrated on Figure 10a and b, respectively.

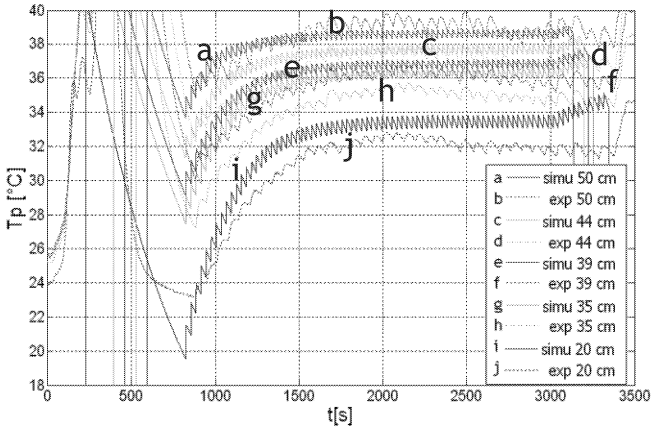

Figure 10a: Product temperatures at different levels

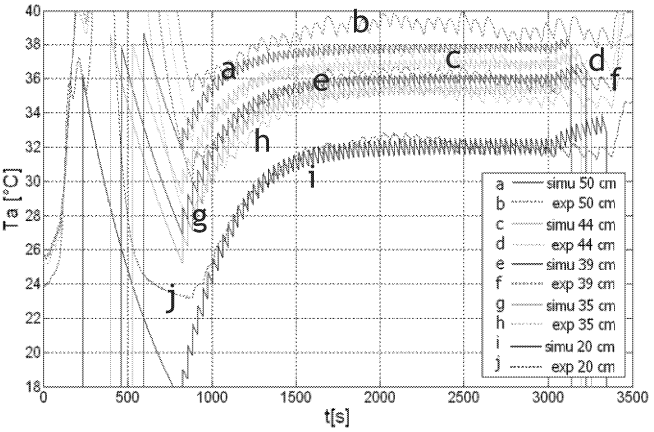

Figure 10b: Air temperatures at different levels

And the associated moisture content and absolute humidity of air are given as shown on Figure 11a and b, respectively.

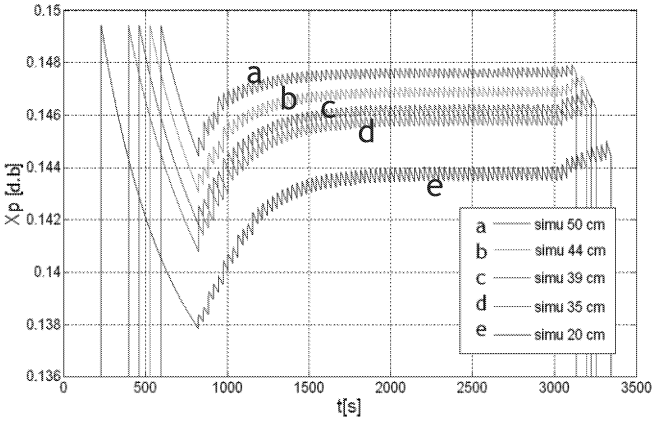

Figure 11a: Pellet moisture content at different levels

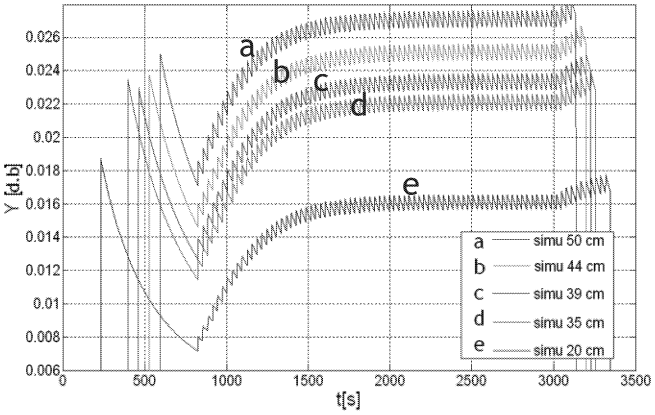

Figure 11b: Absolute humidity of air at different levels

DISCUSSION AND CONCLUSION

As mentioned earlier, our objective in this study is to model drying/ cooling processes of pellets in order to furthermore, optimize their performance in livestock feed production factories, in term of quality management and energy efficiency.

The process deals with very complex systems, with distributed parameters, nonlinear and involving discontinuities at many parts. One can remark that there is indeed no steady state throughout the cooling-drying process, as switches (discrete events) happen over and over again before reaching any equilibrium point.

Nevertheless hybrid approach is undoubtedly the best tool to overcome those problems and helping us to understand better the pellets behavior during the process.

Despite of simplification and assumptions in the modeling, the approach has shown coherence and relatively good shape in describing the process dynamics. In order to describe better the drying process, the continuous-time model shall take into account more parameters, such as air velocity variation during the filling phase at different levels, product temperature and humidity variation during the fall of pellets, etc.

By comparing measurement and simulation, it is true that actually we cannot yet talk about accuracy on values.
For the time being, only temperatures are measured on-line at real time during the process, while we measure the product humidity off-line on inlet and outlet points.

The model-based simulations will help us in predicting the tendency of the product humidity evolution, knowing the temperature at different levels of the pile of pellets.

Furthermore, 'Know-how' and expertise of industrialists will lead us to implement control strategies in order to fulfill the objectives.

REFERENCES

Alur, R., C. Courcoubetis, N. Halbwachs, T.A. Henzinger, P.-H. Ho, X. Nicollin, A. Olivero, J. Sifakis and S. Yovine. 1995. "The algorithmic analysis of hybrid systems". *Theoretical Computer Science*, 138: 3-34

Bird, R. B., W. E. Stewart and E. N. Lightfoot. 2002. *Transport phenomena*.

Boillereaux L., H. Fibrianto and J. M. Flaus. 2002. "Switched linear modelling approach for high-pressure thawing process analysis". *International Journal of Control* (special issue, Nov. 2002), Vol. 75, No 16/17, p. 1260-1268.

Courtois, F. 1991. "Dynamic modeling of drying to improve processing quality of corn". *PhD thesis report*, ENSIA Massy, France.

Courtois, F., A. Lebert, A. Duquenoy, J.C. Lasseran and J.J. Bimbenent. 1991. "Modelling of drying in order to improve processing quality of maize". *Drying Technology* 9(4): 927-945.

Courtois, F., M.A. Archila, C. Bonazzi, J.M. Meot and G. Trystram. 2001. "Modeling and control of a mixed-flow rice dryer with emphasis on breakage quality". *Journal of Food Engineering* 49(4), 303–309.

Fairfield, D.A. 2003. "Pelleting for profit- part 1". *National Grain and Feed Association Feed and Feeding Digest* 54:1-5.

Fibrianto, H., L. Boillereaux and J. M. Flaus. 2003. "Some supervisory solutions for high-pressure thawing modelled by hybrid automata". *IEEE Trans. on Control Systems Technology*.

Fibrianto, H., L. Boillereaux and J. M. Flaus. 2003. "Hybrid Automata: an approach for linearizing the model of High Pressure Assisted Thawing". *Control Engineering and Practice* (Nov. 2003) Vol. 11, Issue 11, p. 1253–1262.

Henzinger, T.A. 1996. "The theory of hybrid automata". In *Proceedings of the 11th Annual IEEE Symposium on Logic in Computer Science*, pp.278-292.

Maier, D.E. and Bakker-Arkema, F.W. 1992. "The counter flow cooling of feed pellets". *Journal of Agricultural Engineering Research*. 53(4):305-320. Purdue AES No. 13420.

BIOGRAPHIES

LIONEL BOILLEREAUX is currently Professor at ONIRIS (College of Veterinary Medicine, Food Science and Engineering of Nantes, France) and exercises his research activity within the Laboratory for Process Engineering, Environment and Food, which is a joint research unit of the CNRS (GEPEA – UMR 6144). With a PhD obtained in 1996 in the Process Control Laboratory of Grenoble, he developed a transverse research activity (Process Control / Chemical Engineering) in the field of Modeling and Control of biotechnological, Food and Thermal processes. His activity generates more than 75 publications in international reviews or peer-reviewed conference proceedings, and he supervised ten PhD students in the field of Process Control or Chemical Engineering.

FRANCIS COURTOIS is currently Professor at AGROPARISTECH (France) and exercises his research activity within the joint research unit of the INRA (GENIAL – UMR 1145). With a PhD obtained in 1991 in the Food Process Engineering Laboratory of MASSY (formerly known as ENSIA), he developed a transverse research activity (Process Control / Chemical Engineering) in the field of Modeling and Control of Food processes. His activity has generated more than 170 publications in international reviews or peer-reviewed journals, books and conference proceedings, and he has supervised 15 PhD students in the field of Food Process Engineering.

HADYAN FIBRIANTO was born in Yogyakarta, Indonesia and is actually research engineer at ONIRIS/TECALIMEN. Holding Bachelor degree in 1997 in Mechanical Engineering from the University of Bordeaux I, France, then Master in 1998 and PhD degree in 2001 in Automatic Process Control Engineering in Nantes (ENITIAA/ONIRIS) and Grenoble (LAG/INPG), France, and experienced in research for food engineering and environment/ biotechnology, also in manufacturing industries (2005-2012), his research interests are quite large, from mathematical modeling, numerical approaches and simulations up to process controls with various applications, like food engineering, environment and biotechnology.

CHARLENE LAMBERT is actually a PhD student in a joint research unit AgroParisTech/INRA/CNAM (UMR1145 – GénIAl). She works in the COOPERE-2 project funded by the French "*Agence Nationale de la Recherche*". She held an Engineering degree (equivalent to a master) in 2009 in Massy (AgroParisTech) in food process Engineering. Her research interests are quite large, from mathematical modeling, numerical approaches and simulations up to energy process optimization with various applications in drying and more globally in food engineering.

FABRICE PUTIER, 52 years old, is managing director at TECALIMAN since 2005. Engineer from the Agro Sup Dijon (Dijon - France) in 1986, school on biological science applied on the food and nutritional research. He is working in TECALIMAN since 24 years on several issues concerning feed safety, such as thermal treatment for detoxification of peas and rapeseed (Hydrothermal treatment and extrusion), HACCP on Salmonella contamination of the feed, HACCP on the additive control (carry-over and mixing behavior), evaluations of the behavior and physical characteristics measurement of the additives, and research of new external tracers for carry-over and mixing measurement tools.

SANDY ROUCHOUSE is engineer at TECALIMAN, a technical center for feed industries, since 2006. Holding a degree in Agricultural Engineering of ENSAIA in Nancy in 2005, she is expert in animal feed production. She works on several topics such as shrinkage in food processing, pelleting process, heat treatment.

FOOD PROCESSING AND SAFETY

Transfer of *Salmonella* during slicing of a turkey breast based product

Guiomar Denisse Posada Izquierdo[a], Arícia Mara Melo Possas[b], Antonio Valero Diaz[a], Fernando Pérez Rodríguez[a], Rosa Maria Garcia Gimeno[a]

[a] Department of Food Science and Technology. International Campus of Excellence in the AgriFood Sector ceiA3. University of Cordoba. Campus de Rabanales. 14014, Córdoba (Spain)

[b] Department of Food Science, Faculty of Food Engineering, State University of Campinas (UNICAMP), Campinas-SP, Brazil

Keywords
Cross-contamination with *Salmonella* during slicing. Transfer of *Salmonella* to turkey breast based product. Use of essential oil in packaging innovation of sliced meat products. Essential oils as natural preservatives of meat products

Abstract
The present study focused on meat product innovation applying essential oil of thyme with antibacterial effect against *Salmonella*, as proposal for an improvement of the active packages. The scenario of a possible cross-contamination during slicing was chosen. Four conditions were evaluated combining food product of turkeys breast, one with preservative and another without, and covered or not with thyme oil. Good results have been obtained, a significant reduction of bacteria was observed and at the same time the product covered with essential oil was sensory acceptable.

1. Introduction

There is a growing interest and intense research about natural antimicrobial substances that can be applied in the food industry, especially read-to-eat products (Mohammad Jouki et al. 2014). These substances can be incorporated in active packaging, like edible coatings, and this system can extend the shelf-life of foods and reduce the risks associated with their consumption (Hyldgaard et al., 2012).

Among these substances with antimicrobial potential are the essential oils, which are secondary metabolites of plants. Thyme and Oregano essential oils are commonly studied to be applied in the meat industry, since their major compounds, such thimol and carvacrol, have their antimicrobial property already recognized (Juneja et al., 2012; Solomakos et al., 2008). The essential oils are very versatile, since they can be used in food industry as flavoring, antimicrobial and antioxidant ingredients (Nowak, et al., 2012).

Cross contamination is one of the most important contributing factors in foodborne illnesses originating in household environments. The slicing process of meat is well known to be one of the vehicles of cross-contamination in foods, principally in the read-to-eat meat products industry (Chen et al., 2014). *Listeria monocytogenes*, *Salmonella* and *E.*

coli O157:H7 are the pathogens most associated with cross contamination on these environments. For this reason, the risks of cross-contamination are increased by the contact of foods and contaminated surfaces, like the slicer blade of the slice machine (Carrasco et al., 2012; Pérez-Rodríguez et al., 2008). So, the slicing procedure is of special concern as it is conducted at ambient temperature and the equipment is used in a random way and in an intermittent manner.

The slice machines have been associated with pathogens in retail RTE meat products (Hoelzer et al., 2011). These circumstances increase the risk on the safety of these products, information that is confirmed in the report of the FDA (2013), and was studied by several researchers (Pérez-Rodríguez et al, 2007; Hoelzer et al, 2012; Chaitiemwong et al., 2014).

The latest consumer trends show their tendency towards ready to eat products and with different formulations, such as reduced-salt, no preservatives, formulations that make these types of products to be recognized as healthy. These circumstances may favor bacterial growth, therefore, in this study we evaluate the antimicrobial activity of thyme essential oil, a natural antimicrobial, against *Salmonella* during the slicing process of turkey breast based products, simulating an active packaging system.

2. Material and Methods

2.1. Meat product

A turkey breast based product was used to simulate a delicatessen meat product that could be cross contaminated during slicing. Two turkey breast based formulations, produced by different companies, were analyzed: A and B. The formulation A doesn't contain preservatives, colorants and fat. The formulation B has the same characteristics of fat as product A, but contains preservatives commonly used in meat conservation (E-306, E-331, E-250) and has a reduced salt concentration. Furthermore, the meat products were treated or not with a solution containing thyme essential oil before procedure.

2.2. Preparation of thyme essential oil solution

The products were treated or not with a solution of thyme essential oil (La Casa de Jabones, Spain), to evaluate its antimicrobial activity on a meat product when used in coatings composition. The minimum inhibitory concentration (MIC) of this essential oil was previously determined in vitro against the *Salmonella* Enteritidis strain used as inoculum. The solution was prepared with sterilized water containing 10 % (v/v) of Tween 80 (Panreac, Spain) as an emulsifier. The concentration of essential oil used was equivalent to fifty times the MIC value (0,625 µL/mL). This concentration was sensory acceptable in tests conducted previously. The products were introduced in plastic bags with 10 mL of the essential oil solution, and massaged for 10 minutes so the products were coated with it, simulating the transfer of essential oil that could be achieved with the use of edible coatings.

2.3. Inoculum preparation

Salmonella Enteritidis (ATCC 13076), obtained from the Spanish Type Culture Collection (CECT),

was maintained at -18 °C in cryovials containing beads and cryopreservative (Microbank). Two days before each experiment, a bead of each strain was transferred to a tube containing 4.5 mL of Brain Heart Infusion broth (Oxoid, UK) and incubated at 37 °C for 24 h. Then, 0.5 mL of the initial subculture was pipetted into a tube containing 4.5 ml of BHI, and incubated at 37 °C for 24 h, until the bacteria reached the early stationary phase (approximately 20 hours). Subsequently, we proceeded to remove the growth broth (BHI) through three consecutive washings with 5.0 mL of Phosphate Buffer Solution (PBS, Oxoid, UK). The meat broth was used to simulate soiled conditions on the blades. An aliquot of 1.0 mL was serially diluted and surface plated onto Xylose Lysine Deoxycholate agar (XLD, Oxoid, UK) and colonies were counted to determine the initial concentration of the studied culture, which was nearly 10^9 cfu/mL.

2.4. Preparation of meat broth

A meat broth was used to simulate soiled conditions on the blades. To obtain sterile meat broth, meat cubes (2 x 2 x 2 cm) of turkey breast based product were homogenized with 10 mL of saline solution in the Stomacher equipment for 2 minutes, and then filter-sterilized (through a 0.22 microns filter, Millipore, USA). The meat broth was stored under refrigeration and before use it was thawed at room temperature for 1 h. Tween 80 was added to the meat broth in a concentration of 10 % (v/v) in order to facilitate the dispersion of inoculum on the blades. An aliquot of 0.5 mL of the culture of *Salmonella* prepared as cited previously were transferred to a tube containing 4.5 mL of meat broth, so as to obtain a final concentration of 10^8 cfu/mL on the blades.

2.5. Slicing machine and artificial contamination

Before use, a domestic slicer and polished stainless steel blades (Bosch, Germany) were washed and disinfected with 70 % (v/v) ethanol (Panreac, Spain) and exposed to UV radiation for 10 min. The ethanol was allowed to evaporate prior to any contamination step. Subsequently, 0.5 mL of meat broth containing inoculum at a concentration of 10^8 cfu/mL was evenly distributed on the blades with the aid of a pipette (Figure 1). The inoculums were allowed to dry in a laminar flow cabinet for 30 minutes, at 25 °C and 50 % relative humidity. Before the experiments, a test with the evaluated *Salmonella* strain showed that it was able to survive on stainless steel surfaces under soiled and cleaned conditions.

2.6. Transfer of *Salmonella* Enteritidis from contaminated blades via the slicer to uninoculated meat product by slicing

After drying, the inoculated blades were placed in the slicer, and then the turkey breast based products were sliced up to 21 times to yield slices (14–16 g each), as can be seen in Figure 1. Each slice was picked up as it came off the machine using a pair of sterilized pincers and placed in sterile stomacher bags. Three repetitions for each treatment were performed. The products had a plain and uniform surface of slicing, so all slices had a similar area and weight.

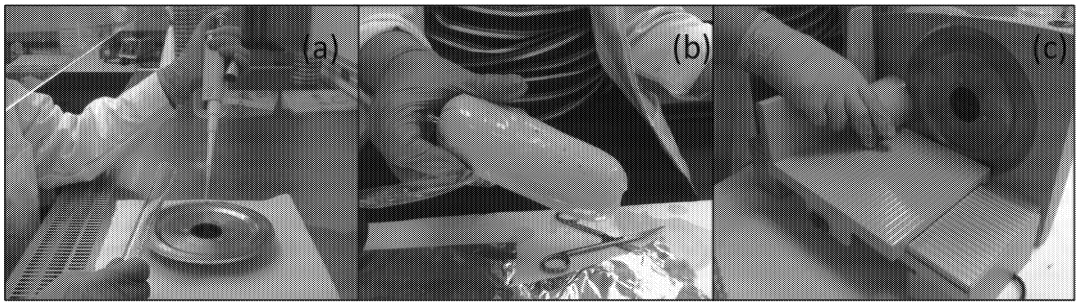

Figure 1- Experimental procedure: (a) artificial contamination of the blade; (b) turkey breast product to be sliced (c) slicing of the turkey breast product with transfer of the studied pathogen from the blade.

2.7. Quantification of transfer

To estimate the number of viable cells transferred during the slicing process (up to 21 slices), slices were placed independently into sterile stomacher bags and filled with peptone buffer water at 1 % and then homogenized in the Stomacher for 2 min. The volume of peptone water in each bag varied according to the weight of each slice, in order to achieve a decimal dilution. Serial decimal dilutions were prepared in the first six slices with peptone water. In all cases the homogenized was cultured on XLD agar plates with the Spiral Plate equipment (Eddy Jet, IUL, SA), incubated at 37 °C for 24 hours, and the number of viable cells was determined. The homogenized of the first slice was also cultured on Plate Count Agar (PCA, OXOID) plates, in order to verify the natural microflora present on the products. As required, the samples giving no detectable counts by direct plating were submitted to the filtration using filters of 0.22 µm. The filters were directly placed onto XLD agar plates, incubated at 37 °C for 24 hours, and the number of viable cells was determined in each case. The detection limit varied depending on the slice weight and inoculated area.

2.8. Data and statistical analysis

The concentration of pathogen on the slices was expressed per cm² of slice and logarithmically transformed (log cfu/cm^2) in Excel (Microsoft Corporation) spreadsheet. In this study, it was estimated the transfer coefficient which is the logarithm of the proportion (%) of bacterial cells transferred from the blade to each slice (expressed per cm^2). The transfer coefficient were tested by analysis of variance (ANOVA), and Duncan's multiple-range tests using STATISTICA® software, version 10, for the factors, type of turkey breast meat formulation and the treatment with or without thyme essential oil coating solution.

3. Results and Conclusions

The transfer of *Salmonella* from the contaminated blades during slicing of the turkey breast based product was significant ($p \leq 0.05$). *Salmonella* could be detected in all the 20 slices evaluated when formulations were not treated with essential oil, though it was verified that the strain used in this study is really sensitive under stress

conditions. So, it is clear that cross-contamination with this microorganism can happen between the blade and the meat product during slicing.

Cells transferred per slice decreased logarithmically from the first documented slice to the last slice in all treatments evaluated. As expected, the first slices had the highest contamination levels, and the risk of illness would be higher after eating these compared to the subsequent slices. Cells could not be detected in the last slices of the formulations treated with thyme essential oil. These results are graphically represented in Figure 2.

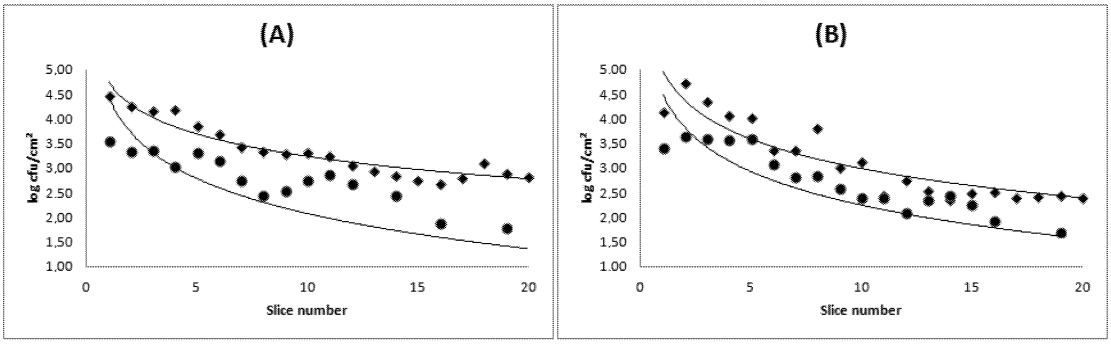

Figure 2- Transfer (log cfu/cm²) of *Salmonella* from an inoculated slicer: (A) Formulation A; (B) Formulation B; (◆) Formulations not treated with essential oil; (●) Formulations treated with essential oil.

In the case of the product coated by a solution of thyme essential oil, it could be observed that the number of viable cells detected after slicing was lower in comparison with the number of viable cells detected on the formulations that were not coated, showing that this essential oil have an antimicrobial effect against *Salmonella*. The incorporation of thyme essential oil on active packaging could be a good alternative to the use of chemical preservatives in the conservation of the evaluated meat product.

The presence of food preservatives in formulation B doesn't seem to influence the transfer of *Salmonella* to the meat product during the slicing procedure in comparison with formulation A. However studies to determine how the formulation of these meat products affects the survival capacity of *Salmonella* during the shelf-life at different temperatures are currently being conducted by our research group.

4. Acknowledgements

The research has been funded by the Project of Excellence P08-CT5-3620 from the Andalusia government and the European Regional Development Fund (ERDF). This work has been performed by the AGR-170 research group, HIBRO, of the Research Andalusian Plan. Arícia Mara Melo Possas is holder of a scholarship of the "Santander Formula" program, of the Santander bank.

5. References

- Carrasco, E., Morales-Rueda, A., & García-Gimeno, R. M. (2012). Cross-contamination and recontamination by Salmonella in foods: A review. *Food Research International, 45*(2), 545-556.
- Chaitiemwong, N., Hazeleger, W., Beumer, R., Zwietering, M. 2014. Quantification of transfer of Listeria onocytogenes between cooked ham and slicing machine surfaces. Food Control

- Chen, D., Zhao, T., Doyle, M. 2014. Transfer of foodborne pathogens during mechanical slicing and their inactivation by levulinic acid-based sanitizer on slicers. Food Microbiology 38, 263–269. FDA, 2013. FDA Draft Interagency Risk Assessment – Listeria Monocytogenes in Retail Delicatessens Technical Report (2013) Available at: http://www.fda.gov/downloads/Food/FoodScienceResearch/RiskSafetyAssessment/UCM351328.pdf
- Hoelzer, K., Pouillot, R., Gallagher, D., Silverman, M. B., Kause, J., & Dennis, S. (2012). Estimation of Listeria monocytogenes transfer coefficients and efficacy of bacterial removal through cleaning and sanitation. *International Journal of Food Microbiology, 157*(2), 267-277.
- Hoelzer, K., Sauders, B., Sanchez, M., Olsen, P., Pickett, M., Mangione, K., Rice, D., Corby, J., Stich, S. Fortes, E., Roof, S.. Grohn Y., Wiedmann, M., Oliver H. 2011. Prevalence, distribution, and diversity of Listeria monocytogenes in retail environments, focusing on small establishments and establishments with a history of failed inspections. Journal of Food Protection, 74, 1083–1095.
- Hyldgaard, M., Mygind, T., & Meyer, R. L. (2012). Essential oils in food preservation: Mode of action, synergies, and interactions with food matrix components. *Frontiers in Microbiology, 3*(JAN).
- Juneja, V. K., Dwivedi, H. P., & Yan, X. (2012). Novel natural food antimicrobials*. *Annual Review of Food Science and Technology, 3*(1), 381-403.
- Mohammad Jouki, Seyed Ali Mortazavi, Farideh Tabatabaei Yazdi, Arash Koocheki. 2014. Characterization of antioxidant–antibacterial quince seed mucilage films containing thyme essential oil. Carbohydrate Polymers 99, 537–546.
- Nowak, A., Kalemba, D., Krala, L., Piotrowska, M., Czyzowska. A. 2012. The effects of thyme (*Thymus vulgaris*) and rosemary (*Rosmarinus officinalis*) essential oils on Brochothrix thermosphacta and on the shelf life of beef packaged in high-oxygen modified atmosphere. Food Microbiology 32, 212–216.
- Pérez-Rodríguez, F., Valero, A., Carrasco, E., García, R. Ma, & Zurera, G. (2008). Understanding and modelling bacterial transfer to foods: a review. *Trends in Food Science and Technology, 19*(3), 131-144. doi: 10.1016/j.tifs.2007.08.003
- Pérez-Rodríguez, F., Valero, A., Todd, E. C. D., Carrasco, E., García-Gimeno, R. M., & Zurera, G. (2007). Modeling transfer of Escherichia coli O157:H7 and Staphylococcus aureus during slicing of a cooked meat product. *Meat Science, 76*(4), 692-699.
- Solomakos, N., Govaris, A., Koidis, P., & Botsoglou, N. (2008). The antimicrobial effect of thyme essential oil, nisin, and their combination against Listeria monocytogenes in minced beef during refrigerated storage. *Food Microbiology, 25*(1), 120-127.

MODELING OF SHRINKAGE, MICROBIAL SPOILAGE AND COLOR DEGRADATION OCCURRING IN CONVECTIVE DRYING OF VEGETABLES

Stefano Curcio*, Vincenza Calabrò, Gabriele Iorio.
Department of Computer Engineering, Modeling, Electronics and Systems
Laboratory of Transport Phenomena and Biotechnology
University of Calabria – Ponte P. Bucci, cubo 39/c
Rende (CS) – Italy
E-mail: stefano.curcio@unical.it

KEYWORDS
Transport Phenomena, Shrinkage, *Listeria monocytogenes*, Food quality, Food safety.

ABSTRACT

In this work, the formulation of a theoretical model aimed at providing a complete description of vegetables convective drying was presented. The proposed approach was based on the coupling of four different models. In particular, a multiphase transport phenomena model predicted the simultaneous transfer of momentum, heat and mass, occurring in both the drying chamber and the food. A structural mechanics model estimated the sample deformations, strictly related to food shrinkage, as due to moisture loss. A product decontamination model calculated the microbial inactivation kinetics of *Listeria monocytogenes* and, finally, a macroscopic model estimated the vegetables color changes, expressed in terms of the Hunter parameters. The system of non-linear, unsteady-state, partial differential equations modeling the drying process was solved by an Arbitrary-Lagrangian-Eulerian-based finite elements formulation, which, by a proper modification of the integration domains (food and air), allowed accounting for shrinkage effects. The effects of operating conditions on drying performance were ascertained by analyzing the time evolution of several variables. Among these, the spatial distributions of temperature, water activity, moisture content, strain and stress, as well as the variation of food dimensions, as due shrinkage, the color degradation, chosen as a reference quality parameter, and the microbial population decay, chosen as a measure of food safety, were considered as the most important.

INTRODUCTION

Drying represents one of the most important techniques for preservation of biological products. When moisture removal is promoted by a heating process, like in the case of hot convective drying, the decontamination of food surface could be achieved, particularly if drying air temperature is properly chosen. The main aim of convective drying, hence, is to ensure that surviving microorganisms are reduced to an acceptable level, which delays spoilage of food product, thus enhancing its safety (Halder et al. 2011). Besides the heat effects, the associated reduction of water activity promotes food preservation, by avoiding microbial growth and chemical reactions causing deterioration. Most spore-forming organisms (e.g., Bacillus species) do indeed not grow at water activity values smaller than a threshold, usually equal to 0.93 (Valdramidis et al. 2006). However, during thermal drying, food quality could worsen; the loss of water is indeed responsible for profound modifications of mechanical and structural properties of dehydrated foods (Bernstein and Noreña 2014), as well as for the degradation of many essential organoleptic characteristics. The removal of water from a porous solid material is indeed responsible for the development of a field of contracting stresses in the matrix (Kowalski and Mielniczuk 2006). An ever-different mechanical equilibrium of the material is attained and a change both of its shape and dimensions is observed. Drying methods as well as the exploited operating conditions differently affect both the quality and the main characteristics of dried foods (Panyawong and Devahastin 2007). Among these characteristics, color is traditionally considered as one of the key quality attributes of foods and vegetables due to its strong relationship with flavor and aroma (Spence et al. 2010).

The chosen set of operating conditions in which dehydration process is performed, plays a key role on both dried product quality and its safety (Calín-Sánchez et al. 2013). The exploitation of drastic operating conditions, namely high dry bulb temperatures and low relative humidity of drying air, generally results in higher drying rate, in more efficient reduction of microbial population (improvement of food safety), but also in more significant deterioration of food organoleptic characteristics (lower product quality) (Fernández-Sandoval et al. 2012). The utilization of mild or very mild operating conditions generally determines an opposite behavior: the organoleptic properties of dried foods do certainly improve, but proper decontamination of final product may not be assured (Ahmad-Qasem et al. 2013). It is, therefore, necessary to identify a specific set of operating conditions, which have to be chosen so to achieve a trade-off between high quality and safe dried foods. The identification of such a set of operating conditions can be attained by defining, in a systematic and rigorous way, an optimization problem whose solution, actually representing the best compromise among several conflicting demands, has to be calculated by efficient algorithms. To be efficient, any optimization method requires, as a fundamental starting point, a reliable mathematical model capable of predicting how system responses may change, with time, under the influence of both external disturbances and manipulated variables. However, in the case of food convective drying,

the formulation of such a theoretical model may represent a rather challenging task. A simultaneous transfer of heat and water (both as liquid and as vapor) takes place so that heat is transported from air to the material, whereas water is transported from the food core, then to its surface, and, eventually, to drying air (Chua et al. 2002). In addition, the dependence of food transport properties on the local values of temperature and moisture content, the complex fluid-structure interactions as caused by airflow, the time variation of food shape and its dimensions are to be accounted for to properly predict drying process behavior. Datta's research group proposed several comprehensive and general multiphase models aimed at estimating the heat and mass transfer rates in different industrial processes involving foods (Datta 2007, Dhall and Datta, 2011). In Datta's papers, the transport phenomena occurring at food/air interfaces were described in terms of heat and mass transfer coefficients estimated from semi-empirical correlations and referred to samples having a constant characteristic dimension. When food shape is not regular or it even changes with time, i.e. when shrinkage is significant, the exploitation of literature correlations might significantly limit the model accuracy, thus providing unreliable predictions. The transport phenomena occurring in the air and the complex interactions between air and food significantly affect the interfacial heat and mass transfer rates and, therefore, the overall process performance (Curcio et al. 2008). A rigorous analysis of the transport phenomena occurring in air as well as in food results in coupled non-linear partial differential equations that can be solved by cumbersome numerical methods (Curcio 2010), which are time-consuming and difficult to incorporate in on-line control devices. In a previous work, one of the authors of the present paper already developed an accurate theoretical model aimed at describing the transport phenomena occurring both in the food and in the drying air and at predicting the time evolutions of food temperature and moisture content distributions (Curcio 2010). A multiphase approach was adopted; the model, due to its versatility, provided reliable predictions of convective drying and was tested over a wide range of operating and fluid-dynamic conditions on vegetables, available in different shapes.

As compared to the drying models available in the literature, the main innovations introduced by the present paper regarded: a) the description of the anisotropic change of food dimensions, as determined by the local values of moisture transfer rate. b) The evaluation, without resorting to any semi-empirical correlation, of the interfacial heat and mass fluxes; in the case of shrinking materials, this definitely represented a significant breakthrough since the correlations currently available were obtained defining a constant characteristic geometric dimension, generally referred to regular shapes. The present model, instead, accounted for the continuous variation of food shape, as well as of the exposed surfaces, thus allowing reliable predictions of real driers performance. c) The calculation of the actual microbial inactivation kinetics and color changes occurring during vegetables drying.

The formulated model can be exploited to analyze the convective drying behavior over a wide range of process conditions and to develop computational tools aimed at attaining specific control objectives, represented by a trade-off between quality and safety of dried foods.

THEORETICAL

The food under study was a cylindrical potato sample characterized by fixed initial values of both length and diameter. The potato sample was placed on a stainless steel ultrathin wide-mesh net, 0.040 m far from the inlet section of a cylindrical drying cell, whose length and diameter were fixed, as well. Drying air, characterized by definite values of temperature (T_a), relative humidity (H) and velocity (v_0) measured at drier inlet section, was continuously flowing in the axial direction, parallel to food sample length. The present model was referred to spatial domains (food and air), which changed their shape and dimension because of potato anisotropic shrinkage.

The main assumptions exploited to formulate the transport model were: a) cylindrical symmetry, which allowed restricting the analysis to a 2D geometry. b) Thermal equilibrium of all the phases involved in the drying process. c) Negligibility of any possible interaction, regarding both transport phenomena and structural mechanics calculations, at the contact points between food and net.

As compared to the studies already published by the authors of the present paper (Curcio et al. 2008; Curcio 2010; Curcio and Aversa 2014), some simplification hypotheses were dropped out. In particular, food sample was considered as a hygroscopic porous medium and not as a fictitious continuum. Then, the gas pressure gradients, necessary for a proper calculation of both liquid water, vapor and air transport in the food were considered as relevant and, therefore, included in the multiphase transport model. The convective heat transfer in food sample was taken into account, as well.

The unsteady-state heat and mass balance equations, referred to the transport of liquid water, vapor and air in the food sample were formulated and coupled to the unsteady-state momentum balance, to the continuity equation and to the energy and water vapor/air balance equations, referred to air domain. It is worthwhile remarking that the proposed model allowed calculating, by the well-known k-ω model, the velocity field of drying air, flowing, in turbulent conditions within the drying chamber, around the potato sample. A set of initial and boundary conditions was exploited to complete the definition of the transport model and, therefore, to carry out the numerical simulations, which were aimed at determining the effect of operating conditions on food shrinkage, on microbial inactivation kinetics and on potato color changes.

The structural changes occurring in potatoes as drying proceeded were estimated combining the above-described transport model to a structural mechanics model, which allowed calculating the stresses developing in the sample as a result of water removal. It was assumed that potatoes behavior was elastoplastic within a not large strain region. In addition, the local total strains, actually depending on the total displacements, were assumed equal to the changes both of mechanical strains, i.e. the constrained deformation due to mechanical elastoplasticity, and of shrinkage strains, representing the free deformation due to moisture loss. The

stress–strain relationship was expressed through the elastoplastic stress-strain matrix, which accounted for the Young modulus, the Poisson ratio, the strain-hardening rate, the shear modulus, the equivalent stress, and the deviatoric stresses. To complete the formulation of the present transport/structural mechanics model, it was assumed that the variation with time of the free shrinkage strain was proportional to the water concentration variation, defined with reference to the initial water concentration in the sample; the validity of such an assumption was already proven in a previous paper (Curcio and Aversa 2014). The virtual work principle was eventually formulated to obtain the equilibrium equation necessary to complete the structural mechanics model. It was assumed that zero body and surface forces were applied to food.

The above-described model, however, did not give any indication about the progress of product decontamination and the color changes of dried potatoes. For this reason, two additional models were incorporated in the transport/ structural mechanics model, with the specific aim of relating the calculated time evolutions of food moisture content and temperature distributions, strictly dependent on drying operating conditions and on food volume variations, to both microbial inactivation and color degradation. Among the bacteria that might proliferate on vegetables surface, *Listeria monocytogenes* was taken into account due to the safety problems arising when such a microorganism is not properly inactivated during food drying. As proposed by Valdramidis et al. 2006, potatoes decontamination was described considering the strong relationship between microbial population decay and both temperature and water activity on food exposed surfaces. Therefore, a model predicting the time evolutions of microbial population was formulated as a function of the so-called specific inactivation rate, whose value depended on the actual distributions of temperature and water activity, as calculated by the transport/structural mechanics model, on food external surfaces. It is worthwhile remarking that, according to the model, no decontamination can be attained if surface potato temperature is lower than 320.75 K, defined as the "growth–no growth boundary".

To predict the kinetics of color changes occurring during drying, the simplified model proposed by Krokida et al. 1988 was exploited. Such a model expresses the time variation of each of the so-called Hunter parameters, namely redness, yellowness and lightness, in terms of a first order kinetics, depending on both dry-bulb temperature and relative humidity of air at the inlet section of drying cell.

NUMERICAL PROCEDURE

On the basis of the above discussion, it is evident that the time evolution of food moisture content had a strong influence on the total strains and, therefore, on sample displacements. These, in turn, were responsible for a time variation of food shape and dimensions. Such a variation significantly affected the transport phenomena occurring at the food/air interfaces and the actual drying rates, too. The local changes of both water activity and temperature on food external surfaces had an effect on the local values of specific inactivation rate and, therefore, on *Listeria monocytogenes* population decay. In addition, it is worthwhile remarking that the chosen set of operating conditions did actually affect not only the transfer rates and the shrinkage extent, but also the changes of Hunter parameters.

The continuous and anisotropic variation of food/air interfaces, as determined by shrinkage, was described by introducing a local modification of food and air domains. The transport equations, written for both air and food, the virtual work principle and the models predicting both the food color changes and the microbial population decay represented a system of unsteady, non-linear, partial/ordinary differential equations that could be solved only by a numerical method. The Finite Elements Method (FEM), implemented in Comsol Multiphysics 4.4, was exploited. The system of PDEs was referred to a time dependent deformed mesh, accounting for food shrinkage. The variation with time of integration domains was described by an Arbitrary-Lagrangian-Eulerian (ALE) method. The deformed mesh motion, strictly dependent on moisture removal and resulting from the solution of the structural mechanics problem, was modeled by the Laplace smoothing. Food and air domains were discretized into a total number of 27612 triangular finite elements leading to about 381000 degrees of freedom. In particular, the mesh consisted of 7823 elements (with a minimum element quality of 0.88) and of 19789 elements (with a minimum element quality of 0.81), respectively, for food and air. The considered mesh provided an adequate spatial resolution for the system under study. The solution was independent of the grid size, even with further refinements. Lagrange finite elements of order two were chosen for all the state variables defining the problem, but for pressure, for which a linear interpolating function was chosen. The time-dependent problem was solved by an implicit time-stepping scheme, leading to a non-linear system of equations for each time step. The Newton's method was used to solve each non-linear system of equations, whereas a direct linear solver was adopted to solve the resulting systems of linear equations. On a quad-core computer running under Windows 8, a typical drying process lasting 5 hours was simulated in about 3 hours.

RESULTS AND DISCUSSION

The proposed transport/structural mechanics approach, combined with the models predicting both the microbial population decay and the color changes, allowed achieving a detailed description of the influence of operating conditions on several variables, which definitely play a key role on drying process behavior. The formulated model is definitely a reliable tool for the identification of the regions (or the points) where potato moisture content, strictly related to water activity, and its temperature might determine microbial spoilage. In addition, both the strains and the stresses developing within food sample and resulting from moisture removal may provide very useful indications about dried potatoes mechanical properties, which certainly represent important indexes ascertaining food quality. A comprehensive analysis about the mutual interactions among the operating conditions, the distribution of some key variables, namely temperature, moisture content, water activity, strains, stresses, and the product quality and its safety may certainly pave the way for a true optimization of

vegetables drying process. As described in the following, such an optimization is based on the definition of a proper objective function that, subjected to a set of constraints, has to be minimized (maximized) by changing the operating conditions in which drying is performed.

Fig. 1 shows, in a typical case, the time evolution of food moisture content distribution (on a dry basis), X_b, referred to the half section of potato sample. Food had not an isotropic deformation; this is due to strain and first principal stress distributions (data not shown) developing in food as drying proceeds. Such a deformation, caused by moisture transfer from food to drying air, determined a progressive reduction of food sample dimensions (shrinkage). In addition, it should be noted that external surfaces got dry quickly than the inner regions and that the process was much faster on the surface where drying air did actually impinge.

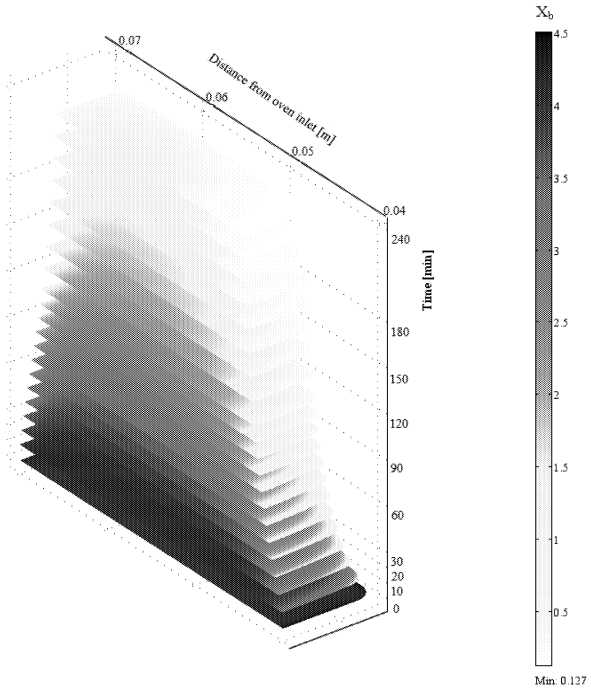

Figure 1: Time evolution of food moisture content distribution and of food sample shrinkage (T_a = 348 K, H = 40%, v_0 = 2.2 m/s, Xb_0 = 4.5)

The present model, however, could also describe the behavior of drying process from a macroscopic point of view, by analyzing the time-evolution of some characteristic quantities averaged either over the entire sample volume or over each of the external food surfaces. This is particularly interesting for the identification of some "critical" boundaries/points on which the combination of temperature and water activity may determine an improper decontamination of food surface. In particular, it was found that, as drying proceeded, potato rear surface, due to the existence of a rather wide segregation region resulting in an inefficient air circulation (Curcio et al. 2008), was characterized by an almost constant temperature (equal to air wet bulb temperature) and by water activity values close to unity and, therefore, well above the threshold value of 0.93 below which most spore-forming organisms do not grow. It is worthwhile observing that, in some of the tested conditions, the rear surface temperature, practically corresponding to air wet bulb temperature for most of the considered timespan, was even lower than the so-called "growth–no growth boundary" that represented the threshold below which no *Listeria monocytogenes* inactivation actually occurred (Valdramidis et al. 2006). The calculated dynamic inactivation curves of *Listeria monocytogenes*, expressed as the logarithm of the ratio between actual microbial population and initial microbial population, N/N_0, are shown, with reference to food rear surface, in Fig. 2. It can be observed that decontamination process is more efficient and faster at higher values of air relative humidity inflowing the drying cell. This is due to the higher values of food surface temperature that are attained as H increases. Although the operating temperature was rather large, it can be observed that, when H was equal to 35%, the microbial population reduction was only three orders of magnitude lower than the initial microbial population; this could be unacceptable in many cases. A deeper analysis of the process under study shows that a rather wide combination of possible operating conditions (Tab. 1) is actually characterized by a wet bulb temperature (to which food rear surface temperature tends to be equal) lower than the growth–no growth boundary. Such combinations of T_a and H should be carefully exploited (or even avoided) if a proper product decontamination has to be attained.

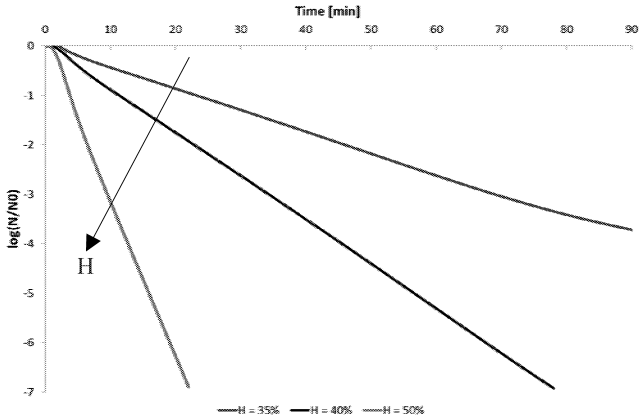

Figure 2: Dynamic inactivation of *Listeria monocytogenes* on the rear surface of potato sample (T_a = 343 K)

Table 1: Values of wet bulb temperature corresponding to different combinations of T_a and H (**bold** values are lower than the "growth–no growth boundary")

H [%]	T_a = 323 K	T_a = 333 K	T_a = 343 K	T_a = 353 K	T_a = 363 K
20	***301.3***	***307.8***	***314.5***	321.4	328.4
30	***305.3***	***312.7***	***320.2***	327.9	335.7
40	***308.7***	***316.8***	324.9	333.2	341.5
50	***311.8***	***320.3***	328.9	337.6	346.4

Fig. 3 shows the calculated variations of yellowness (Δb), representing one typical quality attribute, as a function of the exploited operating conditions. As drying proceeded, more evident color changes are observed as drying temperature decreases and, correspondingly, relative humidity increases.

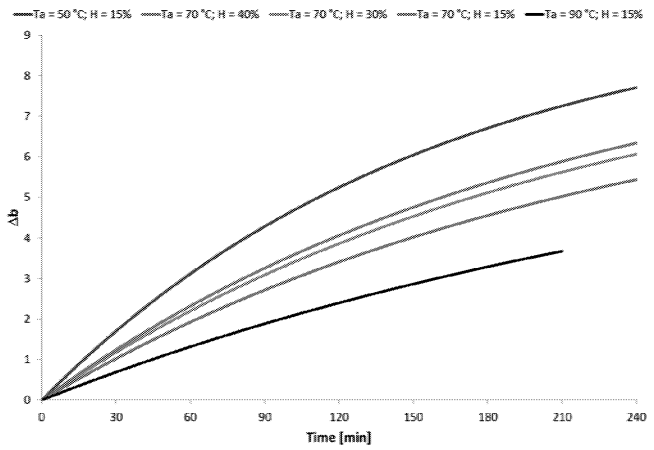

Figures 3: Color difference Δb (yellowness) for potatoes during convective drying at different values of temperatures and air relative humidity

A versatile optimization model was finally formulated to analyze different scenarios, each of them characterized by a definite objective function and a set of constraints to be satisfied. In particular, the above-described mathematical model, given as the combination of the transport phenomena/structural mechanics model, of the product decontamination model and of the model describing the kinetics of color changes, predicted how drying process responses changed, with time, under the influence of operating conditions in which convective drying was performed. The distributions of water activity and temperature on food surfaces allowed determining the time evolution of microbial population (N/N_0), which represented one of the chosen design variables; in addition, the variation of both redness (Δa) and yellowness (Δb) with respect to their initial values were chosen as key parameters expressing food quality. The versatility of the present optimization model allowed choosing different objective functions and describing different scenarios. The technical feasibility of several sets of operating conditions and the resulting effects on both color degradation and product decontamination were, therefore, analyzed assuring, however, that a complete decontamination of dried vegetable had to be achieved. Attention was paid, in particular, to the critical points located on the rear surface, where the combination of temperature and water activity could result in an inefficient (or unacceptable) decay of microbial population. A derivative-free method, called Conjugate Direction with Orthogonal Shift (CDOS) was chosen as the optimization algorithm. The CDOS routines were coupled to the formulated mathematical model in order to determine the values of operating conditions that are to be used to achieve the minimization of specific objective functions subject to a set of constraints.

CONCLUSIONS

A general approach to predict a series of crucial variables, namely the extent of food shrinkage, the microbial population decay and the color changes occurring during food convective drying was presented. It was proven that the proper integration of different models in a unique computational environment allows simulating convective drying over a wide range of operating conditions and may also represent the core of a rigorous optimization model, aimed at achieving specific control objectives. The proposed computational tool can be exploited to determine the set of operating conditions, which enhance the quality and the safety of dried vegetables, thus minimizing expensive and time-consuming pilot test-runs.

REFERENCES

Ahmad-Qasem, M. H.; Barrajon-Catalan, E.; Micol, V.; Cárcel, J. A. and Garcia-Perez, J.V. 2013. *Influence of air temperature on drying kinetics and antioxidant potential of olive pomace.* J. Food Eng. 119, 516-524.

Bernstein, A. and Noreña, C. P. Z. 2014. *Study of Thermodynamic, Structural, and Quality Properties of Yacon (Smallanthus sonchifolius) During Drying*. Food Bioprocess Tech. 7 (1), 148-160.

Calín-Sánchez, A.; Figiel, A.; Hernández, F.; Melgarejo P.; Lech, K. and Carbonell-Barrachina, A. A. 2013. *Chemical Composition, Antioxidant Capacity, and Sensory Quality of Pomegranate (Punica granatum L.) Arils and Rind as Affected by Drying Method*. Food Bioprocess Tech. 6, 1644–1654.

Chua, K. J.; Chou, S. K.; Hawlader, M. N. A.; Mujumdar, A. S. and Ho, J. C. 2002, *Modelling the Moisture and Temperature Distribution within an Agricultural Product undergoing Time-varying Drying Schemes*. Biosyst. Eng. 81, 99-111.

Curcio, S.; Aversa, M.; Calabrò, V.; and Iorio, G. 2008. *Simulation of food drying: FEM analysis and experimental validation*. J. Food Eng. 87, 541–553.

Curcio, S. 2010. *A multiphase model to analyze transport phenomena in food drying processes*. Dry. Tech. 28, 773-785.

Curcio, S. and Aversa, M. 2014. *Influence of shrinkage on convective drying of fresh vegetables: a theoretical model*. J. Food Eng. 123, 36–49.

Datta, A. K. 2007. *Porous media approaches to studying simultaneous heat and mass transfer in food processes. I: Problem formulations*. J. Food Eng. 80, 80-95.

Dhall, A., Datta, A. K. 2011. *Transport in deformable food materials: A poromechanics approach*. Chem. Eng. Sci. 66, 6482–6497.

Fernández-Sandoval, M.T.; Ortiz-García, M.; Galindo, E. and Serrano-Carreón, L. 2012. *Cellular damage during drying and storage of Trichoderma harzianum spores*. Process Biochem. 47, 186-194.

Halder, A.; Dhall, A.; Datta, A. K.; Black, D. G.; Davidson, P.M.; Li, J. and Zivanovic, S. 2011. *A user-friendly general-purpose predictive software package for food safety*. J. Food Eng. 104, 173–185.

Kowalski, S. J.; Mielniczuk, B. 2006. *Drying-Induced Stresses in Macaroni Dough*. Dry. Technol. 24 (9), 1093-1099.

Krokyda, M.K., Tsami, E. and Maroulis, Z.B. 1998. *Kinetics on colour changes during drying of some fruits and vegetables*. Dry. Technol. 16, 667-685.

Panyawong, S. and Devahastin, S. 2007. *Determination of deformation of a food product undergoing different drying methods and conditions via evolution of a shape factor*. J. Food Eng., 78, 151–161.

Spence, C.; Levitan, C. A.; Shankar, M. U. and Zampini, M. 2010. *Does Food Color Influence Taste and Flavor Perception in Humans?* Chemosens. Percept. 3, 68–84.

Valdramidis, V.P., Geeraerd, A. H., Gaze, J.E., Kondjoyan, A., Boyd, A.R., Shaw, H. L. and Van Impe, J. F. 2006. *Quantitative description of Listeria monocytogenes inactivation kinetics with temperature and water activity as the influencing factors, model prediction and methodological validation of dynamic data*. J. Food Eng. 76, 79-88.

ENVIRONMENTAL FACTORS AND FOOD EXPOSURE

MODELING AND SIMULATION OF EPIDEMICS CAUSED BY CONTAMINATED WATER

Bartłomiej Fajdek
Radosław Pytlak
Marcin Stachura
Tomasz Tarnawski

Warsaw University of Technology
Institute of Automatic Control and Robotics
ul. Sw. A. Boboli 8, 02-525 Warsaw
b.fajdek@mchtr.pw.edu.pl, pytlak@mchtr.pw.edu.pl,
m.stachura@mchtr.pw.edu.pl, t.tarnawski@mchtr.pw.edu.pl

KEYWORDS

Water distribution system, epidemic models, foodborne diseases, SIR model.

ABSTRACT

The paper describes an approach to modeling the spread of epidemics originating in contaminated water coming from town water distribution system. In the approach, we assume that we can separate the description of water distribution and the evolution of epidemic caused by the contaminated water. First, the water distribution together with pathogen concentration in water network nodes is evaluated by performing simulation of water network – to this end the EPANET environment is used. Having information on water consumption at water network nodes sources of epidemic outbreak are created. To a set of water network nodes an extended SIR model is assigned which then describes the evolution of infected and recovered populations. Extended SIR models are derived from models related to epidemics of food borne deseases and take into account partirtioning the population into subpopulaitons e.g. in different residential areas. Migrations of people between such areas is also taken into account in one scenario. The proposed approach is illustrated by applying it the Walkerton epidemic caused by the presence of E.coli bacteria in the community water distribution network. Presented simulation results show that the built and simulated integrated model can describe the Walkerton epidemic with adequate accuracy.

INTRODUCTION

Water contamination is a major global problem. It requires ongoing evaluation and revision of water resource policy at all levels. The current research shows that water pollution is the leading worldwide cause of deaths and diseases. Disease-causing microorganisms are referred to as pathogens. Although the majority of bacteria are harmless, some pathogenic bacteria can cause a serious disease. Waterborne diseases are caused by pathogenic microorganisms that most commonly are transmitted in contaminated fresh water. Infection commonly results during bathing, washing, drinking, in the preparation of food, or the consumption of food thus infected. Such diseases have a significant, negative impact on both health of the citizens and a local economy. Hence, a possibility of modeling the spread of epidemics coming from town water distribution system might reduce these negative effects.

WALKERTON TRAGEDY

The Walkerton is a small community in the Canadian province of Ontario. Walkerton is a town of about 5,000 inhabitants. In May 2000, the drinking water in Walkerton was contaminated with the highly dangerous O157:H7 strain of E.coli bacteria and Campylobacter jejuni. About 2300 of people began to simultaneously experience bloody diarrhea, gastrointestinal infections. The water contamination in the town was a terrible tragedy. Many segments of society were affected by the crisis. Seven people died directly from drinking the E. coli-contaminated water. In Figure 1 the water distribution system of Walkerton network is presented, with the marked as *W* placed of contamination.

Figure 1: The Walkerton Water Distribution Network with the Marked as W placed of contamination.

The primary, if not the only, source of the contamination was manure that had been spread on a farm near Well 5 (marked as W on the water distribution network). The owner of this farm followed proper practices and should not be faulted. The scope of the water contamination could be significantly reduced if the Walkerton operators of water distribution system had measured chlorine residuals at Well 5 daily, as they should have, during the critical period when contamination was entering the system.

WATER DISTRIBUTION SYSTEM AND EPIDEMIC MODELING SOFTWARE

The WDSE (Water Distribution System and Epidemic Modelling) software was used for modeling and simulation of water distribution system. Developed water network modeling environment is based on one of the most famous and appreciated modules called EPANET, which is created by the US EPA (United States Environmental Protection Agency). The EPANET application comes with a package of libraries written in C/C++ which allows to customize computational engine to suit needs. It is possible to use supplied function in the own 32-bit applications that can be created in C/C++, Delphi, Pascal, Visual Basic. A specialy designed C++ library was created, which integrates WDSE application with the computional engine of EPANET library. The WDSE system consist of several interacting software modules. The general structure of presented system is shown in Fig. 1.

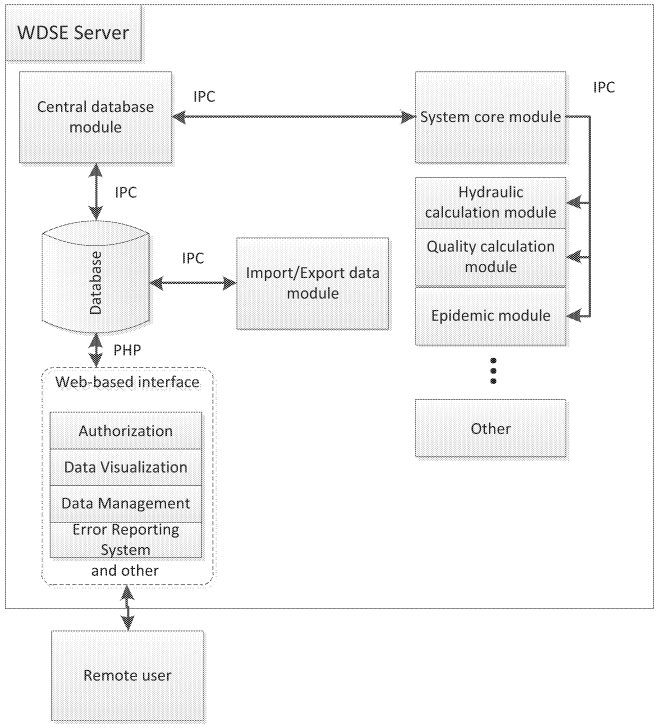

Figure 2: The Simplified Structure of System with Main Software Components.

One can distinguish the following elements of the system (Stachura, Fajdek and Studziński 2012):

a) **system core module** – provides the essential system components that allow operation and integration of all other modules of the system; it contains the links to all the optional modules and includes graphical user interface implementation (the mechanism by which the user communicate with the system), a core module is built around the central database module,
b) **import/export data module** – provides the interface to import/export data to/from external servers; eg import data from GIS (Geographic Information System), import data from water company database etc.,
c) **central database module** – in the system MySQL database is running on the central server; it is used to store all process related information such as: configuration and internal data of system modules, detailed information on water supply networks, archival information about network demands, archival information about faults in the network etc.; all necessary tables of relational database have been created in SQL (Structured Query Language) and are linked to each other using a primary key,
d) **hydraulic calculation module** – it allows to perform calculations of water flow in each pipe, the pressure at each node, the height of water in each tank in a network; the hydraulic model is described by linear and nonlinear algebraic equations; to solve equations hybrid node-loop (Gradient Method)(Todini and Pilati 1987) approach has been applied; hydraulic calculation module was implemented using EPANET programming toolkit,
e) **quality calculation module** – it allows to perform calculations of water quality at each node and pipe in a network; water quality solver are based on the principles of conservation of mass coupled with reaction kinetics (Rossman and Boulos 1996); water quality analysis allows to compute a concentration of a chemical species (eg chlorine concentration) throughout the network during the simulation period; in addition water age and source tracking can also be simulated; water quality calculation module was implemented using EPANET programming toolkit,
f) **web-based interface** – the set of modules that run on the www server and web browser side responsible for realizing the graphical user interface to all the data stored in the central database; the module will perform several basic task such as: visualization and management of data stored in central database which includes information from monitoring system (process variables) and management related data (eg faults history, revitalization history etc), user management (including the division into the different roles and groups) and advanced permission management system etc.; the module will be implemented using Web-desktop technique, which is based mainly on JavaSript and Ajax technology; the server partof the module will be implemented in PHP language; using the module we can remotely access to the system through Internet network without installing any additional software.
g) **epidemic module** – it carries out the simulation of epidemics spreading in the populations, where the sources of simulated new infections may be two-fold: through consumption of contaminated water (where the data on water demands and quality is received from abovementioned modules) and through contact with infected population members. The elements of the implemented model describing the epidemic spreading within the population are based on the extended SIR models discussed in leter sections.

MATHEMATICAL DESCRIPTION OF THE WATER DISTRIBUTION SYSTEM

The main task of a water supply system is to provide a a sufficient amount of water at the appropriate pressure to the

to all users of the system. Hence, each waterworks consists of three main components: pumps, storage tanks and distribution network. Most systems require pumps that allow to raise the water to the desired height and to cover energy losses due to friction. The pipes can be fitted with devices to control the flow, such as control, or relief valves.

Flows in the water supply system are calculated in accordance with the principle of conservation of mass and energy. In the mass conservation law shows that the entire mass stored in the system is equal to the difference between inlet and outlet to flows. In the pressurized water distribution network, it is not possible to store water in pipes, although the levels in the tanks may change over time. For this reason, the input and output flow for each node in the network and the water supply pipe has to be balanced.

Assume we have a pipe network with N junction nodes and NF fixed grade nodes (tanks and reservoirs). Let the flow-headloss relation in a pipe between nodes i and j be given as:

$$H_i - H_j = h_{ij} = rQ_{ij}^n + mQ_{ij}^2 \quad (1)$$

where H is nodal head, h is headloss, r is resistance coefficient, Q is flow rate, n is flow exponent, and m is minor loss coefficient.

The value of the resistance coefficient will depend on which friction headloss formula is being used (see below). For pumps, the headloss (negative of the head gain) can be represented by a power law of the form

$$h_{ij} = -\omega^2 \cdot \left(h_0 - r \cdot \left(\frac{Q_{ij}}{\omega}\right)^n\right) \quad (2)$$

where h_0 is the shutoff head for the pump, ω is a relative speed setting, and r and n are the pump curve coefficients. The second set of equations that must be satisfied is flow continuity around all nodes:

$$\sum_j Q_{ij} - D_i = 0 \quad dla \quad i = 1, \dots, N \quad (3)$$

where D_i is the flow demand at node i and by convention, flow into a node is positive. For a set of known heads at the fixed grade nodes, we seek a solution for all heads H_i and flows Q_{ij} that satisfy Eqs.(1) and (2).

A E.Coli bacterias will travel down the length of a pipe with the same average velocity as the carrier fluid while at the same time reacting (decaying) at a given rate. Longitudinal dispersion is usually not an important transport mechanism under most operating conditions. This means there is no intermixing of mass between adjacent parcels of water traveling down a pipe. Advective transport within a pipe is represented with the following equation:

$$\frac{\partial C_i}{\partial t} = -u_i \cdot \frac{\partial C_i}{\partial x} + r(C_i) \quad (4)$$

where C_i is a concentration (mass/volume) in pipe i as a function of distance x and time t, u_i is a flow velocity (length/time) in pipe i, and r is a rate of reaction (mass/volume/time) as a function of concentration.
The rate of reaction can generally be described as a power function of concentration. In this work the following formula was used:

$$r = K_b C^n \quad (5)$$

where k is a reaction constant and n is the reaction order.

MODELLING THE POPULATION

The WDSE environment is equipped wih models of epidemic spread. Since we assume that an epidemic can be caused mainly by the contact with contaminated water these models are not standard SIR models as described, for example in (Kermack and McKendrick, 1927), (Kermack and McKendrick, 1932), (Kermack and McKendrick, 1933), (Bailey, 1975), (Murray, 1993), (Murray, 2001), (Sterman, 2000), or (Capasso, 1993). Our models are derived from the models developed for food-borne deseases ((Bhunia, 2008), (Joshua and Etukudo, 2011), (Levine, 2009), (Mari et al, 2012), (Mukandavire et al, 2011)). In these models there exists a substance containing pathogen which in contact with people causes an epidemic. Depending on a pathogen the epidemic can also develop due to personal contacts (as in typical SIR models), that mechanism is also reflected in our models.

In the WDSE package the population may either be modeled as a single unit, or as a collection of several disjoint populations. In the most basic case, then, there is a single, uniform population linked with to the whole water distribution network, but in a more complex one, there may be a number of populations, where each is connected to its own set of nodes of the water pipelines. In addition, the different (sub-) populations may be described with differing evalues of their parameters (e.g. describing their susceptibility to a given pathogen).

Infections due to consumption of contaminated water at a particular node are guided by the following set of parameters and variables:

f_{cons} – fraction of the water consumed by people (out of the whole water drawn);

$C(t)$ – pathogen concentration in the node;

$D(t)$ – water flow demand node;

PA – pathogen aggressiveness;

S – size of the susceptible population.

The overall equation of infection rate, i.e. the rate for increasing the size of the infected population I (for the moment assuming, that infections due to personal contact are negligible) is given by the formula:

$$\frac{dI}{dt} = \vartheta_C \cdot S = f_{cons} \cdot PA \cdot C(t) \cdot D(t) \cdot S \quad (6)$$

Since both pathogen concentration and water demand differs from node to node, in the implementation they are appropriately calculated and summed, based on the results received from the hydraulic simulation. Such rate of increase of the Infected population is equal in value (and opposite in sign) to the reate of change in the Susceptible population.

Together with the standard equation for inter-human infections (from the SIR approach), the complete forula for the rate of flow from Susceptible to Infected is:

$$\frac{dS}{dt} = -\vartheta_C \cdot S - \vartheta_P \cdot S \cdot \frac{I}{N} \quad (7)$$

where v_C can be referred to as individual's infection rete due to contamination, v_P – individual's infectious contact rate (rate of infection due to contacts with infected people) and N is the size of the whole population.

When following SIR-like models, one also has to supplement the equation describing the Infected population with two additional flows: from Infected to Recovered (through healing) and from Infected to Deceased (in the cases when patients die of the disease). In result, we get the complete formula:

$$\frac{dI}{dt} = \vartheta_C \cdot S + \vartheta_P \cdot S \cdot \frac{I}{N} - \gamma I - \delta I \quad (8)$$

while for the Recovered and Deceased, T, (sub-)populations the equations take the form, respectively:

$$\frac{dR}{dt} = \gamma I \quad (9)$$

$$\frac{dT}{dt} = \delta I \quad (10)$$

Together, the equations (7) – (10) define the epidemic model in is simplest (single population) form.

Generalization onto multi-population is rather straight forward. It requires definition of respective vectors: $\boldsymbol{S}$, $\boldsymbol{I}$, $\boldsymbol{R}$, $\boldsymbol{T}$, in which e.g. *i*-th Infected population will be denoted as $[\boldsymbol{I}]_i$ (i-th element of the vector), a vector $\boldsymbol{v_C}$ of infection rates caused by water consumptions at particular populations' areas and a migration matrix $\boldsymbol{M}$, where each element $[\boldsymbol{M}]_{i,j}$ defines relative amount of time that members of i-th population spend visiting the area of j-th one. Each row of the matrix must sum to unity, the diagonal elements refer to time spend in own area (so therefore a unit matrix will describe a situations of separated populations with no migrations).

In the generalized model, the process of infections (flow from $\boldsymbol{S}$ to $\boldsymbol{I}$ populations) must take into account getting infected through drinking water and contacting Infected people in all areas that members of a given population visit, hence the formula (7) defining the outflow from the $\boldsymbol{S}$ populations takes the form:

$$\frac{d[S]_i}{dt} = -\sum_{j=1}^{n}\left([\boldsymbol{M}]_{i,j}\,[\vartheta_C]_j \cdot [\boldsymbol{S}]_i + [\boldsymbol{M}]_{i,j}\vartheta_P \cdot [\boldsymbol{S}]_i \cdot \frac{[I]_j}{N}\right) \quad (11)$$

for all i in the appropriate range. Corresponding modifications in (8) will equate the inflow to $\boldsymbol{I}$ with the identical outflow from $\boldsymbol{S}$. Formulas (9) and (10) stay unchanged as they do not depend on migrations.

SIMULATION RESULTS

The presented model and its implementation in the form of WDSE software package was used on the data describing the Walkerton case. It is extremely applicable, as both the water distribution system data and history of the epidemics are well documented and the information is easily available. Basing on the hydraulic and water quality data describing the time of the Walkerton tragedy the epidemic simulation was executed in the tree following scenarios:

a) **single population** – one population unit (of 5000 people) was connected with the whole water distribution network,
b) **2 populations, no migrations** – the population was divided into two separate units based on the analysis of the pathogen propagation in the water distribution system; the first selected population covers an area of water distribution system where high concentration of the pathogen occurred; the second selected population covers an area of water distribution system where the water pathogen infection practically not occurred; the populations sizes were estimated based on water demand data, i.e. the whole population was divided into parts of 61% and 39% of total, lack of migrations was forced by unit migration matrix
c) **2 populations, with migrations** – the population was divided in the same way, but at this point the migration matrix was set with migration coefficients of 0.7 for "stay at home" and 0.3 to "travel to the other population".

In all tree cases we assumed, that the only mode of infection was through drinking contaminated water and there was no secondary infections from person-to-person contact (in food borne epidemics this is usually a justified first order approximation) – i.e. the contact rate coefficient v_P in formula (11) was set to zero.

The first, simplest scenario was initially used to verify (and adjust) the values of the model's parameters. It turned out that the course of epidemics may be easily replicated both in terms of total infections counts (roughly 2500) and the number of deaths (near 7). Figure 3 shows the time series for the S, I and R populations in the first scenario.

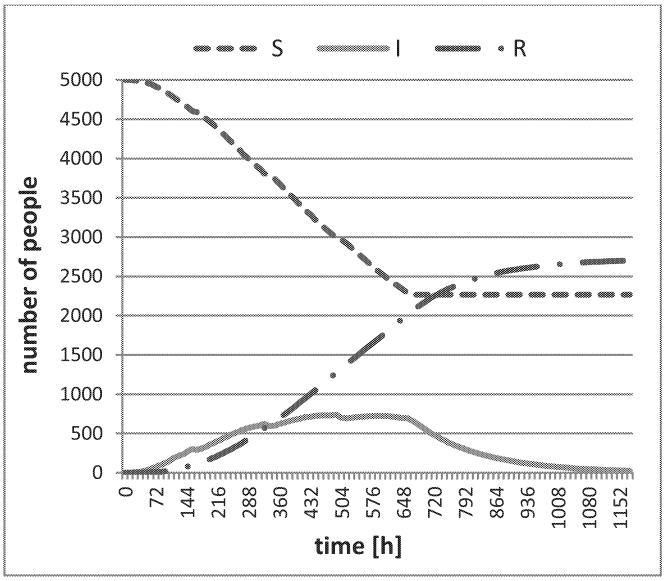

Figure 3: The Walkerton epidemic simulatied with single population (S – susceptible, I – infected, R – removed).

The second scenario, although using the same parameter values (as all later executions did), produced a significantly different results. As one could expect, only 'Population1', the part of population residing in the area where contaminated water was present, significantly experienced the disease. However, as the size of 'Population1' was below 2000, the total number of sick reached about 1770 (1675 in 'PopulationA' and below 100 in 'Population2'), well below scenario a) and historical data (see Figure 4). It was a hint, that migrations and consuming water outside of one's area of residence was also a factor in the spread of the disease.

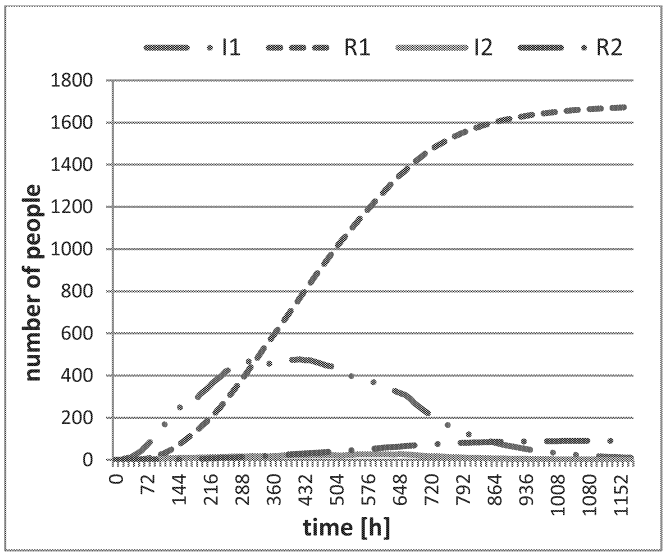

Figure 4: The Walkerton epidemic simulation with two subpopulations with no migrations. The vast majority of contaminated nodes were in the area of Population1.

The third scenario, where a fair "amount" of migration was introduced, produced again results similar to the ones received for the first scenario (and ones that replicate the actual historic course of the Walkerton epidemic. Its simulation results are shown on Figure 5. This provides a fair indication, that migrations outside own residence areas (most likely: commuting to work, as this is the main mode of intra-city migrations nowadays) and drinking water also there played an important role in increasing the number of people influenced by the epidemic.

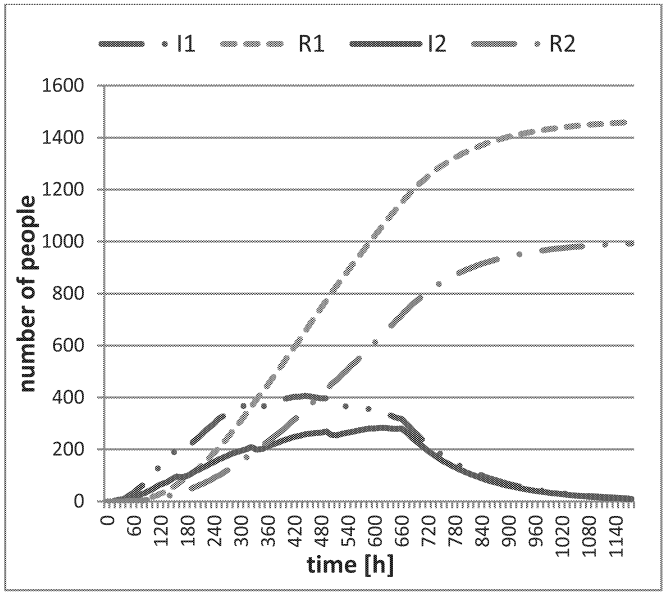

Figure 5: The Walkerton epidemic simulated with two populations. Although Population2 resides in a "clean" area, it suffered significant infections due to migration.

CONCLUSIONS

The paper presents the approach for building simulation models describing the evolution of an epidemic caused by contaminated water. The essential feature of the approach is the integration of two submodels: the first one shows how contaminated water is distributed in water network; the second one is the extended SIR model, related to food borne deseases, which is able to describe the evolution of infected and recovered populations residing in different areas. In the paper we show one variant of integrated models which can be built by the following the approach. In the variant the trajectories of water distribution and pathogen concentrations are first obtained and then they are fed to extended SIR models as exogenous variables. However, one can also build another variant of the integrated model in which simulated values of SIR submodels provide feedback to water network simulation models reflecting the changes in populations linked to simulated water distribution network.

REFERENCES

Bailey, N.T.J. 1975. *The Mathematical Theory of Infectious Diseases*. Griffin, London, second edition.

Bhunia, A. K. 2008. Escherichia coli. In *Foodborne Microbial Pathogens*, 183-200. Springer New York.

Capasso, V. 1993. *Mathematical Structures of Epidemic Systems*. Lecture Notes in Biomathematics. Springer.

Joshua, E. E., Etukudo, U.E. 2011. Mathematical model of the spread of typhoid fever. *World Journal of Applied Science and Technology*, Vol. 3, No. 2, 10- 20.

Kermack, W.O., McKendrick, A.G. 1927. Contributions to the mathematical theory of epidemics. *Proc. R. Soc. Lond. A*, 115:700–721.

Kermack, W.O., McKendrick, A.G. 1932. Contributions to the mathematical theory of epidemics. *Proc. R. Soc. Lond. A*, Vol. 138, 55–83.

Kermack, W.O., McKendrick, A.G. 1933. Contributions to the mathematical theory of epidemics. *Proc. R. Soc. Lond. A,* Vol. 141, 94–122.

Levine, M.M. 2009. Typhoid fever. In Philip S. Brachman and Elias Abrutyn, editors, *Bacterial Infections of Humans*, 913-937. Springer US.

Mari, L., Bertuzzo, E., Righetto, L., Casagrandi, R., Gatto, M.,Rodriguez-Iturbe, I., Rinaldo, A. 2012. Modelling cholera epidemics: the role of waterways, human mobility and sanitation. *Journal of The Royal Society Interface*, Vol. 67, No. 9, 376-388.

Mukandavire, Z., Liao, S., Wang, J., Ga, H., Smith, D.L., Morris, J.G. 2011. Estimating the reproductive numbers for the 2008-2009 cholera outbreaks in Zimbabwe. *Proceedings of the National Academy of Sciences*.

Murray, J.D. 1993. *Mathematical biology. I. An introduction*, Springer-Verlag, Berlin, Heidelberg, New York.

Murray, J.D. 2001. *Mathematical biology. II. Spatial models*, Springer-Verlag, Berlin, Heidelberg, New York, 2001.

Rossman, L.A., Boulos, P.F. 1996. Numerical methods for modeling water quality in distribution systems: A comparison, *J. Water Resour. Plng. and Mgmt*, Vol. 122, No. 2, 137-146.

Stachura, M., Fajdek, B., Studziński, J. 2012. Model Based Decision Support System for Communal Water Works. *Industrial Simulation Conference 2012* (Brno, June 4-6).

Sterman, J.D. 2000. *Business Dynamics*, McGraw-Hill.

Todini, E., Pilati, S. 1987. A gradient method for the analysis of pipe networks. *International Conference on Computer Applications for Water Supply and Distribution* (Leicester Polytechnic, September 8-10).

BIOGRAPHIES

BARTŁOMIEJ FAJDEK was born in Warsaw, Poland. He studied at Warsaw University of Technology, in 2007 he received a M. Sc. Degree in the field of Automatic Control and Robotics. After studies he started to work at the Warsaw University of Technology.

MARCIN STACHURA was born in Szczecin, Poland. He studied at Maritime Academy of Szczecin, in 2004 he received a B. Sc. degree in the field of studies in the field of Mechanics and Machine Construction. Next he moved to Warsaw, and studied at Warsaw University of Technology. In 2007 he received M. Sc. degree in the field of Automatic Control and Robotics. After studies he started to work at the University. He received Ph. D. degree in the field of Automatic Control and Robotics in 2011.

TOMASZ TARNAWSKI was born in Szczecin, Poland. He studied at Military Academy of Technology in Warsaw, where in 2000 he received a M. Sc. degree in Computer Science. After working for several years at the Academy, both in research and didactics, he received Ph. D. degree in the field of Computer Simulation and Optimization in 2006.

RADOSŁAW PYTLAK is a professor at the Institute of Automatic Control and Robotics of Warsaw Technical University. Before joining Warsaw University of Technology he worked at Military University of Technology where he led the group of Information Management Systems. From 1990 to 1998 he worked at the Centre for Process Systems Engineering at Imperial College in London. He does research in the field of optimal control and optimization. He has published several papers in the leading journals of the field and published two books in Springer-Verlag: *Numerical methods for optimal control problems with state constraints*, Lecture Notes in Mathematics 1707, 1999; *Conjugate gradient algorithms in nonconvex optimization*, 2009.

ASSESSING RISK FOR AFLATOXIN EXPOSURE THROUGH MAIZE FOOD INTAKE IN VERACRUZ CITY (MÉXICO)

Hiram Alejandro Wall-Martínez
Guadalupe del Carmen Rodriguez-Jimenes
Victor José Robles-Olvera
Miguel Angel Garcia Alvarado
Alejandra Ramirez-Martinez
Marco Antonio Salgado-Cervantes.
Chemical and Biochemical Engineering Department
Instituto Tecnológico de Veracruz
Av. Miguel A. de Quevedo 2779, Veracruz, Ver. 91860, Mexico

Nathalie Wesolek
Alain Claude-Roudot
Alejandra Ramirez-Martinez
Université de Bretagne Occidentale
Laboratoire d'Evaluation du Risque Chimique pour le Consommateur
6 avenue Le Gorgeu, 29238 Brest cedex 3, France
alain-claude@univ-brest.fr

Violeta T. Pardio Sedas
Zoo Technology Faculty of Veterinary Medicine
University of Veracruz

KEY WORDS
Probability exposure, probability density function, aflatoxin, frequency questionnaires, maize.

ABSTRACT

Maize is one of the most consumed foods in Mexico and the world. Added to this there is evidence of the presence of large amounts of mycotoxins produced by mushrooms in corn. Besides the quality of maize products, it is essential to know if the population is consuming a significant amount of these products because high consumption can lead to health problems. Therefore, the objective of this study was to determine the consumption of maize products to assess aflatoxin exposure in a major city in Mexico (Veracruz). To achieve this objective two types of questionnaires were used: a Food Frequency Questionnaire and a recall record. The resulting consumption data were expressed in terms of maize content (g maize/day). Results showed tortillas were the product with the highest intake. Average consumption of tortilla corresponds to 241.15 g maize/day and 157.54 g maize/day for men and women, respectively. Aflatoxin exposure was higher for men compared with women exposure.

INTRODUCTION

Measuring food consumption levels in a population requires a rigorous sampling step. Most common methodologies used to estimate food daily ingestion correspond to food daily record, follow-up of 24 hours and consumption frequency questionnaire. Questionnaires construction depends on the objectives and type of study, and the available budget. Consumption frequency questionnaires allow obtaining information of population food intake. This type of questionnaires has several advantages: it is easy to subjects to complete them, they are inexpensive and they simplify processing of data. Moreover, they do not alter the consumption pattern of surveyed subjects. In addition, consumption frequency questionnaires allow classifying individuals of a population under different groups (ranking) which facilitate realizing comparisons and identifying high risk pathways (Warneke *et al.*, 2001).

The fact that consumption frequency questionnaires allow identifying diet patterns permit to make predictions in the long term. Predictions let to explore the relationship among diet and health risk. Selection of food item to be assessed is the first step in the construction of the questionnaire (Jackson *et al.*, 2011).

The major cereals, regarding worldwide production, are maize, wheat, rice, barley, sorghum and oats. Maize represents 39 % of world total grain production for the 2010-2011 harvest year. Maize grains may become contaminated by molds while in the field and during storage. Some of these molds can produce mycotoxins (FAO, 2013).

Mycotoxins are secondary metabolites produced by several fungi. These toxins are commonly found on cereal grains and have been linked to esophageal and liver human cancer. Mycotoxins that commonly occur on cereal grains and other products are not completely destroyed during food processing operations and can contaminate processed finished foods. The most commonly mycotoxins associated with corn are aflatoxins (Wild and Gong, 2010).

Aflatoxins have been established as potent mutagens, carcinogens, and teratogens. They are classified as Group 1 carcinogens by the International Agency for Research on Cancer, meaning that they primarily affect liver (IARC, 1995). Particularly, few studies have been conducted to estimate an acceptable daily intake value (ADI). Moss (2002) estimated an intake level value ranging between 253 and 441ng/day. Previously, Bruce (1990) arrived to an estimate of 322 ng/day.

In Mexico, maize is destined for human consumption. This cereal is consumed through several traditional foods: atole, tamales, chilaquiles, antojitos, and especially tortillas. Nearly 60 % of maize national production is destined for the production of tortillas (Secretaría de Economía México, 2012).

The objective of this study was to determine maize consumption of the population of Veracruz City and therefore aflatoxins exposure. To achieve this objective,

consumption data of traditional foods were obtained from two different questionnaires. These data were then expressed in a maize basis and used along with aflatoxin contamination obtained from published values.

METHODS

Data used for contamination levels

In the case of aflatoxins contamination, we used data available from literature. Particularly, Castillo *et al.*, 2011 reported raw data for total aflatoxins levels measured from tortillas in Mexico City. Aflatoxins levels were obtained from 2 kg samples taken amongst 198 tortillerías (tortilla shops) located at different districts of Mexico City. At each district, three supermarkets and three tortilla shops were chosen. Samples were collected during two consecutive years (2006 and 2007). A total of 396 tortilla samples were collected. The survey revealed that 17% of sampled tortillas contained aflatoxins at levels of 3–385 μg/kg. Of these samples, 13% contained aflatoxins above the regulatory limit (12 μg/kg) and 87% were below the regulatory limit.

Contamination level distribution for maize products was obtained by assuming that contamination levels for maize products were similar to that of tortillas. This assumption was based on the fact that all maize products are processed using of the same process (nixtamalization). At nixtamalization process, raw material consists in maize. In consequence, we chose to express consumption data of maize products in terms of maize content (Table 1). Then contamination data of maize tortillas in Castillo *et al.*, 2011 (already expressed in terms of maize content) were used to perform a PDF of aflatoxin contamination for each maize product. By this means the result was expressed as μg total aflafoxin per grame of maize for all cases.

TABLE 1: Maize content in maize products

Product	Maize Content (g)		
Size	Small	Medium	Big
Taco	13	15	20
Tamales	25	32	40
Tostadas	13	15	20
Esquites	15	20	30
Antojitos	15	20	30
Atole	10	13	15
Chilaquiles	60	90	120
Tortilla	13	15	20

Consumption data obtainment

In order to have a random and representative sampling of the population of Veracruz City, a computer program was used (MATLAB). MATLAB generated 35 random geographical points of the city, under the Latin hypercube sampling type (Figure 1).

For each geographical coordinate two households were randomly selected. Consumption data were obtained through to two types of questionnaires.

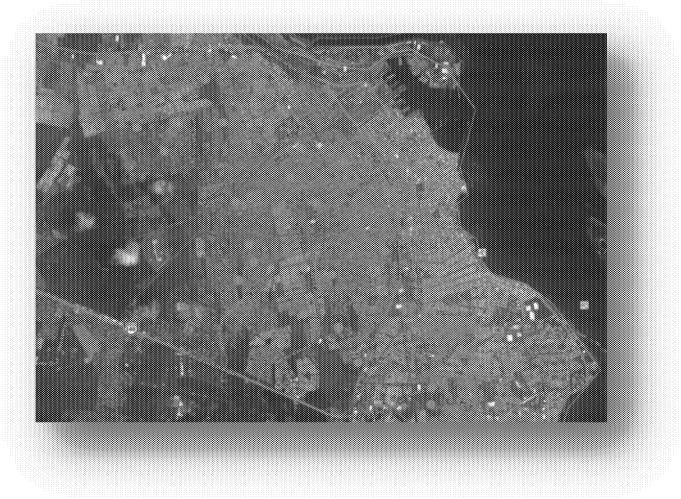

FIGURE 1: Location of apply sites of food frequency questionnaires

Once the household selected, one of the two questionnaires was left to household members for fill in. The first questionnaire was a food diary about the consumption levels of tortilla during each meal over a three day period. Respondents consisted of each of the inhabitants of the selected household. Each inhabitant wrote down the number of tortillas consumed. The second questionnaire was a recall record about the consumption frequency per week or per month, depending on the food type. Information about consumption of maize products (tacos, toasted tortillas, tamales, antojitos, atole and chilaquiles) was assessed by this questionnaire. Moreover, the portion size for each product was recorded by the respondent, using a photography book. Thus, use of the two questionnaires allowed obtaining the global consumption levels of the main products made from maize.

Additional information on body weight, age and gender of each household member as well as the level of education and occupation of the head of the household were requested. A total of 172 food frequency questionnaires were filled out and in the case of the food recall method, 122 questionnaires were completed.

Theoretical distribution fitting

Population was classified under 2 groups in order to differentiate the consumption among men and women. The classifications according to age, education and profession will be analyzed in future work.

For each gender, the consumption of the consumers' population solely was adjusted to a lognormal distribution. The proportion of consumers and non-consumers was the input of a binomial function. Then the distribution of the combination of consumers and non-consumers was computed.

Similarly, binomial distribution was used to differentiate sample uncontaminated and sample contaminated, the contaminated sample was adjusted by a lognormal distribution.

A function of probability density for the weight of men and one for women was performed; both were adjusted to a lognormal distribution.

Exposure calculation

Descriptive statistics and Probability Density Functions of the daily consumption estimated for each food were determined and analyzed using @Risk6 (Palisade, Inc.). Descriptive statistics of daily consumption include the mean, median, standard deviation and the 95th percentile. Furthermore, Probability Density Functions (PDF) for aflatoxin concentration, body weight and consumption of the inhabitants of Veracruz City were generated. Calculation of probability density functions is based in the Monte Carlo simulation method.

Exposure was determined by the Equation (1)

$$Exp = \sum_{k=1}^{p} \frac{(x_{iAft})(C_i)}{W} \qquad (1)$$

Where

Exp = Exposure per day (ng Aflatoxin per kg body weight per day)
X_{iAFt} = concentration of Aflatoxin in the food (µg/kg)
C_i = Maize consumption in the food (g/day)
W= Body weight (kg)
P= Number of maize products were aflatoxin exposure is assessed

Exposure was calculated using different methods:

- A deterministic calculation where a fixed food consumption value and a fixed contamination level for each of maize products were considered.
- A probabilistic calculation, called "worst case" where exposure distributions for each maize products were added, not taking into account consumers and non-consumers
- A probabilistic calculation taking into account this difference (everybody do not eat all maize products)
- A probabilistic method -similar to the last one- but adding the consumption correlations between the different products. This one is the more realistic exposure evaluation.

RESULTS AND DISCUSSION

Descriptive analysis results for the consumption of maize products are given in Tables 2 and 3.

Table 2: Consumption of maize products by women from Veracruz City (g maize / day)

Food	Consumers (%)	Consumption level	Median	Standard Deviation	95th Percentile
Tacos	94.21	19.50	11.43	24.86	60.00
Tamales	66.12	7.82	6.40	8.20	21.33
Tostadas	90.08	8.67	6.40	7.87	24.00
Esquites	57.85	3.75	2.14	4.56	15.50
Antojitos	93.38	22.54	14.29	18.56	60.00
Atole	25.62	1.59	0.87	1.37	4.29
Chilaquiles	95.86	10.57	6.40	19.04	27.43
Tortillas	95.60	159.68	151.04	78.47	281.00

Table 3: Consumption of maize products by men from Veracruz City (g maize / day)

Food	Consumers (%)	Consumption level (g maize/day)			
		Mean	Median	Standard deviation	95th Percentile
Tacos	95.5	23.12	13.71	32.42	60.00
Tamales	65.5	8.26	6.40	6.94	27.73
Tostadas	85.5	9.55	6.40	8.64	27.43
Esquites	60.0	3.85	2.14	4.72	15.50
Antojitos	92.7	21.87	14.27	17.46	51.43
Atole	27.8	1.17	0.87	1.01	3.71
Chilaquiles	96.4	7.88	6.40	6.24	19.20
Tortilla	97.4	251.33	208.67	143.73	542.33

Data show that foods with a higher percentage of consumers correspond to tacos, tostadas, antojitos, chilaquiles and tortillas, knowing that tortillas are consumed at the highest consumption level.

Descriptive analysis of the probability density function of the body weight of the inhabitants of the city of Veracruz is given in Table 4.

Table 4: Body weight statistics of the inhabitants of the city of Veracruz

	Weight (kg)			
	Mean	Median	Standard deviation	95th Percentile
Men	73.94	74	8.52	90
Woman	66.55	65	8.57	80

Figure 2 shows the probability density function of consumption of tortillas expressed in terms of maize consumption per day among men. These data may suggest that men consume an average of 310 g of maize flour per day. Furthermore, Figure 2 illustrates that 5% of men eat less than 39 g of maize per day, 90% eat between 39 and 662 g of maize per day and the remaining 5% more than 662 g of maize per day. Regarding aflatoxins contamination, the estimated probability density function led to a mean of 3 µg/kg of maize with a standard deviation being 13 µg/kg and a 95th percentile of 18.27 µg/kg.

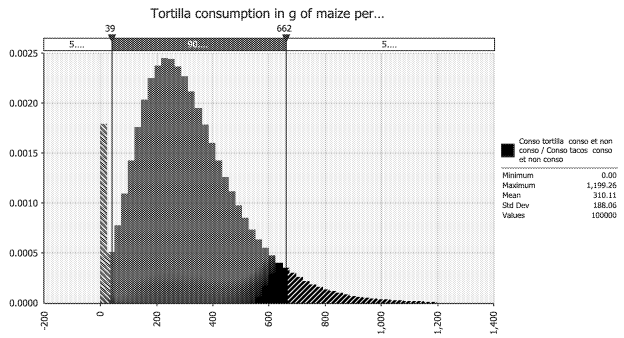

FIGURE 2: Probability density function of consumption of tortilla among men

Tables 5 and 6 show the results of a Monte Carlo simulation for aflatoxin exposure of each product derived from maize.

Table 5: Probabilistic Aflatoxins exposure in men due to the consumption of maize products

	Aflatoxin exposure (µg/kg bw/day) for different scenarios for men			
	Mean	median	Standard deviation	95th Percentile
With correlation	0.0144	0.000818	0.0637	0.0637
Without correlation	0.0149	0.000823	0.0886	0.0642
With correlation and without tortilla	0.0032	0.000350	0.0144	0.0136
Without correlation and without tortilla	0.0031	0.000351	0.1270	0.0136
Worst case	0.0157	0.001250	0.0773	0.0662

Table 6: Probabilistic Aflatoxins exposure in women due to the consumption of maize products

	Aflatoxin exposure (µg/kg bw/day) for different scenarios for women			
	Mean	Median	Standard deviation	95th Percentile
With correlation	0.0122	0.00104	0.1590	0.0531
Without correlation	0.0121	0.00101	0.0564	0.0520
With correlation and without tortilla	0.0036	0.00047	0.0134	0.0157
Without correlation and without tortilla	0.0036	0.00047	0.0122	0.0156
Worst case	0.0133	0.00014	0.1590	0.0550

As correlations between consumption of the different maize products are very low, they do not greatly influence the total exposure. The 95th percentile for exposure estimation indicates the value of a distribution with 95% percentage of the values equal to or below it. Thus, this percentile value corresponds to an exposure limit of 95% of the population.

Exposure values given in Table 4 and 5 were assessed using a probabilistic approach. In order to compare exposure assessed by using different calculation approaches (deterministic and probabilistic), a deterministic value was also calculated. To achieve this, a point estimate value was performed at the 95th percentile contamination value and the sum of the average consumption for each of maize products. Body weight value used in calculation corresponds to the mean body weight for males and females combined. Exposures to aflatoxin *via* maize consumption calculated in this way correspond to 0.0761 µg/kg bw/day for men and 0.063 µg/kg bw/day for women. The greatest exposure comes from tortilla consumption for men and women as shown in Figures 3 and 4.

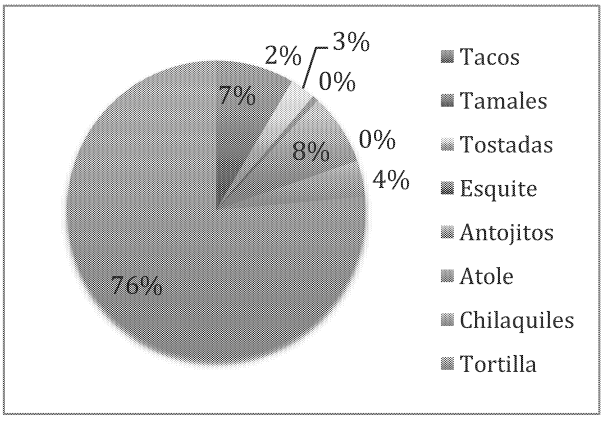

FIGURE 3: Aflatoxin exposure in men by product

The deterministic method is a global evaluation without any descriptive characteristics of consumption or contamination. Results show that, in our case, deterministic value is far more protective than probabilistic ones. However, in the probabilistic approach all variability are taken into account, in consequence, exposure values obtained by this method give us a more complete idea of the exposure distribution.

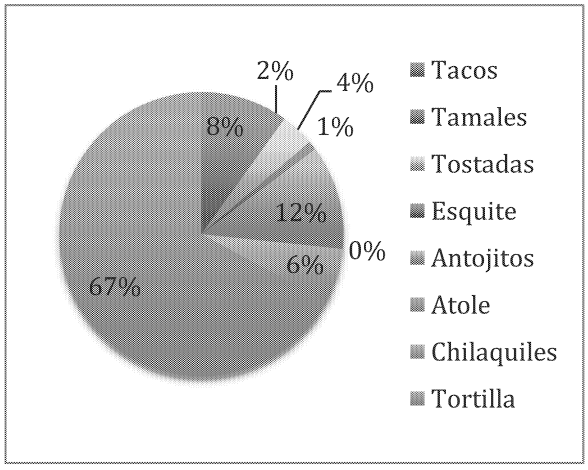

FIGURE 4: Aflatoxin exposure in women by product

CONCLUSION

Probability density functions for aflatoxin concentration, body weight and consumption of maize products of the population of Veracruz City were performed.

Exposures to aflatoxin via maize consumption by using probabilistic and deterministic methods were calculated. The probabilistic method provides improved information regarding the distribution of risk exposure of the population as well as being more protective. Probabilistic method is more protective due to the fact that it takes into account exposure distribution.

ACKNOWLEDGEMENT

This work was partially supported by an ECOS-Nord (Mexico-France copperation) grant.

REFERENCES

Bruce, R.D., 1990. Risk assessment for aflatoxin: II. Implications of human epidemiology data Risk Analysis 10, 561–569.

Castillo-Urueta P., Carvajal M. Mendez I., Meza F. and Galvaez A. 2011 Survey of aflatoxins in maize tortillas from Mexico City *Food Additives and Contaminants*: Part B Vol. 4, No. 1, 42–51.

FAO. 2013. FAOSTAT World food situation.

IARC 1995. "IARC Monographs on the Evaluation of Carcinogenic Risks to Humans" , Vol. 62, *Wood Dust and Formaldehyde*, Lyon, IARCPress, pp. 217–362.

Jackson, M.D.; Walker, S.P.; Younger, N.M.; Bennett, F.I. 2011. "Use of a food frequency questionnaire to assess diets of Jamaican adults: Validation and correlation with biomarkers" *Nutr J*, 10, p. 28.

Moss M.O. 2002. Risk assessment for aflatoxins in foodstuffs. *Int Biodeterior Biodegrad*; 50(3-4): 137-142.

Secretaría de Economía (México). 2012. Analisis del valor del maíz-tortilla situación actual y factores de competencia local. Dirección General de Industrias Básicas.

Warneke, C.L.; Davis, M.; De Moor, C.; Baranowski, T.A. 2001. "7-item versus 31-item food frequency questionnaire for measuring fruit, juice, and vegetable intake among a predominantly African-American population" *J Am Diet Assoc*, 101 (7), pp. 774–779.

Wild, C.P. and Gong, Y.Y. 2010. "Mycotoxins and human disease: a largely ignored global health issue" *Carcinogenesis* 31 (1), pp. 71–82.

MONITORING ENVIRONMENTAL FACTORS IN MEKONG DELTA OF VIETNAM USING WIRELESS SENSOR NETWORK APPROACH

Bao Hoai Lam
Hiep Xuan Huynh
Can Tho University, Vietnam; LAB-STICC, UMR CNRS 6285, France. Email: lhbao@cit.ctu.edu.vn
DREAM Team/UMI 209 UMMISCO-IRD; Can Tho University, Vietnam. Email: hxhiep@ctu.edu.vn

Mahamadou Traoré
Université Gaston Berger, Saint Louis, Senegal. Email: mahamadou.traore@ugb.edu.sn

Pierre Yves Lucas
Bernard Pottier
Université de Bretagne Occidentale, LAB-STICC, UMR CNRS 6285, France. Email : {pierre-yves.lucas, pottier}@univ-brest.fr

KEYWORDS
Mekong Delta, Brown Plant-Hopper, BPH, Wireless Sensor Network, WSN, NetGen.

ABSTRACT

The paper is about monitoring the environment in the Mekong Delta of Vietnam. The delta is an important food supply area in Vietnam, with several environmental issues that may endanger the production. Among the issues are pest insects, saltwater intrusion, floods and water pollution. We are considering Wireless Sensor Networks (WSN) for understanding and controlling risks. A top down design method is investigated that allows geographic deployment, optimization of the layouts, and robust algorithms. This method is based on a simulation technique compatible with the synchronous behavior of the WSNs and future real time interactions.

INTRODUCTION

The Vietnam Mekong Delta is one of the great fertile plains in Southeast Asia and in the world. The natural area of the delta is 39,763 km^2 and the population in the end of 2010 was approximately 18 million (Nguyen Minh Sang 2011). The delta is a key food production area of Vietnam in which it is the largest food producers and has favorable conditions for the development of large-scale farming, especially raising coastal or fluvial aquaculture; for the high quality fruit-growing regions (Nguyen Minh Sang 2011).

Rice is an important production of the Mekong Delta. Although the area of the Mekong Delta represents only 12.1% the area of Vietnam, half of the production and the majority of rice exports from the country is coming from this region. The average food per capita in the Delta is 2.3 times higher than the national Vietnam average (Nguyen Trung Tien 2011).

The Mekong Delta also has a very strong aquaculture. Firstly, the delta is a key area for *brackish water shrimp* farming. In 2012, the shrimp farming area of the Mekong represented 90.6% of the total area in Vietnam, and reached 595.7 thousand hectares. In addition, production of shrimp harvested in the coastal provinces of the Mekong Delta contributed for 75.2% of whole Vietnam's production. Another fishery product of the delta is *shark catfish*. In fact, shark catfish (pangasius hypophthalmus) ranks in the 2nd position of seafood exports to foreign countries, shrimp holding the first rank (Department of Aquaculture, Ministry of Agriculture and Rural Development 2013). Shark catfish lives mainly in the Mekong Delta and is raised in almost provinces in the delta, especially An Giang and Dong Thap. In 2012, the turnover of shark catfish export reached $1.74 billion, with a mass of about 1,255,500 tons (Ministry of Agriculture and Rural Development 2013).

However, The Vietnam Mekong Delta confronts with many environmental conditions that may endanger its food production. Although there exist practical solutions for these dangers, Information Technology tools are rarely used. This paper explains benefits coming from Wireless Sensor Network for remote data collection, understanding of biological processes, and eventual real time reaction to threats. The case used in this paper is the case of Brown Plant Hopper (BPH), a typical pest insect in Vietnam Mekong Delta, with the data collection in Dong Thap province, a typical rice province in Vietnam Mekong Delta.

This paper is organized as follows. Section 2 depicts some environmental factors that affect to Vietnam Mekong Delta and some current solutions for them in Vietnam. This is a followed by the explanation of WSN to monitor and control environment, in section 3. This section also mentions some tools to operate the simulation. Next section describes the design flow in NetGen (NetGen project) and some simulation results in light traps data in Dong Thap. In the last section we draw some conclusion regarding the presented work in particular, as well as possible future approaches in general.

The background of this paper is a work direction at Can Tho University, JEAI Dream group from the IRD, working in cooperation with the WSN group at University of Brest, Lab-STICC.

SOME ENVIRONMENTAL FACTORS INFLUENCING THE VIETNAM MEKONG DELTA

This section presents main characteristics of threats: pest insects, saltwater intrusion, floods, and water pollution.

Pest insects

The production of rice is the major target of several insects: *green leafhopper*, *zigzag leafhopper*, *white-backed plant-hopper*, *brown plant-hopper*, *rice whorl maggot*, *pink*

stem-borer, and several unidentified species of leaf folders and stem borers (R. Kisimoto 1979).

The brown plant-hopper (BPH) is a major insect pest of rice in Mekong Delta, southern Vietnam. From 2005-2006, an outbreak of BPH occurred and two virus diseases were transmitted by BPH. Rice Ragged Stunt Virus disease (RRSV) and Rice Grassy Stunt Virus (RGSV) disease (Akira Otuka 2009), spread over in the delta, resulting in big loss of rice production. Furthermore, in the same period, national rice production, and particularly the Mekong Delta production, suffered a major setback when outbreaks of BPH caused a loss of ~400,000 tons (1.1% of national production) (Kong Luen Heong 2007).

The outbreak of virus diseases transmitted by BPH has been the big challenge for the rice breeders, to find out the rice varieties with high yield and good grain quality, tolerant to BPH and virus diseases, suitable to different soil conditions. Some of the results were promising rice varieties tolerant to BPH, yellowing dwarf virus diseases, resistant to blast high and stable yield, tolerant to acid sulfate soils, suitable to alluvial soils and adapted to intensive cropping systems (MTL590, MTL603, MTL614, MTL631, MTL634, MTL637, MTL642, MTL645, MTL649, MTL653, MTL661, MTL662, MTL665, MTL706, MTL708 (Phạm Thị Phấn. 2011)).

Farmers may use pesticides to destroy BPH by direct spraying on young seedling of rice and seed treatment methods. By direct spraying, some pesticides are effective (such as Etofenprox, Fenobucarb, Carbosulfan, Thiamethoxam). By seed treatment methods, some insecticides are used: Thiamethoxam, Difenoconazole, Fludioxonil, Fipronil (Tran Van Hai et al. 2007).

Besides this, insect light trap is one of the effective tools of insect pest management in organic agriculture. It mass-traps almost all of insect pests and also substantially reduces the carryover pest population. By monitoring the light traps, farmers will know better what types of insect are in their fields and if they are in a controllable level, or not (Dr. C. Vaithilingam. 2013).

To forecast the population of BPH, a sampling distribution with more than 340 light traps has been deployed in the Mekong Delta since 2005 (Viet Xuan Truong et al. 2011).

A light trap uses light as an attraction source. Light traps depend on the positive photo tactic response of the insects, as physiological as well as abiotic environmental factors can influence the insect behavior (in Brown planthopper: Threat to Rice 1979). In the Mekong Delta, the light is usually turned on at 7:00pm everyday and the sample is collected and analyzed by farmers in the next morning (Dinh Van Thanh et al. 2009).

Figure 1: A *light trap* in the Delta. Top to bottom, there are rain cover, low energy bulb, reflectors, basin with water (sometimes insecticide) to kill insects that fall down. The power comes from a farmer house at tens of meters.

Figure 2: Layout of light traps (green spots) in Dong Thap

Figure 2 depicts light trap layout in Dong Thap province, a typical rice province in Mekong Delta. Green dots are light trap positions. Currently, 23 light traps have been established in Dong Thap.

The following figure (Figure 3) illustrates the number of BPH in three light traps in Dong Thap province. 'No power' means that there was no electricity in that night. The density of BPH in a light trap *is calculated sorting by hand.*

Light trap	07/11/2011	08/11/2011	09/11/2011	10/11/2011	11/11/2011	12/11/2011	13/11/2011
Sa Rài	13	2	16	0	131	36	No power
Tân Thành A	85	78	93	325	11	1,250	No power
Long Thuận	No power	324	390	410	450	515	5,200

Figure 3: BPH data from some light traps in Dong Thap from 07/11/2011 - 13/11/2011

Saltwater intrusion

Currently, the situation of drought and saltwater intrusion in the Mekong Delta are at an alarming rate and affect social life. In most estuaries and coastal areas of the Mekong Delta, saltwater encroaches on inland about 40-60 km, in 4-5 months (Doan Thu Ha 2013). Many provinces in the Mekong Delta get troubles with tap water. In a few regions, the

situation is particularly serious: people do not have running water; therefore, it makes a great influence on the lives and health. On the other hand, farmers often use river water to irrigate their fields, vegetable gardens and fruit trees. Freshwater aquaculture is also a common industry in rural areas of the Mekong Delta. All these activities are very sensitive to salinity.

The first solution to confront saltwater intrusion is to regulate water in salt prevention sluice gates. Opening and closing the outlet of a sluice gate plays an important role which has a great impact on aquaculture activities as well as saline prevention solution of locals. Therefore, reasonable opening and closing outlet may protect the ecology system, ensure the locals life, and improve salinity intrusion in the dry season (Center of Environmental Engineering 2012).

Another practice is plant choice restructuring to adapt to saline land. Some rice varieties adapting to saline land are now used. In addition, rice-prawn model has brought high economic efficiency and is contributing to structural economic shifts of the coastal provinces. Breeders continue research on breed salt-tolerant rice varieties that are suitable for current cultivation conditions and to overcome climate change in the Mekong Delta (Center of Environmental Engineering 2012).

From 2012 to 2014, Can Tho Climate Change Office has been performing the project: *Improving the capacity to respond saltwater intrusion due to climate change in Can Tho city*. This project is to build a network of automatic salinity monitoring stations in Can Tho to immediately warn about saltwater intrusion. This leads to enhancement with quick warning about changes of the salinity in some main rivers in Can Tho. Besides, residents have access to saltwater intrusion situation easily and quickly by connecting to salinity warning SMS system (Can Tho Climate Change Office. 2011).

Floods

Every year, the Mekong delta faces with floods and their impacts. The term *flooding season* implies an annual basis from July to November in the Mekong Delta. In the past, the Mekong Delta had more than 10 big floods, occurring in 1937, 1961, 1966, 1978, 1984, 1991, 1994, 1996, 2000, 2001, 2002... (Trần Như Hối 2009). Floods make a big damage to crops, livestock, and fisheries. For instance, in the flood 2012, about 27,000 hectares of rice crops were damaged; the area of industrial crops, fruit trees were flooded nearly 12,000 hectares; the total damage was estimated about 1,000 billion VND (Nguyet Anh 2012).

Governments and farmers in Mekong River delta have been constructing and maintaining dyke and embankment system surrounding their agricultural fields to control flood, and protect crops. Thanks to this system, two or three crop farms are annually cultivated in many places in Mekong River Delta. In 2008, there were approximately 1,000km^2 of three crop rice farms, 10,000km^2 of two crop and 1,300 km^2 of single crop farms (Huu Ninh Nguyen 2008).

In 2012, Southern Hydrometeorological Station built and equipped 89 meteorological stations and 117 flood warning piles in order to create a system to monitor floods in the Mekong Delta. This system has operated since then. Stations have been installed with modern equipments to automatically collect data of rain water level. Next, data is transmitted instantaneously to the provincial Hydrometeorological Centre and the Southern Hydrometeorological Station. This allows to process, compute, forecast fast and accurately some weather conditions such as tropical storms, floods (Vietnam's National Center for Hydrometeorological Forecasting. 2012).

Floods are not always negative. During the five month flooding period, 460 billion m^3 of water flowed through the delta each year, carrying some 200 million tones of alluvial, a mineral rich sediment that has high potential for soil enrichment. This type of flooding water also provides a nutrition source for fish and shrimp, while crops and livestock also benefits during flooding seasons. Flooding water can be regarded as a natural resource which local people can live with and take advantage of, even contribute to lessen the poverty rate in the region, thereby reducing the level of vulnerability to disasters (Huu Ninh Nguyen 2008).

Water pollution

Water pollution causes significant economic losses in operations agricultural production and aquaculture. Aquaculture production (especially fish cage farming on the river) has been decreased due to river water pollution problems. For example, from 2/2012-3/2012, in Soc Trang, 30% tiger prawn died because of water pollution. In Tra Vinh, after the first month of the prawn crop 2012, almost prawns died in 600/6,000 hectares of aquaculture due to diseases (Vietnam Environment Administration 2012).

Aquaculture has become a traditional craft and plays an important role for the national economy. However, aquaculture activities are sources of environmental pollutions on rivers in the Mekong Delta. In these activities, the main source of pollution is deposited-silt, which is wasted annually, in aquaculture ponds. In addition, in feed ingredients in aquaculture, only 17% dry weight of food is converted into biomass, the rest is discharged into the environment as manures or rotting organics. Another important problem comes from the industrial pond wastes. They are the source may cause environmental pollution and aquatic diseases in water (Vietnam Environment Administration 2012).

Up to 2012, there were 61 industrial zones in Vietnam Mekong Delta, creating jobs for more than 70 thousand labors. Most industrial parks have been located along the Tien River and Hau River. The discharge of untreated waste water or non-standard processes cause environmental pollutants for these rivers (Vietnam Environment Administration 2012).

To confront with water pollution, local governments in Vietnam Mekong Delta enhance monitoring agricultural activities and aquaculture in basins of Tien River and Hau River to closely control chemical pollutions in river basins due to fertilizer residues and chemical substances in plant protection (Vietnam Environment Administration 2012).

ARCHITECTURES FOR INFORMATION TECHNOLOGIES

Technologies

Information technology can help for controlling and understanding environmental behaviors, thanks to progresses

achieved on size reduction for integrated circuits, radio communications, energy saving and harvesting. This section describes system organizations that are under investigation in projects of UCT, and the resulting service organizations.

Figure 4: Radio module with pinout for serial control and data acquisition. Such modules can emit from few meters to kilometers depending on standards. They can fit Arduino boards

Sensor networks

Sensors are used to connect information systems to the physical world. A basic sensor is a physic system that reacts to real world changes by producing current or voltage changes. These last changes can in turn be measured and transformed into digital values.

A common practice to interface sensors is to use Micro-controller units (MCU) that have Analog to digital converters (ADC) and other capabilities, then to connect these MCUs to sensors. Other possibilities include Smart sensors, where processing is done on the same circuit as data acquisition. Image processing is a good case for such devices.

Such "intelligent sensors" can help in local control, without interface to IT systems. However more and more of the sensing systems are now connected to register history of changes and to take into account surrounding contexts. By correlating histories together, by observing and computing relations between histories, research can build new knowledges, and warn the society on potential risks.

Interconnecting sensors together is now feasible at low price using radio communications. Resulting networks can work in different ways conforming to transmission and system standards.

As an example IEEE 802.15.4 standards define several frequencies (regional 700/800/900 Mhz and worldwide 2.4 Ghz bands), medium access control (MAC) protocol and network topologies usable for sensor systems: *star topologies*, or *peer to peer with possible mesh organization* (IEEE 802.15: Wireless personal area networks). Access to the medium can be achieved in different ways which includes *CSMA/CA* for random access, and *beacon based*, periodic access under control of coordinators. This last method is well suited to sensor networks having periodic sampling behaviour, since it takes care of sleeping periods, and provide a schedule for communications from *coordinators and superframes* (Figure 5).

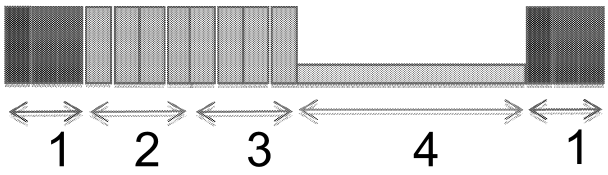

Figure 5: Superframe showing (1) beacon information, (2) slots with contention, (3) guaranteed communication slots, (4) sleeping time

Beside IEEE 802.15.4, other radio solutions exist, such as the use of cellular phone infrastructures, ZigBee and ISM variants (300-450Mhz).

Recent circuits from chip providers propose MCU, digital and analog interfaces, and radio transceiver on the same die, producing low cost solutions for sensor controls with protocol stacks. Radio modules and modular sensor boards allow to build swiftly sensor prototype systems and test new applications (Figure 4). Thus WSN have open the way to new control practice with impressive applications binding together thousands of sensors to save resources.

A WSN can also be an efficient tool to monitor and control the environment on a wider scale. Management of several problems of the Mekong Delta using this new technology is under investigation.

IT integration

In sensor vocabulary, the *cover* is the part of the physical process in which the sensor can operate, collecting values. In practice, several physical interfaces to the real world can be associated to a system, therefore multiple covers can exist for one system. To give an example, light traps can attract insects to less than 10 meters, so their cover is at most this distance.

However, by sampling insects in several locations, and doing an interpolation between measures, a distribution of sensors can reflect the reality of a situation on large ground surfaces. By adding time labels to samples, it is also possible to appreciate how a situation is evolving with changes in densities and moves of an insect cloud.

The role of IT tools is to keep track of measures in the long term, and to propose synthesis through display and alert mechanisms to final users, farmers in the case of BPH.

Some requirements for integration are the following:

- a localization of sensors on geographic systems
- a modeling of the environment (sea, rivers, ...)
- the collection of data on sensors at given times, and probably given frequencies
- the computation of physical characteristics *inside the WSN*, necessary for runtime decisions
- a propagation of results and measure histories to gateways and external servers, answering queries
- the representation of the physical evolution on geographic systems or databases
- the analysis of measures and decision making

The geographic system data is critical for the layout of an observation system, the internal computations, and final interpretation.

To support these requirements and the simulations described in next section, a set of tools are developed.

Map browsers

This kind of tools is of common use to obtain geographical information as well as satellite pictures. A first implementation has been used to select geographic zone of interest; to specify sensor positions, to represent expected network connections, simulated or actual sensor values. The second generation browser produced swift moving and zooming over maps and access to several map databases, notably OpenStreetMap. They both have support for geographic localization.

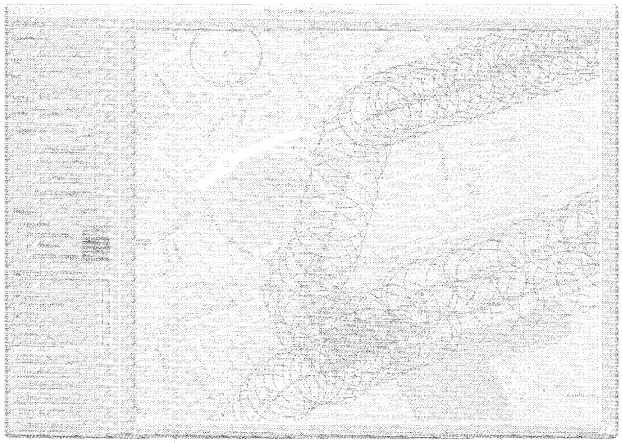

Figure 6: 1st generation browser displaying the Smart Santander european sensor experiment in real-time. 7 different networks are displayed which sensor connection range is tuned to 100meters. This browser is able to produce simulation architectures and to present data from simulation processes

Figure 7: 2nd generation browser displaying map of the Mekong delta from OpenStreetMap data. The browser can move its display presentation at pixel level, under program control. The Dong Thap provine appears above the city of Can Tho.

Specifications of deployment: picking tools

These specifications are achieved on pictures rather than map systems. Both sensors layouts and mobile paths can be produced and expressed on abstract models.

Image analysis

From the picking tools there is the possibility to produce layouts for geographic objects suitable for physical process simulation, running concurrently with network simulation. These tools consist of image segmentation and block classification according to min, max, mean in the RGB space. We expect to run physical simulation in various way, including cellular automata representing diffusions such as fires, insects, car traffic.

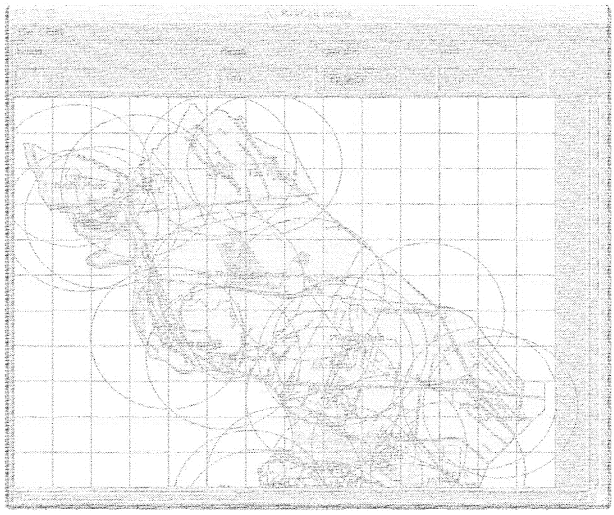

Figure 8: Sensor deployment preparation corresponding to current light-traps. The picture also shows a segmentation in 50 x 50 pixel blocks. Menu options allows to produce a graph model according to the selected range.

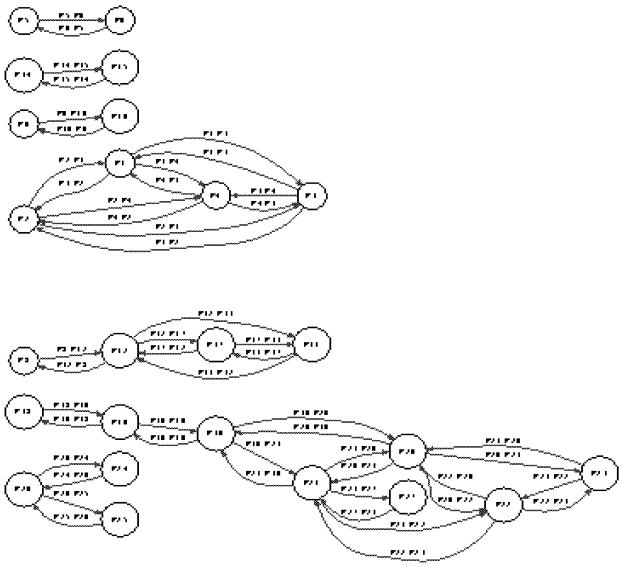

Figure 9: As the selected range is not large enough, the connections does not allow a completely connected network to be built. In this case, 7 networks appear in the logical graph. These graphs are traduction of the abstract model in *dot* file format for the *graphviz* program.

Figure 10 presents a layout extracted from the map. Each of the RGB component has been divided in 2 giving 8 cubes over the product of useful intervals for each color component. The *minimum* value in blocks was considered as classification criteria. By selecting the *mean* in these blocks, the 27 green spots for light-trap appear with very little noise as 5 additional block errors. Preparing such data partition can serve as a preparation of further physical simulations.

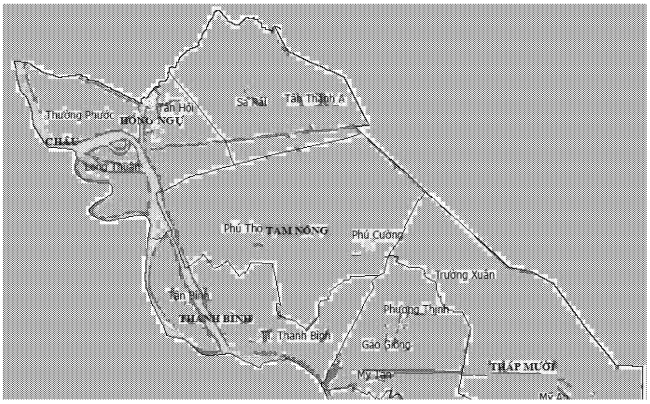

Figure 10: Segmentation was operated according to 5x5 pixel grid. RGB cubes had been generated according to 2x2x2 partition. This is the map extraction corresponding to coordinates 0,1,3 for the minimum pixels in cells This map would allow to represent the river as an actor in a physical simulation.

CONTROL SYSTEMS DESIGN AND SIMULATION

This set of tools is aggregated in the *NetGen* generic project names having a public documentation available on *github* (NetGen project). NetGen is a flow for wireless sensor code simulation, and production (Figure 11).

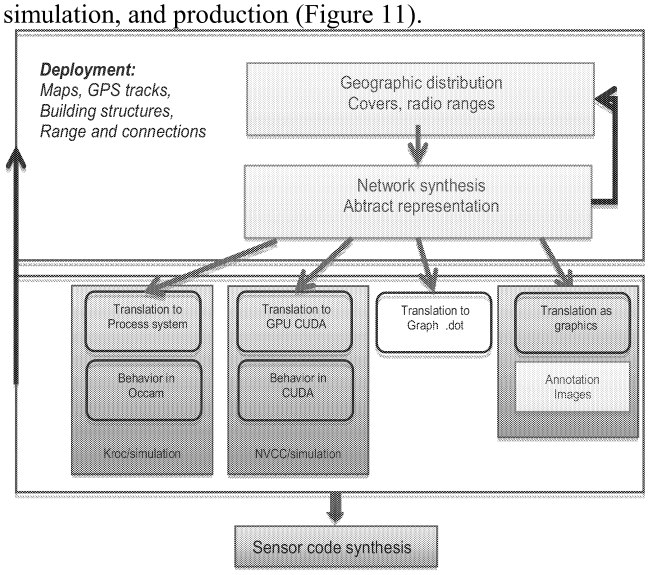

Figure 11: NetGen design flow showing 3 stages for sensor layout and network estimations, production of simulators, then reproduction of distributed code into actual sensor programs

Simulation code synthesis

The role of simulations is to validate cooperative work inside the network. This is done by *distributed algorithms,* that compute local decision in group of sensors, that optimize the number of transfers according to network topology, that allows external devices to access data inside the network, building routing supports. Since these networks have a *dynamic nature*, it is very important to let them decide how to proceed (Nancy Lynch and Morgan-Kaufman 1996). Internal basic activities in network are achieved over the communication links, by procedures executed synchronously by nodes. As example:

- Diameter computation provides in each network the maximum number of steps necessary to propagate knowledge from each node to each other node.
- Leader computation provides a unique identifier in each network, plus a potential controller for various algorithms.
- Route computation provides in each node the capability to propagate packets on a shortest pat to any target.
- Local computations on bounded radius allow to get cumulated operations in the neighborhood.

These procedures also provide designers with estimation on cost of communications, delays, latencies, and casual risk of failures. They are fundamental for application design, in relation with the network architecture.

NetGen has two working translators from graphs to network representation, expressed as asynchronous process systems (Occam Language), or high performance synchronous execution on Graphic Processing Units (GPU, and CUDA tools), see Figure 11. Both of these translators cleanly separate *cooperative behavior*, and *architecture description*. The first one is a manual programming tasks, while the other is fully automatic, freeing the designer from practical issues management related to topologies. Refer to NetGen project for more details.

Estimation on Mekong Light trap system

Simulation is run as a concurrent system of Occam processes that communicate over blocking channels. The periodic sampling shown Figure 4 is reproduced by having neighbor processes progressing synchronously in locked step fashion (Nancy Lynch and Morgan-Kaufman 1996), thus, simulation is strictly equivalent to what happens in the real network.

When the *architecture description* is produced, a trace process is added to collect information from each simulated nodes. In this case, we have produced numbers for *leaders* and for *diameters.* The number of different *leaders* give the number of networks, while the *diameter* gives the number of useful hops inside networks.

Table 1: Static and dynamic information from simulation runs for ranges from 95 to 170. The 2 last rows are produced by the simulation in similar way as what happens in real case

Range	95	100	105	110	115	120	170
Fan in	1	1	1	1	1	1	2
Fan out	4	4	4	6	6	6	10
channels	48	50	58	70	78	84	142
processes	24	25	26	26	27	27	27
networks	7	7	6	3	2	2	1
max diameter	4	4	6	9	9	7	8

Notice that the first range embedding all sensor nodes is obtained for range = 115, and the first solution *fully connected* is obtained for range = 170, with a diameter of 8. This means that any algorithm willing to propagate values inside the resulting network will need 8 steps to proceed. The number of channels and maximum fan out represent the communication load on some node, with up to 10 neighbor inputs to handle. The choice of range = 120 can be better to save energy if it is feasible to join a common gateway from the two isolated networks.

To demonstrate neighborhood computations, we had developed and run a computation constrained by a radius (logical distance) around each node. The principle is an Occam program reproducing this algorithm:

- *Initially* each node set up a table *T* holding records *R* with *Id, distance, value.* The first entry is for the node itself, other entries are invalidated
- *For each step,*
  - nodes emit *T* and receive *Ti* tables to/from neighbors.
  - For each incoming table *Ti,* the table is swept and its contents is aggregated to *T, without duplicating entries for any Id*
- *After count step,* T is swept, computing a global value is produced (mean, global condition, sum)

The Table 2 displays the minimum and maximum count of neighbors on a *radius of 2* for each sensor in the previous networks. Notice that time stamps are also necessary to distinguish moment of measures, they can be deduced from the *distance* parameter in *R* records.

Table 2: Minimum and maximum number of neighbors (Ids) computed dynamically for Dong Thap light trap systems, range from 95 to 170

Range	95	100	105	110	115	120	170
neighbor min	2	2	2	2	3	3	5
neighbor max	8	8	8	11	12	14	20

CONCLUSION AND FINAL REMARKS

In this paper, WSN has been investigated as an information technology tool to monitor some environmental conditions in Vietnam Mekong Delta. These conditions may be threats such as pest insects, saltwater intrusion, floods, and water pollution.

Pest insect threats are currently monitored manually using light traps. With an additional research effort, automatic traps, able to classify and count insects, could replace these devices. With this hypothesis; it is attractive to connect traps using small radio following sensor network standards. We simulate several WSN options for light traps network in Dong Thap province in the Mekong Delta using NetGen. The network range 170 is fully connected, meanwhile, the transmission range is large enough to cover all sensor nodes leading to a single well-balanced network. However, the choice of range 120 is more energy saving if we can use a common gateway for the two isolated networks.

WSN can be used to face other threats. For example, sensors can be used to analyze the water pollution data in rivers in Mekong Delta. These measures will be useful for aquaculture households in Mekong Delta. Another usage of sensors is to monitor salinity in rivers to immediately warn about saltwater intrusion. They can be an efficient tool to monitor floods as well.

This work was done at an abstract level targeting system and algorithm design. Ongoing investigations include study of radio capabilities for connection of traps and information servers. As range 100 in Figure 8 represents 12km, one can see that the expected distances between light traps are medium range, going from 11 to 20km, thus providing indications on radio technologies and transceivers that could be used for this case (Digi.com, XBee RF features), perhaps with the addition of wired solutions.

WSN appear to be a very promising technology for the protection, of environment and agriculture activities.

REFERENCES

AHMED Ahmed. 2013. “Simulation and modeling of physical processes (Master report)”, http://wsn.univ-brest.fr/pottier/ahmedReport.pdf,

Akira Otuka. 2009. “Rice Planthoppers in Vietnam and Their Migration”. National Agricultural Research Center, Tsukuba, Ibaraki 3005-8666, Japan.

Can Tho Climate Change Office. 2011. “Improving the capacity to respond saltwater intrusion due to climate change in Can Tho city”. Asian Cities Climate Change Resilience Network, Phase 3 Proposals – City Level Intervention (in Vietnamese)

Center of Environmental Engineering. 2012. “Proposal to restrict saltwater intrusion in Soc Trang” (in Vietnamese)

Department of Aquaculture, Ministry of Agriculture and Rural Development. 2013. Conference of Aquaculture in the coastal provinces of the Mekong River Delta, Tien Giang (in Vietnamese)

Digi.com. XBee RF features. http://www.digi.com/pdf/chart_xbee_rf_features.pdf

Dinh Van Thanh, Lai Tien Dzung, Nguyen Thi Duong, Phan Thi Bich Thu, Nguyen Nhu Cuong. 2009. “Management of Rice Planthoppers in Vietnam”. Plant Protection Research Institute, Ha Noi- Vietnam.

Doan Thu Ha. 2013. “Impact of climate change on rural water supply in the Mekong Delta and response solutions”. Annual Conference of Science of Water Resources University.

Dr. C. Vaithilingam. 2013. “Role of insect light trap in organic agriculture”. Romvijay Biootech Private Limited.

Huu Ninh Nguyen. 2008. “Flooding in Mekong River Delta, Viet Nam”

IEEE 802.15: Wireless personal area networks . http://standards.ieee.org/about/get/802/802.15.html

International Rice Research Institude. 1979. “Brown planthopper: Threat to Rice”.

J.Markoff. “Can't find a parking spot? Check smartphone.” http://www.nytimes.com/2008/07/12/business/12newpark.html?_r=0

Kong Luen Heong. 2007. “Research issues on the brown planthopper/virus problem in rice in Vietnam”. International Rice Research Institute, Philippines.

Ministry of Agriculture and Rural Development. 2013. Conference of review the production and consumption of catfish in the Mekong Delta in 2012 (in Vietnamese)

Nancy Lynch, Morgan-Kaufman. 1996. “Distributed algorithms”

NetGen project. https://github.com/NetGenProject

Nguyen Minh Sang. 2011. “Positions, roles, potential, and the strength of the key economic zone Mekong Delta”. Ministry of Planning and Investment. http://www.vietrade.gov.vn/vung-kinh-te-trong-diem-dbscl/2403-vi-tri-vai-tro-tiem-nang-va-the-manh-cua-vung-kinh-te-trong-diem-vung-dbscl.html (in Vietnamese)

Nguyen Trung Tien. 2011. “Development of rice production in the Mekong Delta”. Kien Giang Seed Center. http://cayluongthuc.blogspot.com/2011/08/phat-trien-san-xuat-lua-gao-vung-bscl.html (in Vietnamese)

Nguyet Anh. 2012. “Heavy losses in Mekong Delta due to flood”. Vietnam Academy for Water Resources. http://www.vawr.org.vn/index.aspx?aac=CLICK&aid=ARTICLE_DETAIL&ari=1402&lang=1&menu=tin-trong-nuoc&mid=177&parentmid=131&pid=2&storeid=0&title=dong-bang-song-cuu-long-thiet-hai-nang-ne-do-lu (in Vietnamese)

Phạm Thị Phấn. 2011. “Breeding and varietal selection for high quality rice varieties for the Mekong Delta of Vietnam in the period of 2009-2010”. Journal of Science Can Tho University.

R. Kisimoto. 1979. “Brown planthopper migration, Brown planthopper: Threat to rice production in Asia”. IRRI, pp. 120-131.

Santander on FIRE: http://www.smartsantander.eu/

Tran Van Hai, Nguyen Van Hai, Truong Vu Linh, Ly Yen Minh. 2007. “Evaluating the efficacy of some common pesticides against Brown Plant Hopper Nilaparvata lugens Stal.”. Science workshop proceedings of Sustainable development in Mekong delta after Vietnam joined World Trade Organization. Can Tho University, pp.322-330.

Trần Như Hối. 2009. “Some typical floods and flood zoning in the Mekong Delta”. Collection of science and technology: 50 years of construction and development.

Viet Xuan Truong, Hiep Xuan Huynh, Minh Ngoc Le , and Alexis Drogoul. 2011. “Estimating the Density of Brown Planthoppers from a Light-Traps Network based on Unit Disk Graph ”. AMT’11 Proceedings of the 7th international conference on Active media technology, pp. 276-287.

Vietnam Environment Administration; National environmental report. 2012

Vietnam's National Center for Hydrometeorological Forecasting. 2012. “Building a flood warning system in Vietnam Mekong Delta”

Uncertainties and Variabilities Evaluation in Food Exposure Assessment

Alain-Claude Roudot
Université de Bretagne Occidentale
Laboratoire d'Evaluation du Risque Chimique pour le Consommateur
UFR des Sciences et des Techniques
6 avenue Le Gorgeu, CS 93831
29238 Brest cedex 3
France
alain-claude.roudot@univ-brest.fr

Keywords
Uncertainty, fuzzy number, probabilistic analysis, hybrid analysis, exposure

Abstract
When realizing exposure analysis to chemical contaminants in food, one must take into account a lot of possibilities of uncertainties and variabilities. Classically, when exposure is very low from a risk threshold, a deterministic approach is made with no evaluation of variabilities or uncertainties. A probabilistic approach can be done when a large number of data are given by experiments. The results are given under the shape of a distribution of exposure among the population studied, and two main parameters remain: the median and the 95th percentile of the distribution. When few experimental data exist, this last method is very difficult to apply and a fuzzy approach can be chosen. Its advantage is that a prior idea of the « hidden » distribution is not needed, but only the upper and lower limits of such parameters. The obtained result of such analysis is far more informative than the deterministic results or even the probabilistic ones. However, the main problem of this method is to find an easy interpretation way.

1- Introduction

Health-risk assessment is a quantitative evaluation of information on potential health hazards from exposure to various agents. In order to make this assessment, different steps are needed: sampling the population, sampling the food eaten, calculating the intake, measuring contamination, calculating the exposure. During all these steps numerous possibilities of uncertainties appear (Mesa-Frias et al. 2012; Ben-Haim, 2012), which necessitate an evaluation of the uncertainty on the final result in order to make this final exposure usable by risk managers. Different attempt were made in this analysis but points such as evaluating the quantities eaten, or evaluating chemical analysis precision are very often forgotten in the analysis because of a lack of information. The different food safety agencies have approved for years, using a probabilistic approach for some parameters when there are numerous data to be collected. But when few data are present, this method is very difficult to implement and may create more uncertainties (model uncertainties which are never evaluated) than solving the problem. The main alternative is then to use a deterministic approach, which means using an average of the parameter under consideration for instance (or any other value: maximum, median etc. but just one value). That solution means that you consider that no variability exist, and then the result may be under or over evaluated, which is the worst case because you do not know where you really are (fig. 1). A solution could be a fuzzy approach of the parameters which are uncertain and not clearly defined.

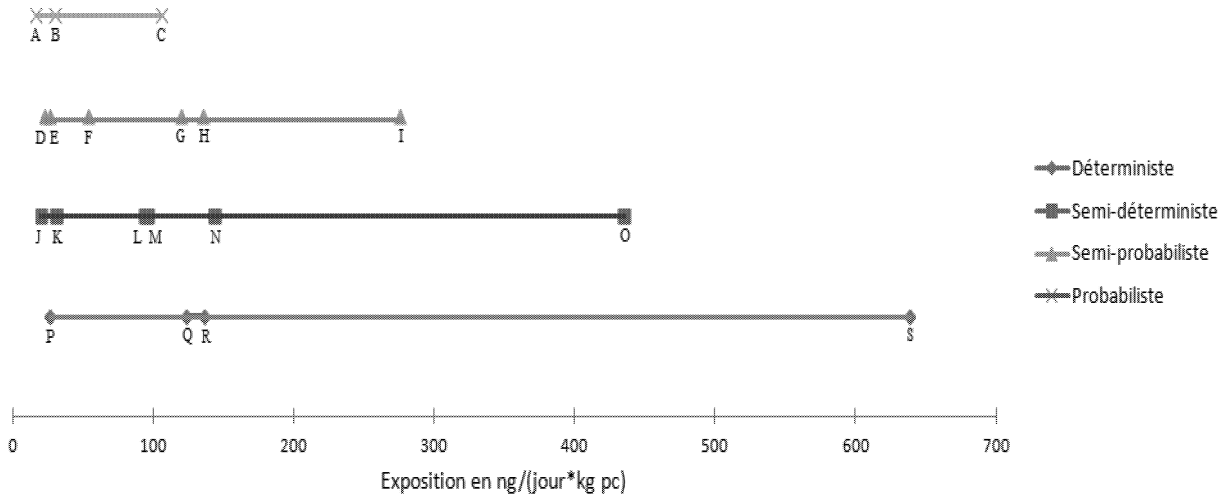

Fig. 1: Comparison of deterministic and probabilistic evaluation of an exposure to phycotoxins. Consumption comes from a 500 individuals' survey, and contamination from 10 chemical measures. One can see that the larger possibilities are obtained with deterministic evaluation (low curve), while the probabilistic one (upper curve) gives the more robust results. A and C median and P95 of the distribution of exposure, P: exposure obtained with median consumption and contamination, S exposure obtained with P95 consumption and contamination. The second line use a distribution for consumption and a deterministic approach for contamination, and the third line is the opposite.

2- Theory

21- The fuzzy numbers

Fuzzy logic was invented in the 1960's by Lofti Zadeh (Zadeh, 1965) and was then used in numerous technical and technological areas, such as neural networks, process regulation and, very recently, in risk assessment (Tazid and Palash, 2012). Its main idea is that Boolean logic is insufficient. In Boolean logic you can choose between 0 and 1, in fuzzy logic you can choose any number between these limits. It is a continuous logic. Among the different aspects of fuzzy logic what is usable in our area is the notion of fuzzy number. A fuzzy number necessitates different elements: an interval (which is called the core) and a belonging function. Each value inside the core has a belonging function, which is a value between 0 and 1 giving its belonging to the fuzzy number. For instance (Fig. 2), the core of the fuzzy number N can be the interval [1 ; 3] and the belonging function can be 0 for number 1 ; 0.5 for number 1.5 ; 1 for number 2 ; 0.5 for number 2.5 and 0 for number 3. This gives a triangular fuzzy number, for which one can say that number 1.5 has a 50 % belonging to N, or number 2 has a 100 % belonging to N. With this method you can be partly inside and partly outside the number.

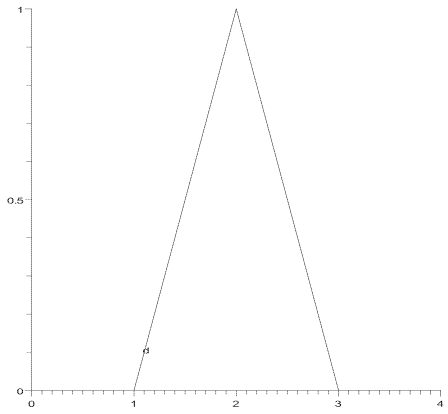

Fig. 2: example of a symmetrical fuzzy number [1;3]

In our area, the interest of fuzzy numbers is to define an interval of belonging around the average or median value: for instance the measured contamination is 20 mg/kg but if you take into account the uncertainty using fuzzy number you can use a core [10; 30] for a symmetrical triangular fuzzy number with maximum belonging for 20mg/kg and minimum for 10 and 30 mg/kg.

Using fuzzy numbers in such cases necessitates having at least one value and an expert advice of the usual uncertainty around that value (Roudot, 2013).

22- The probabilistic distribution

The main solution used and preconize for evaluating uncertainties is the use of probabilistic distribution. That implies that you have a lot of data, and that you can adjust these data with a probabilistic distribution. The main distributions are normal, lognormal or decreasing exponential functions. The interest relies on the use of real data and then on a real evaluation of the uncertainties. These ones are then modelled using an adjustment in order to be able to calculate further parameters such as exposure or daily intake.

The condition of use of this probabilistic method is the necessity of having a great number of data in order to be able to adjust the function. Consequently, that method is very useful with data obtained from surveys such as quantities eaten by a population, but difficult to use with contamination measurement for instance.

23- The hybrid method

In the exposure area, consumption data are generally in great quantities (some hundreds), and contamination in low quantities (some unities). Then the same modelling method is not the best one. The proposal is to use a distribution approach for consumption and a fuzzy approach for contamination. This mixed method is called the hybrid one. The choice is possible for all parameters in the model used to calculate exposure.

3- Examples

In order to calculate an exposure analysis to chemicals in food, one needs to obtain different parameters:

- consumption of the population
- contamination of the different food items
- body weight of the population

Consumption can be obtained using different methods but concerning the quantities eaten, the main solution used is to show pictures of plates with different quantities (classically three : few, lot and medium) and people choose between them the «good» one. This point is a critical point in consumption evaluation and uncertainty on that evaluation is never analysed. It can come from the creation of the pictures or from the choice by the consumer. In fact it is very difficult to give the good answer when it is not shown! So we obtain one solution from each consumer but with a great amount of uncertainty. In that case, fuzzy number can be a good approach, the quantity being centered on the plate chosen and with a core between the two plates in its neighbourhood. That means you will have to create two virtual plates with maximum and minimum contents.

Frequency can be obtain using different method such as a frequency questionnaire or a 24h recall which give data which can be modelled by probabilistic distribution.

For contamination, as data are in few quantities, it is almost impossible to adjust the experimental values to a probabilistic distribution. Then, a fuzzy number centered on the median value with a core between the maximum and minimum measured value could be used. One can see that, with that method, problems of left censorship of chemical values due to limits of detection does not occur because the belonging function can grow from null contamination to limit of detection and then to median value. The only problem could occur if more than 50 % of data are left censored.

Another point, never taken into account, is the precision of the chemical analysis which vary with the method and with its value. This point can be also modelled by fuzzy method.

4- Applications

In order to show the differences between the different exposure calculation methods, one has calculated a virtual chemical intake using deterministic, probabilistic and hybrid methods. The exposure was calculated using only two parameters: consumption and concentration.

In the deterministic approach, consumption is evaluated with an average of 50 g/kg bw/d and a chemical contaminant concentration of 15 µg/g. The immediate result is an exposure of 750 µg/kg bw/d. One can see that there is

absolutely no information on the possible uncertainties.

In the probabilistic approach, consumption is evaluated as a lognormal distribution of mean 50 and standard deviation 15, when contamination is modelled with a normal distribution of mean 15 and standard deviation 2. The result is given with Figure 3 which gives a cumulated distribution function (CDF) of the product: consumption X contamination.

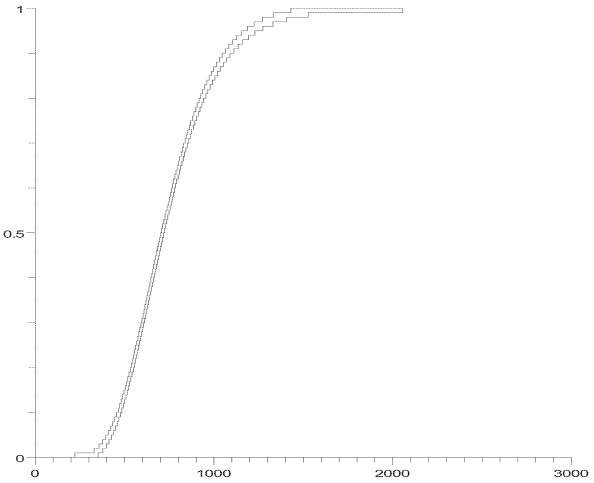

Fig. 3: CDF of probabilistic evaluation of the exposure

This curve gives a mean value of 750 µg/kg bw/d , and a standard deviation of 248 µg/kg bw/d (median : 710 µg/kg bw/d and P95 : 1220 µg/kg bw/d). In that case one can see that an evaluation of the uncertainty is made. Far more information is known in order to make a risk characterization.

In the hybrid approach, consumption is modelled as in the probabilistic one and contamination using a fuzzy number [10, 20] which means maximum belonging function (100%) for 15 and minimum (0%) for 10 and 20. The result is given in figure 4.

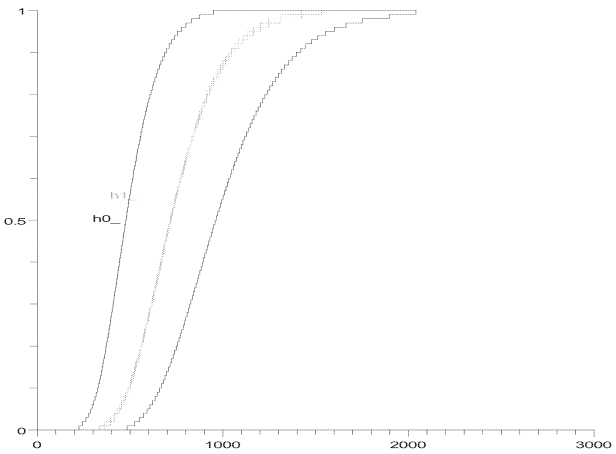

Fig. 4: Hybrid evaluation of the exposure

On this result one can see that the average exposure is comprised between 570 and 900 µg/kg bw/d, while between 17 % and 93 % of the population have an exposure less than 750 µg/kg pc/j. Between 80 % and 100 % of the population have an exposure less than 1220 µg/kg pc/j.

One can see that the three approaches give the same average value and that they can complete each other. However, their complexity increases from deterministic to probabilistic and hybrid. The main problem is then to choose the best one for risk managing. One can easily understand that if it is easy to manage risk with the deterministic approach (the exposure must not exceed the legal limit), it is more difficult with the probabilistic one (very often the P95 is used as the reference exposure, but why not the P75 or the P99?) and far more difficult with the hybrid approach because average and P95 (for instance) are only known as intervals!

5- Conclusion

The use of fuzzy logic and more precisely fuzzy numbers seem to be an alternative to semi probabilistic approach when data are missing. The use of hybrid methodology gives a high amount of information about uncertainty. Anyway, the problem is to know what can be practically done with so much information and above all how using these new data in a risk assessment project (Roudot, 2012).

References

Ben-Haim Y., 2012. Why risk analysis is difficult and some thoughts on how to proceed. Risk Analysis, 32(10), 1638-1646

Mesa -Frias M., Chalabi Z., Vanni T., Foss AM. 2013. Uncertainty in environmental health impact assessment: quantitative methods and perspectives. International Journal of Environmental Health Research. 23(1), 16-30

Roudot AC, 2012. Modélisation des incertitudes et variabilités en EQRS. Bulletin de Veille Sanitaire (19), 44-46

Roudot AC. 2013. Influence of uncertainties and variabilities on exposure and risk evaluation. Joint ISEE, ISES and ISIAQ Environmental Health Conference. Basel, 2013/08/ 19-23

Tazid A., Palash D. 2012. Modeling of uncertainty in dose assessment using probability-possibility transformation. International Journal of Computer Applications. 48(12), 1-7.

Zadeh L., 1965. Fuzzy sets. Information and Control, 8, 338-353

AUTHOR LISTING

AUTHOR LISTING